ISSN: 2224-2007
E-ISSN: 2707-7365

MIJST

MIST International Journal of Science and Technology

A Peer Reviewed Online Open Access Journal

Golden Jubilee of Independence Issue

Volume 09
June 2021

Military Institute of Science and Technology (MIST)
https://mijst.mist.ac.bd/mijst
Previously known as:
MIST Journal of Science and Technology

MIJST

MIST International Journal of Science and Technology

EDITORIAL BOARD

DISCLAIMER

ISSN: 2224-2007
E-ISSN: 2707-7365

QUERIES ON SUBMISSION

For any query on submission the author(s) should contact: MIST, Mirpur Cantonment, Dhaka-1216, Bangladesh; Tel: 88 02 8034194, FAX: 88 02 9011311, email: *mijst@mist.ac.bd*. For detailed information on submission of articles, the author(s) should refer to the Call for Papers and About MIJST at the back cover of the MIJST Journal. Authors must browse MIJST website through the journal link (*https://mijst.mist.ac.bd/mijst*) for electronic submission of their manuscripts.

PUBLISHER

Military Institute of Science and Technology (MIST), Dhaka, Bangladesh

DESIGN AND PRINTING

Research and Development Wing
Military Institute of Science and Technology (MIST)
Dhaka, Bangladesh

FOREWORD

Bismillahir Rahmanir Rahim

The Military Institute of Science and Technology (MIST) aims at being one of the leading Institutions of Engineering and Technology in regional and international ranking and it continues to play its role as a centre of excellence in creating and disseminating new knowledge in the cutting-edge areas of Science and Technology. I firmly believe that 'MIST International Journal of Science and Technology (MIJST)', the flagship journal of this Institution has already been able to make an impact with its quality signatures. I am happy to note that MIJST is already indexed by a number of search engines, such as, DOI Crossref, Google Scholar, Microsoft Academic Search, Publons, Semantic Scholar, BaglaJOL, Creative Commons and Open Journal System and working toward getting indexed in SCOPUS, Directory of Open Access Journals (DOAJ) and Web of Science (WoS).

Golden Jubilee of our Independence is a landmark event for us. To make this event memorable, this issue of MIJST has been dedicated to the Golden Jubilee of Independence of Bangladesh. I would like to express my sincere thanks to the MIJST team for its on time publication of consecutive 3 issues of MIJST, despite the COVID-19 Pandemic situation. My deep appreciations to the Authors of this issue for their scholarly contributions. Reviewers are also acknowledged for providing invaluable peer review to the articles to ensure high quality of the papers. Very special thanks to the National and the International Advisory Boards for their invaluable suggestions and guidance in maintaining the quality of the Journal.

I wish continued success of MIJST.

Major General Md Wahid-Uz-Zaman, ndc, aowc, psc, te
Commandant, MIST, Bangladesh
Chief Patron, MIJST, Bangladesh

EDITORIAL

The global havoc caused by COVID-19 pandemic is continuing. However, our commitment to timely publication of MIST International Journal of Science and Technology (MIJST) has not been deterred. We are delighted to inform you that the Volume 09, June 2021 issue of the journal has come out on schedule. It was only possible by the hard work, commitment and synergies of authors, reviewers, editorial and production teams. As always, the journal is fully committed to publishing theoretical and applied research outputs from any fields of science, engineering, and technology that will help our planet earth.

The MIJST is an Open Access bi-annual Journal. The purpose of Open Access policy is to enable readers to unrestricted access from any location across the world allowing diffusion of new knowledge and innovations. Moreover, the publication and access to MIJST are completely free of cost. The Journal is now more visible and indexed through Google Scholar, DOI Crossref, Microsoft Academic Search, Semantic Scholar, Publons, Creative Common, BanglaJOL, and Open Journal System. We are following a roadmap for getting our journal to be indexed in SCOPUS, Web of Science (WoS), Emerging Source Citation Indexing (ESCI) by Thomson Reuters/Clarivate Analytics, and Directory of Open Access Journals (DOAJ).

Academics/faculty members, researchers, professionals, and industry practitioners are urged to submit their unpublished, original, and innovative contributions from any branch of science, engineering, technology, and related fields. All submitted contributions will go through a double-blind peer-review process with effective feedback. We are committed to publishing high quality original, innovative, and latest findings as original articles and review articles (by invitation).

This June issue, 2021 includes six original research articles focussing on water collection methods from plume of a cooling tower, bank-line behaviour of rivers in mangroves, GIS approach for hydrological modelling, behaviour of recycled brick aggregate concrete, applicability of various fuels in SI engines, ecosystem services and disservices in urban environment. Each of these six articles deal with real-world problems and broadens our knowledgebase.

Over and above this, I wholeheartedly thank the Chief Patron, Executive Editor, Associate Editors, Section Editors, Reviewers, other Editors and Proof-readers, Editorial/Advisory Board members (national and international), and web production consultant for their all-out support, commitment, hard work, and passion for this journal. I call upon you to promote the MIST International Journal of Science and Technology (MIJST) among colleagues, research scholars, and library liaison officers.

Your valued feedback, suggestion, and advice for the advancement of this journal are always welcome through telephone +61 3 99256103 and/or email: *firoz.alam@rmit.edu.au*; *mijst@mist.ac.bd*.

Sincerely,

Prof. Dr. Firoz Alam
Editor in Chief

INDEX

MIJST
MIST International Journal of Science and Technology

Experimental Study of Water Collection from Plume of an Induced-Draft Counter-Flow Cooling Tower Using Space Charge Injection

Md. Fahim Faisal Patwary[1*], Isheka Agarwala[2], Rashik Ahmed[3], and Dipak Kanti Das[4]

Department of Mechanical Engineering, Military Institute of Science and Technology (MIST), Dhaka, Bangladesh

emails: *[1]*fahim.mech.mist@outlook.com; [2]isheka.mist@gmail.com; [3]ahmed.rashik4@gmail.com; and [4]dipak@mist.ac.bd*

ARTICLE INFO

Article History:

Received: 19th April 2020
Revised: 10th February 2021
Accepted: 11th February 2021
Published: 27th June 2021

Keywords:

Space Charge
Injection Plume
Abatement Collection
Percentage Air
Ionization Liquid-Gas Ratio

ABSTRACT

Plume collection from cooling towers can be a reliable solution to the water scarcity problem faced in many regions around the world. Meshes are one of the most proposed collectors in this regard that rely upon inertial collision for droplet capture and are inherently limited by aerodynamics. This study quantifies the effect of electrical forces on water collection from the plume of an Induced Draft Counter Flow (IDCF) Cooling Tower by introducing sets of copper tubes at the exit of the tower. The imparting of net charge to the exhaust plume by instigating space charge directs the vapor towards the inside wall of copper tube forming water droplets. This arrangement instead of a mesh or net system, creates a lesser obstruction to flow. Fabrication of fill/packing with a corrugated wave pattern using PVC plastic demonstrates satisfactory cooling performance of the tower. An optimized *L/G ratio* is found to exist for maximum collection efficiency of water from plume at definite entering fluid temperatures by investigating with the entering warm water temperatures at 40°C, 45°C and 50°C while the dry bulb temperature of air ranges from 23.5°C to 30.1°C. The electricity consumption for this arrangement fluctuates from 2.78 kWh/m^3 to 5.13 kWh/m^3 for two *L/G ratios* (23.5 and 28.3). Where maximum collection percentage occurs at two different entering fluid temperatures, the power expended is below the minimum used for typical desalination plants.

1. INTRODUCTION

The cooling tower is equipment most widely used to release excess heat loads from various processes, such as thermal and nuclear power plants, electric power generation units, refrigeration and air-conditioning systems, chemical and petroleum industries, into the atmosphere (Wakil, 1985). Transfer of mass and thermal energy from high-temperature water to coolant air is the basis on which this device operates. In wet cooling towers, a direct interface between coolant air flow and warm water is created as water flows over the fill. As this hot water gets cooled down, a portion of it evaporates and leaves the tower along with the air. So, air's temperature is raised and its relative humidity elevates to 100% causing a vapor fog to escape out otherwise known as plume. While maximum performance is the aim of every cooling system, visible water vapor plumes might be the unexpected result of certain environmental conditions. These plumes have reportedly exerted negative effects on the environment by affecting clarity of view and safety as well as public insight, and decisively delaying permits and jeopardizing project timelines.

In Mechanical-Draft Cooling Towers (MDCT) there have been incidences of fogging at ground level along with icing typically in winter. The updrafts from MDCT have contributed to the formation of cloud. Light snow has also been observed due to this dissipation which was first recorded in 1975 (Carson, 1980). Other effects include possible contribution to severe weather such as thunderstorms, hail and tornadoes along with precipitation generation (Huff *et al.*, 1971). In areas with frequent fog, visibility problems are caused by the descent of this condensing vapor plume. There have also been instances of toxic component formation due to mixture of plume with gaseous emissions of the industry. For example, formation of sulphurous acid mist due to reaction with sulphur-dioxide gases. Supersaturated region created, when the ambient temperature goes below 10-16°C and the relative

humidity exceeds 80%, is also one of its effects. As a result, there have been several researches for dispensing this plume coming out of the towers. One of these processes is adding heat to the tower exhaust thus superheating the plume. The installation and operating cost estimated for this process is $40,000 and $16,000 annually. Discarding the process latent heat without evaporation by altering the cooling method is also one of the processes of plume abatement. Installation and operation cost estimated for the system in practice of this method is $22,000 and $3,000 annually respectively (Veldhuizen & Ledbetter, 1971).

Researchers from MIT (USA) came up with a new approach for fog harvesting mesh in 2018 in which they introduced electrical forces, and aerodynamic drag forces could be overcome by dint of it (Damak & Varanasi, 2018). They measured collection efficiency of fog on single-wires, and meshes and proposed a physical model to quantify it (Damak & Varanasi, 2018). In this paper, a non-identical setup for water collection from the plumes of cooling tower has been proposed, inspired by the principles of electrostatic precipitators (Parker, 2003; Kraemer & Johnstone, 1955; Uchiyama & Jyumonji, 1995). Small copper tubes serve as collectors inside of which there are smaller copper tubes that serve as emitters. Plume is directed to pass in between these tubes while the tubes are maintained at a high voltage of ~-7 kV. Thus, it induces a net charge into the plume droplets and directs them towards the collector. The electric field lines take off from emitter and end at grounded collector. When the electric forces surpass the air drag forces, the droplets travel along the field lines and deposit on the inside wall of collector tube.

Based on prior studies, the main factor influencing the efficiency of a cooling tower is the thermal performance inside the filling zone. This is because 70% of the heat dissipating capacity is based on the filling zone (Williamson *et al.*, 2008). An IDCF cooling tower prototype of the size constructed for this study would produce plume with an inadequate concentration of water. So, instead of straight or zigzag shapes, fill material is used in waveforms for the occurrence of highest possible heat rejection so as to obtain more concentrated plumes (Novianarenti *et al.*, 2019). The primary objective of this experiment is to reduce the water content in the exhaust plume of cooling towers, collect it instead for reuse and hence, diminish some of the harmful effects caused by them. The results from this study have shown that this can simultaneously reduce the current reverse de-salination energy consumption (~3 to 5 kWh/m^3) required for make-up water of cooling towers in power plants by an estimated energy consumption of ~0.2 kWh/m^3 for more concentrated plumes which is on the order of 5000 litres/m^2 per day. It has also been shown that the collection percentage from the evaporative loss is variable depending upon various conditions and specific criteria in this paper.

2. BRIEF THEORETICAL BACKGROUND

During the ionization of air, the dielectrophoretic nucleation of polar water molecules on ions allows for ~16-20% dehumidification (Reznikov, 2003; Reznikov, 2014). However, the electrostatic enhancement of condensation occurs due to the amalgam of three phenomena:

1. the dielectrophoretic (DEP) nucleation of the vapor on electrically charged centres;
2. the electrohydrodynamic (EHD) flow of the vapor as electrically charged droplets create drag; and
3. the temporal (until droplets are discharged) storage of heat energy in electrically charged droplets.

The stability of small droplets is notably affected only by the dielectrophoretic potential. The total latent heat of evaporation is relatively small for small droplets (<10μm) which is shown in Figure 1 (Reznikov, 2015). At a constant droplet volume of $4\pi R^3/3$ where R is the radius of a drop, the heat capacitance is proportional to the second derivative of Gibbs energy, $G = N \times \mu_l$, where N is the number of molecules contained in the cluster (droplet), and μ_l is the liquid chemical potential.

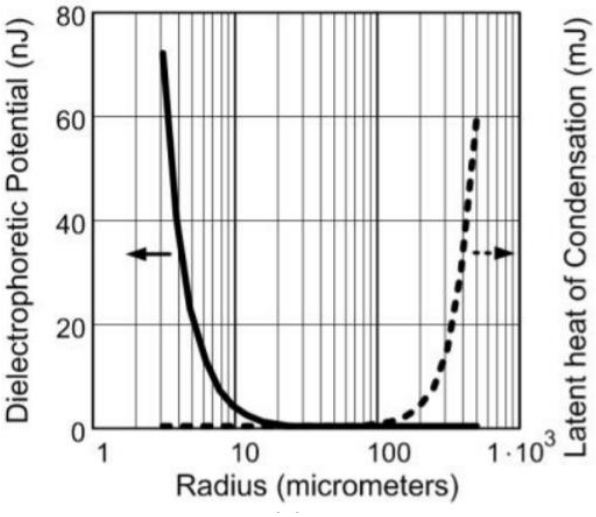

Figure 1: Droplet DEP potential (solid line) contrasted with its latent heat of condensation (dotted line)

Therefore, the isochoric heat capacitance of the droplet is stated as

$$C_{V,N} = -T\left(\frac{\partial^2 G}{\partial T^2}\right)_{V,N} = -T.N\left(\frac{\partial^2(\mu_n - \Delta\mu_{DEP})}{\partial T^2}\right)_{V,} \quad (1)$$

where μ_n is the chemical potential in the neutral droplet and $\Delta\mu_{DEP}$ is the decrement of chemical potential due to dielectrophoretic forces.

$$\Delta\mu_{DEP} = \frac{q^2 v^l}{32\pi^2 \varepsilon_0 R^4} + \frac{q\rho_0}{4\pi\varepsilon_0 R^2} \quad (2)$$

Here, q represents a single electron charge, equal to 1.6×10^{-19} C and v_l is the volume per single molecule in liquid. Therefore, the heat capacitance of the droplet should decrease due to the electric charge. Experimental data from Sundén *et al.* (2009) supports this conjectural conclusion. There are more aiding factors supported by numerical modelling and experimental data from Yu (2005) where it shows that same number of molecules in bulk neutral water contains higher enthalpy in charged droplet form and the excess enthalpy is added as energy in the form of electric polarization.

A decrease in temperature of the droplet at the discharge on the ground condensing wall is induced by the decrement of heat capacitance of the electrically charged droplet. The latent heat of condensation decreases relatively and it is also partially replaced by electrostatic energy which ultimately results in the condensation of droplets on the wall.

3. EXPERIMENTAL PROCESS

A. Experimental Setup

The cooling tower used in this experiment is an induced draft counter flow wet type with a circular cross-section. The installation is done on a steel frame and is accompanied by the following.

- A collection basin for collecting cooled water.
- A hot water reservoir with arrangement for electric heaters to heat up the water.
- A water pump at the bottom to pump from reservoir with a water distribution system up to the top containing spraying nozzles. Heated water is sprayed through nozzles that flows down through the fill to the basin and continues the cycle.
- A draft fan for inducing airflow from the bottom to cool down hot water. This air, rich in water vapor, exits from the top of the tower increasing the air temperature.

The setup is shown schematically and photographically in Figure 2 and Figure 3, respectively.

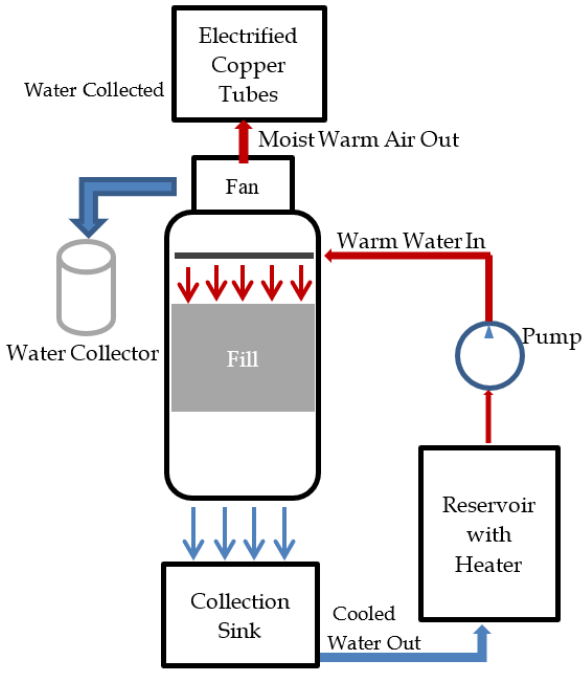

Figure 2: Schematic diagram of the experimental setup

A unique arrangement is built for inducing space charge to the exiting air. This arrangement consists of the following parts.

- A right-angled U-shaped passage tube for turning the flow 180˚ towards gravity. One end of this tube is attached to the exhaust side of the fan while the other end is made such that the exiting air flows through four holes.
- Four cylindrical copper tubes are fixed under these holes with another four smaller tubes inside.
- Electric wiring of copper tubes with D.C. voltage boosters.
- A collector for the condensed water from inside the copper tubes.

Figure 3: Photograph of the experimental setup

A screenshot of the view from the bottom of the water collection system designed in SolidWorks is given in Figure 4. Figure 5 is an image of the actual constructed water collection system. Figure 6 shows a close-up view of the electrified copper tubes, while Figure 7 displays the cross-section of a single pair of copper tubes. The annular space between the inner and outer copper tube is where corona discharge occurs.

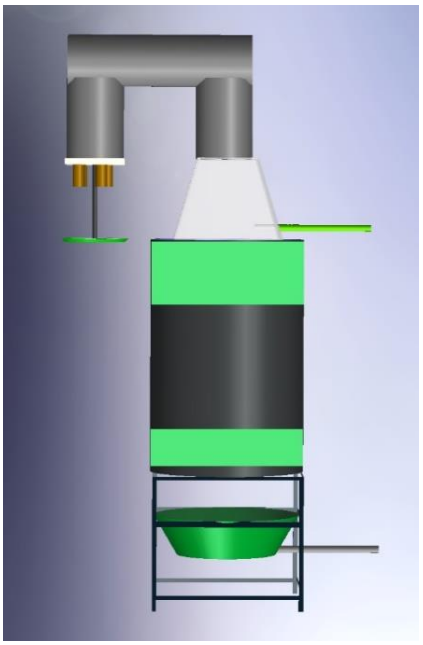

Figure 4: SolidWorks design of water collection system

Figure 5: Photograph of water collection system.

Figure 6: Picture showing spaces inside copper tubes for charge injection

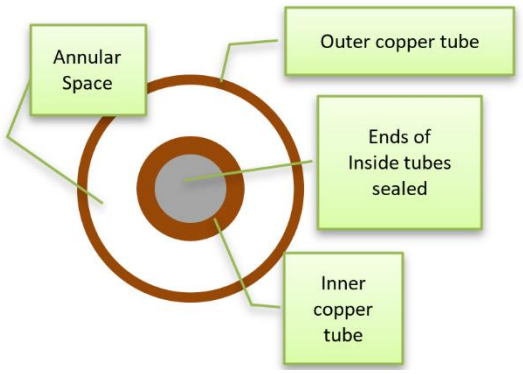

Figure 7: A cross-sectional view of one set of copper tubes

B. Equipment and Parameters

The equipment used in this experiment and their respective specifications are listed in Table 1. The parameters to be monitored and the measuring instrument for each are illustrated in Table 2.

Table 1
Equipment and Specifications

Equipment Used	Specification
Pump	Max head: 40 m Max flow rate: 40 L/min
Induced Draft Fan	Air velocity: 1.5 m/s
Electric Heater	Power: 500 W
High Voltage Generator	Input: DC 3-6V; output: 10kV

Table 2
Monitor parameters and Measurement instruments

Parameters	Measuring Instrument
Inlet dry and wet bulb temperatures (°C)	Alcohol Thermometer
Outlet air temperature (°C)	Alcohol Thermometer
Inlet and outlet water temperatures (°C)	Digital Thermocouple
Air flow velocity (m/s)	Anemometer
Volume of water collected (m3)	Measuring Cylinder

C. Water Collection Mechanism

Sets of two copper tubes of uniform thickness (~1mm) with different diameters are used as the opposing electrodes for space charge injection. 13mm tubes with the ends sealed are placed axially along the centre of hollow 32mm tubes. The plume from the cooling tower outlet is allowed to pass through the space between the copper tubes. The high voltage is generated using D.C. voltage boosters, where each booster is given an input of 3-6 V and produces an output of 7-10 kV. Corona discharge between the copper electrodes is observed at about 7 kV. The electric field produced causes the particles in the air and water mixture passing through the space between the electrodes to become ionized. The ionized water vapor particles deflect inside the field as shown in Figure 8. Upon contact with the surface of the electrodes, the vapor gives off latent heat of vaporization and condenses to liquid water.

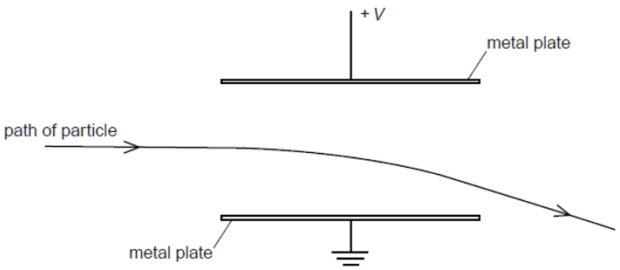

Figure 8: Movement of a particle inside an electric field

D. Experimental Procedure

The experiment is carried out at four different flow rates and using three different inlet warm water temperatures for each. So, 12 cases are developed for this paper based on different pairings of mass flow rate of water and warm water temperature. Cooled water temperature, hot air out temperature, amount of collected water and environmental dry bulb and wet bulb temperatures are read from alcohol thermometers and digital thermocouple with ±1˚C accuracy. The cases are noted in Table 3.

Flow rate of water is controlled using a manually operated flow control valve. Inlet temperature of water was maintained using electric heaters. The U-shaped circular duct with two 90° elbows is used to direct the plume to the copper tubes so that the final output air flows vertically downwards. This was done to facilitate the movement of

condensed water droplets formed in the copper tubes so that air did not flow against them. This can be visualized in Figure 4 and in Figure 7.

Table 3
Tower Operating Parameters

T_1 (˚C)	m_w (kg/s)	T_2 (˚C)	T_{a1} (˚C)	T_{f1} (˚C)	Air (Plume) Temperature at Tower Outlet (˚C)
40	0.047833	37.2	23.5	22.8	26
	0.088467	38.2	24	23.5	27.5
	0.106567	37.9	24	23.5	26.2
	0.1451	38.7	28.9	27.5	32.5
45	0.047833	41.5	29.5	25.5	32
	0.088467	41.9	24	23.5	28
	0.106567	40.9	24	23.5	26.4
	0.1451	42.9	30.1	25.5	33
50	0.047833	45.3	29.5	25.5	32
	0.088467	45.7	24	23.5	28.1
	0.106567	44	24	23.5	26.7
	0.1451	46.8	30.1	25.5	33

4. NOMENCLATURES

a	Approach, °C
C_r	Water Circulation rate
m_l	Air mass flow rate (kg/s)
M_w	Water loss (kg/s)
m_w	Water mass flow rate (kg/s)
T_1	Entering warm water temperature of the tower, °C
T_2	Cold water temperature at the cooling tower outlet, °C
T_{a1}	Inlet air dry bulb temperature, °C
T_d	Temperature difference between hot water in, T_1 and cold air in, T_{a1}, °C
T_{f1}	Wet bulb temperature at tower inlet, °C
V_1	Air specific volume at tower inlet (m^3/kg)
X_2	Humidity ratio at tower outlet (kg water/kg dry air)
X_1	Humidity ratio at tower inlet (kg water/kg dry air)
Z	Cooling range, °C
μ	Cooling coefficient, %

5. METHODOLOGY

The first practical theory and equation set for the performance evaluation of cooling towers developed by Merkel has been widely employed ever since 1925 and is used in Liao *et al.* (2019). However, evaporative water losses are not considered in this model (González Pedraza *et al.*, 2018). This evaporation loss as found by a numerical study conducted on cross flow cooling towers accounts for up to 5.1% of the total inlet water (Bourouni *et al.*, 2008). This percentage is not negligible at all and hence, many models have been proposed to calculate the loss of water by evaporation using the empirical relation of evaporative water loss (Perry & Green, 1997).

$$\text{Evaporation loss} = 0.00085 \times 1.8 \times C_r \times (T_1 - T_2) \quad (3)$$

This study has followed the approach of evaporative water loss equation deduced from the above empirical equation recently by Naik & Muthukumar (2017) that has later been used by Shublaq & Sleiti (2020) and Saber & Maree (2019). For the evaluation of the experimental setup as a regular working IDCF cooling tower, necessary performance parameters of a cooling tower according to (Saber & Maree, 2019, pp. 1-8) are stated below.

The difference in temperature between the hot water entering the tower and the cold water exiting the tower is the cooling range.

$$Z = T_1 - T_2 \quad (4)$$

The difference in temperature of the cold water exiting the tower and the wet bulb temperature of the air is known as the approach.

$$a = T_2 - T_{f1} \quad (5)$$

The cooling coefficient is the efficiency of a cooling tower and is given by

$$\mu = \frac{T_1 - T_2}{T_1 - T_{f1}} \quad (6)$$

Effectiveness of a cooling tower is given by

$$\varepsilon = \frac{T_1 - T_2}{T_1 - T_{a1}} \quad (7)$$

These parameters are plotted versus four different flow rates of water (0.047833 kg/s, 0.088467 kg/s, 0.106567 kg/s, 0.1451 kg/s) with separate curves for each of the warm water temperatures (40˚C, 45˚C and 50˚C).

A certain amount of water is lost due to evaporation in a cooling tower with an open circuit and equals to the amount of makeup water required. This water loss is given by

$$M_w = (X_2 - X_1) \times m_l \quad (8)$$

Mass flow rate of air through the tower is given by

$$m_l = \text{density} \times \text{flow area} \times \text{air speed} \quad (9)$$

Specific density of dry air is measured at the air outlet conditions and air speed is measured at outlet of copper tubes by anemometer.

Liquid Gas Ratio is the ratio of the mass flow rate of water to that of air.

$$\text{L/G ratio} = \frac{m_w}{m_l} \quad (10)$$

Temperature difference between entering warm water and inlet cold air,

$$T_d = T_1 - T_{a1} \quad (11)$$

The percentage of collection, or collection efficiency, is measured with respect to M_w for each of the cases.

$$\text{Collection } \% \;=\; \text{collected water} \times 100 / \, M_w \qquad (12)$$

For understanding the nature of collection efficiency two graphs are shown in the following ways.

i) *Collection %* vs Temperature difference between entering warm water and entering cold air, T_d. The points in the graph are marked for the corresponding *L/G ratios*.
ii) *Collection %* vs *L/G ratio* with separate curves drawn for each of the warm water temperatures.

The electrical energy consumption for each of the 12 cases has been plotted against the corresponding collection efficiencies. Separate curves are drawn for each of the *L/G ratios*.

6. RESULTS AND DISCUSSION

The variation of cooling range with water mass flow rate shown in Figure 9 demonstrates that the cooling range decreases with increasing mass flow rate of water. This is because the amount of heat transfer is dependent on the two mass flow rates. In the case of a large quantity of air that is in contact with a low quantity of water, the result is a larger degree of water cooling. Thus, cooling range is high, but in the case of a larger quantity of water that is in contact with less quantity of air, the result is a lesser degree of water cooling and so cooling range is low. For all cases the cooling range increases with increasing warm water in temperature, T_1 and the best cooling range is obtained for 50˚C at the lowest flow rate (0.047833 kg/s).

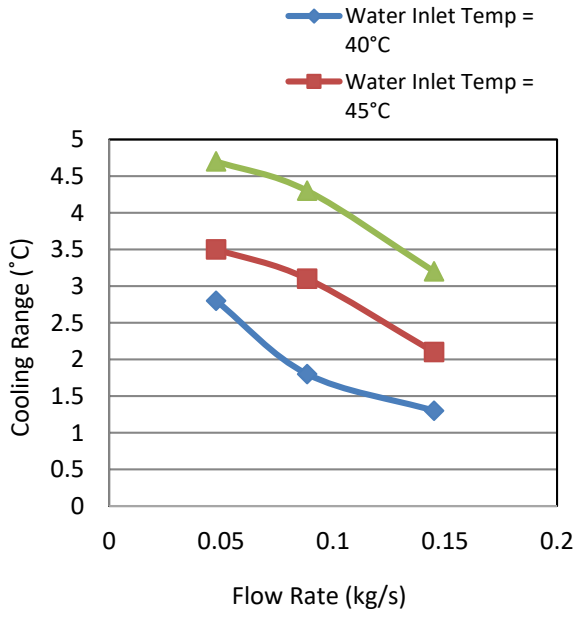

Figure 9: Cooling Range as a function of Flow Rate

Figure 10 illustrates the variation of the approach with water mass flow rate. It shows that the approach is maximum at moderate water flow rates and does not gradually increase with increasing flow rate. A decrease in the corresponding wet bulb temperature reduces the cold-water temperature. The approach increases with increasing warm water temperature and the minimum approach is obtained for 40˚C at the highest flow rate (0.1451 kg/s).

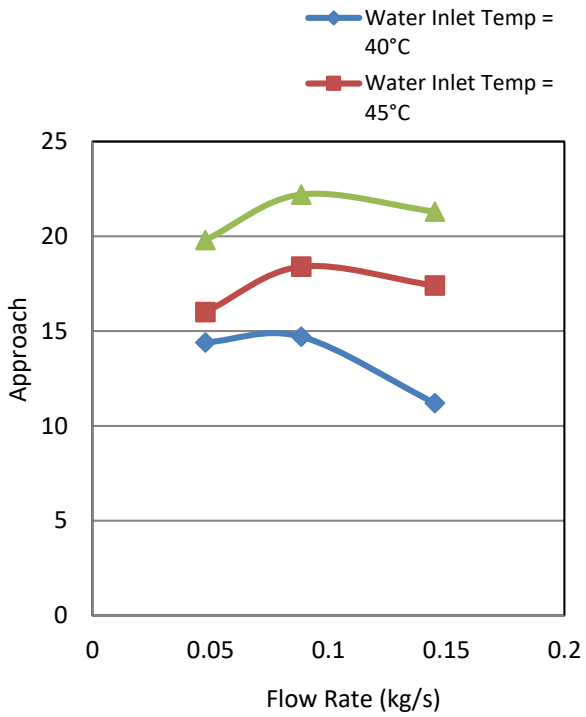

Figure 10: Approach as a function of Flow Rate

The effectiveness decreases with increasing water mass flow rate as shown in Figure 11, and it increases with increasing warm water temperature. The best cooling tower effectiveness is obtained for both 45˚C & 50˚C at the lowest flow rate (0.047833 kg/s).

The cooling coefficient decreases with increasing water mass flow rate as shown in Figure 12. This implies that cooling coefficient is directly proportional to cooling range. Also, the cooling coefficient increases with increasing warm water temperature and the best cooling coefficient is obtained for 50˚C at the lowest flow rate (0.047833 kg/s).

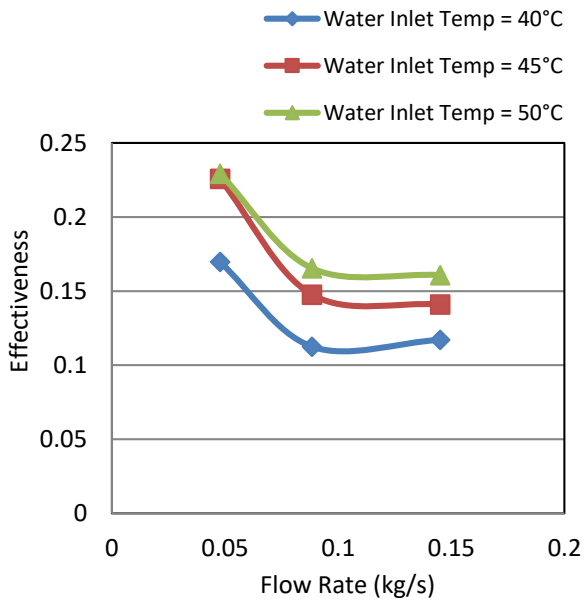

Figure 11: Effectiveness as a function of Flow Rate

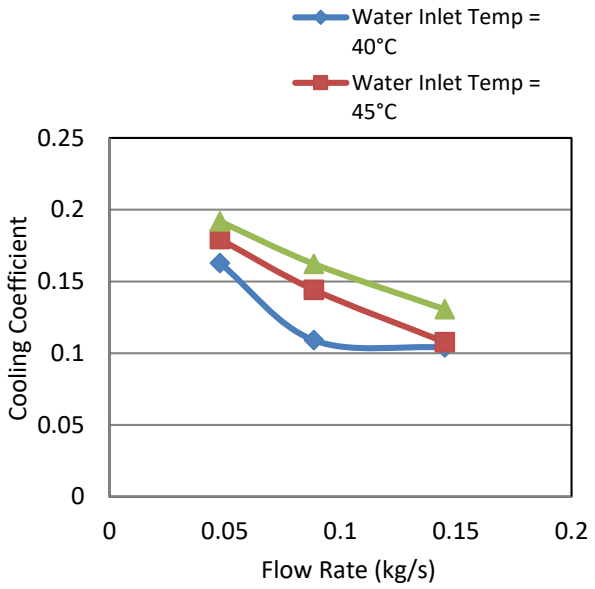

Figure 12: Cooling Coefficient as a function of Flow Rate

The aforementioned figures and their discussion are given to justify our setup as a regular working cooling tower (used mostly in refrigeration and air conditioning sectors). The similarity with the curves from (Saber & Maree, 2019, pp. 1-8) substantiates the validation of the prototype and the addition of a flow-obstructive setup at the outlet of the tower does not affect the relation of cooling effect at any warm water temperatures. The following discussion upholds the distinctive studies from our setup.

The optimum counter flow rates of water and air account for maximum cooling efficiency (cooling coefficient) at definite inlet temperatures. Figure 13 shows that the cooling efficiency decreases with rising value of *L/G ratio*, which is in accordance with Figure 12.

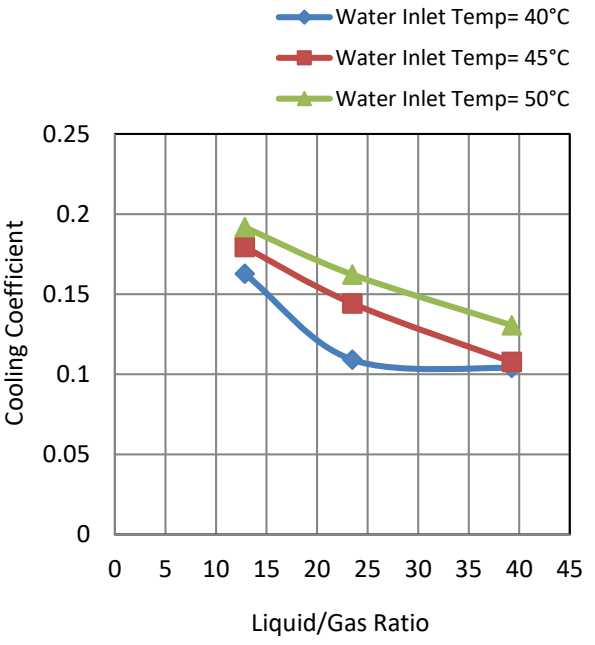

Figure 13: Cooling Coefficient as a function of *L/G ratio*

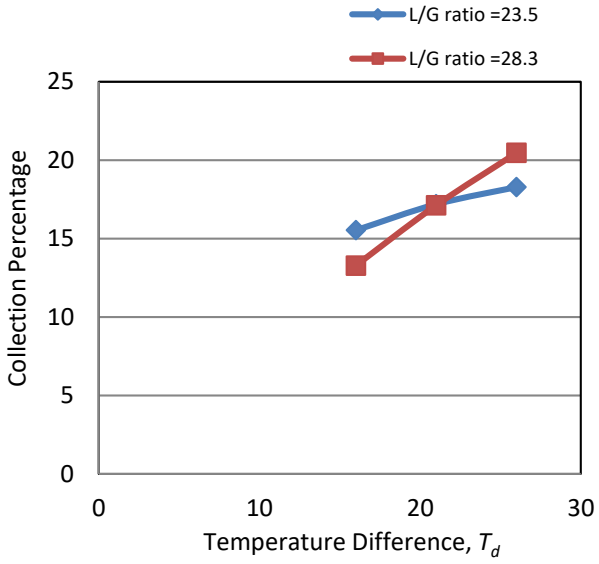

Figure 14: Collection percentage as a function of Temperature difference, T_d for different *L/G ratios*

Figure 14 displays the nature of variation in collection percentages with respect to the temperature difference between the inlet temperatures of the two fluids for two *L/G ratios* (23.5 and 28.3). The curves exemplify a linear relation for these *L/G ratios*.

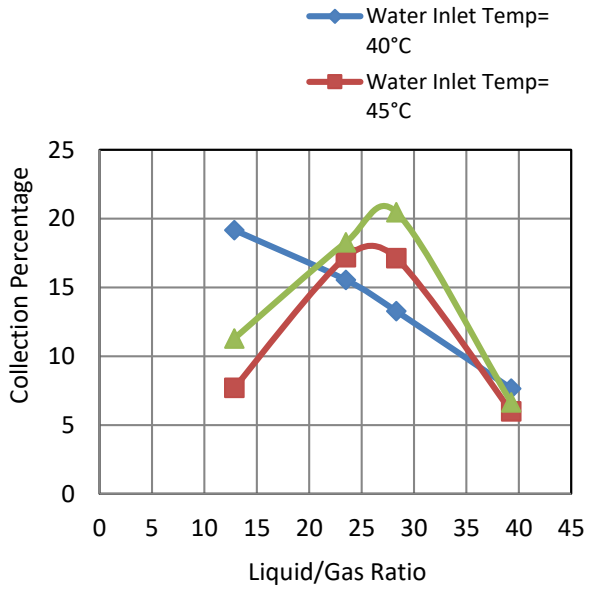

Figure 15: Collection percentage as a function of *L/G ratio.*

Figure 15 illustrates the previously stated fact for the existence of an optimum value of *L/G ratio* which in this case is for maximum collection percentage for any hot water in temperature, T_1. The curves maintain a certain peak value of collection efficiency for higher warm water temperatures, before and after which the value decreases. At the lowest warm temperature, a continuous fall of collection percentage with increasing *L/G ratios* is observed. This could suggest that the peak for this curve is towards the left of the graph. The maximum percentage of collection is observed for *L/G ratio* of 27-28 at hot water inlet temperature of 50˚C.

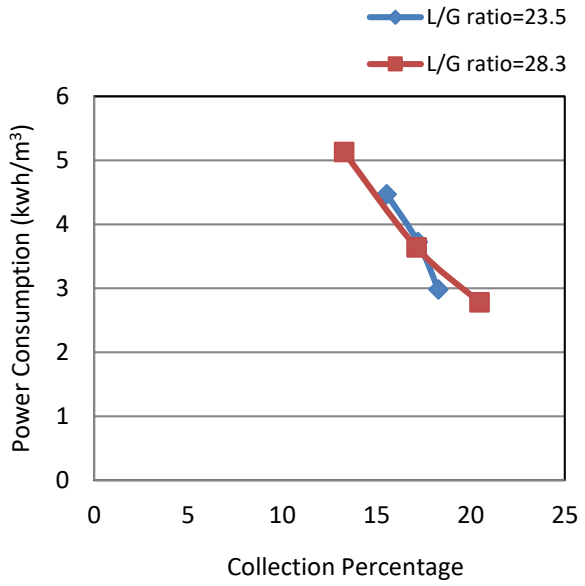

Figure 16: Power consumption as a function of Collection percentage for different *L/G ratios.*

Figure 16 displays the ranges of electricity consumption with respect to the collection efficiency for two *L/G ratios*. The highest electricity consumption is found to be 5.13 kWh/m^3 and the lowest to be 2.78 kWh/m^3. Notably, the lowest power consumption corresponds to the maximum collection percentage (~20%) for the curve of *L/G ratio* 28.3. *L/G ratios* signify the variation of vapor density and so, the trait of the curves varies due to variation in plume density. The maximum collection efficiencies for the two curves consume below 3 kWh/m^3 and offer the possibility of more sets of operating conditions below that. Furthermore, this energy consumption can be minimized significantly for high density plumes that come out of commercial cooling towers.

Figures 14-16 are the original works of this paper which assist in finding out the optimum operating condition required to achieve best collection efficiency of water from the plume keeping the properties of an IDCF tower unhindered. Figure 14 brings out an important fact that the collection efficiencies increase with increasing temperature difference. Additionally, Figure 15 proves that the peak values of collection efficiencies exist at moderate *L/G ratios* (27-28) for the higher warm water temperatures. Figure 16 marks out that *L/G ratios* that are close to these moderate values, being the best operating condition for the tower, can also correspond to a relatively low consumption of power. De-salination plants consume at-least 3 kWh/m^3 (Damak & Varanasi, 2018), and it has been found that more than one cases in our setup consume less than this value.

If optimum conditions for maximum collection efficiency are not prioritized, there are more findings to look for in these figures. Figure 14 indicates that the maximum collection percentage almost corresponds to the maximum temperature difference for higher *L/G ratios*. So, the cooling effect and thus, evaporative loss may be least but only the highest temperature difference, T_d will get back maximum water from the plume coming out of the cooling tower. On the other hand, it is evident from Figure 15 that the collection efficiency for any *L/G ratio* at higher warm water temperatures increases with increasing warm water temperature. Thus, for any fixed *L/G ratio*, these two figures represent a dependency of collection efficiency on two factors, the temperature difference of the inlet fluids and the inlet warm water temperature. This paper evaluates the necessity of finding the relative significance of these two factors on collection efficiency.

Maximum ionization rate ensures highest collection efficiency and depends on exiting velocity, density and temperature of the plume. Plume temperature depends on the heat transfer between water and air, i.e. entering fluid temperatures. At fixed conditions of entering fluid temperatures, a definite value of *L/G ratio* gives out a definite evaporative cooling thus, a definite density of plume as shown in Figure 13. The exiting velocity is constant for all the cases in this study and so, an optimum density must exist for maximum collection efficiency at definite entering fluid temperatures. In most of the cases, Figure 14 shows a subsisting linear relation of collection % with T_d and Figure 15 maintains a bell curve signifying an optimum *L/G ratio* for the peak value. The methods are to be studied on other types and sizes of cooling towers in order to find more relevancy in these findings. Overall, the installation of a duct and tube structure on top of cooling towers instead of the mesh system proposed by MIT (Damak & Varanasi, 2018) unlocked yet another effective way of water collection from the plume expelled by the towers. Based on the results, this new approach of water collection can be successfully implemented in cooling towers.

7. CONCLUSIONS

Any technology that incorporates the generation or saving of usable water in an energy-efficient manner is required for stepping into a sustainable future. The loss of water in cooling towers is what we intend to minimize in order to reduce the harmful effects of plume with a low consumption of electricity. The cooling tower built for this experiment represents an ideal prototype (3:1) of those being utilized in the commercial refrigeration or other industrial sectors. The main conclusive findings of this study are-

1. Introducing a properly designed flow-obstructive structure on top of the tower does not constrain the cooling effect of the tower.
2. The water collection efficiency relies on *L/G ratio* and inlet fluid temperatures in most of the cases. The best collection efficiency is obtained for a condition of warm water entering the tower at 50˚C maintaining a *L/G ratio* of 28.3. This condition is experimented at dry and wet bulb temperatures of 24˚C and 23.5˚C respectively and remarkably uses up the lowest electric energy of about 2.78 kWh/m3.
3. Most importantly, two optimum operating conditions at different sets of entering fluid temperatures are found in this study which consume lower energy compared to the minimum energy used in de-

salination plants (3 kWh/m3) and thus the proposed system can be promisingly eco-friendly as well as cost effective.

8. RECOMMENDATIONS

There is a potential chance of improved collection efficiency with cooling towers of better performance and higher water content in the plume. Designing a curved U-shaped passage instead of 90° bends may offer a lesser hindrance for air flow raising the cooling performance of a cooling tower.

Improved mechanism for air ionization to enhance the collection of water can be studied by

- Varying the space between the electrodes.
- Varying the relative position of electrodes (emitter being held slightly above the collector).
- Varying the overall geometry of copper tubes (spiral, curve, funnel shapes).
- Integrating an edgy, slotted, perforated, wavy, or a combination of designs inside the copper tube
- Using a new metal or alloy instead of copper (aluminium, nickel or alloys)

ACKNOWLEDGEMENTS

This work was supported by the Department of Mechanical Engineering (ME), Military Institute of Science and Technology (MIST), Dhaka, Bangladesh.

REFERENCES

Bourouni, K., Bassem, M. M., & Chaïbi, M. T. (2008). Numerical study of coupled heat and mass transfer in geothermal water cooling tower. *Energy Conversion and Management*, 49(5), 988–994. DOI:10.1016/j.enconman.2007.10.003

Carson, J. E. (1980). The Atmospheric Impacts of Evaporative Cooling Systems. In Atmospheric Pollution 1980: Proceedings of the 14th International Colloquium, UNESCO Building, Paris, France, May 5-8, 1980 (pp. 37–42). Amsterdam, Netherlands: Elsevier Scientific Publishing Company.

Damak, M., & Varanasi, K. K. (2018). Electrostatically driven fog collection using space charge injection. *Science Advances*, 4(6), eaao5323. DOI:10.1126/sciadv.aao5323

González Pedraza, O. J., Pacheco Ibarra, J. J., Rubio-Maya, C., Galván González, S. R., & Rangel Arista, J. A. (2018). Numerical study of the drift and evaporation of water droplets cooled down by a forced stream of air. *Applied Thermal Engineering*, 142, 292–302. DOI:10.1016/j.applthermaleng.2018.07.011

Huff, F. A., Beebe, R. C., Jones, D. M. A., Morgan, G. M., Jr., & Semonin, R. G. (1971). Effect of Cooling Tower Effluents on Atmospheric Conditions in Northeastern Illinois. Source: https://www.ideals.illinois.edu/bitstream/handle/2142/94436/ISWSC-100.pdf?sequence=1

Kraemer, H. F., & Johnstone, H. F. (1955). Collection of Aerosol Particles in Presence of Electrostatic Fields. *Industrial & Engineering Chemistry*, 47(12), 2426–2434. DOI:10.1021/ie50552a020

Liao, J., Xie, X., Nemer, H., Claridge, D. E., & Culp, C. H. (2019). A simplified methodology to optimize the cooling tower approach temperature control schedule in a cooling system. *Energy Conversion and Management*, 199, 111950. DOI:10.1016/j.enconman.2019.111950

Naik, B. K., & Muthukumar, P. (2017). A novel approach for performance assessment of mechanical draft wet cooling towers. *Applied Thermal Engineering*, 121, 14–26. DOI:10.1016/j.applthermaleng.2017.04.042

Novianarenti, E., Setyono, G., & Safitra, A. G. (2019). Experimental Study of The Performance Characteristic an Induced Draft Cooling Tower with Variates Fillings. IOP Conference Series: *Materials Science and Engineering*, 462, 012027. DOI:10.1088/1757-899x/462/1/012027

Parker, K. (2003). Electrical Operation of Electrostatic Precipitators (Energy Engineering). London, United Kingdom: The Institution of Engineering and Technology.

Perry, R. H., & Green, D. W. (1997). *Perry's Chemical Engineer's Handbook* (8th ed.). Kansas, USA: McGraw-Hill Professional Pub.

Reznikov, M. (2003). Dielectrophoretic Dehumidification of Gas Stream in Low and Moderate Electrical Fields. Presented at the ESA-IEEE Joint Meeting of Electrostatics (pp. 230-240), Little Rock, AR, USA.

Reznikov, M. (2014). Electrically Enhanced Condensation I: *Effects of Corona Discharge. IEEE Transactions on Industry Applications*, 51(2), 1137–1145. DOI:10.1109/tia.2014.2354734

Reznikov, M. (2015). Electrically Enhanced Harvesting of Water Vapor from The Air. Presented at the ESA Annual Meeting on Electrostatics.

Saber, H. A., & Maree, I. E. (2019). Experimental study on thermal performance of counter flow wet cooling tower and effect of fins angle. *Anbar Journal of Engineering Science*, 8(1), 1–8. Source: https://www.iasj.net/iasj?func=fulltext&aId=169264

Shublaq, M., & Sleiti, A. K. (2020). Experimental analysis of water evaporation losses in cooling towers using filters. *Applied Thermal Engineering*, 175, 115418. DOI:10.1016/j.applthermaleng.2020.115418

Sundén, A. E. K., Støchkel, K., Panja, S., Kadhane, U., Hvelplund, P., Nielsen, S. B., … Hansen, K. (2009). Heat capacities of freely evaporating charged water clusters. *The Journal of Chemical Physics*, 130(22), 224308. DOI:10.1063/1.3149784

Uchiyama, H., & Jyumonji, M. (1995). Field experiments of an electrostatic fog-liquefier. *Journal of Electrostatics*, 35(1), 133–143. DOI:10.1016/0304-3886(95)00019-7

Veldhuizen, H., & Ledbetter, J. (1971). Cooling Tower Fog: Control and Abatement. *Journal of the Air Pollution Control Association*, 21(1), 21–24. DOI:10.1080/00022470.1971.10469490

Wakil, M. M. E. (1985). *Power Plant Technology* (Rev. ed.). New York, St. Louis, San Francisco: Mc Graw-Hill Book Company.

Williamson, N., Behnia, M., & Armfield, S. (2008). Comparison of a 2D axisymmetric CFD model of a natural draft wet cooling tower and a 1D model. *International Journal of Heat and Mass Transfer*, 51(9–10), 2227–2236. DOI: 10.1016/j.ijheatmasstransfer.2007.11.008

Yu, F. (2005). Modified Kelvin–Thomson equation considering ion-dipole interaction: Comparison with observed ion-clustering enthalpies and entropies. *The Journal of Chemical Physics*, 122(8), 084503. DOI:10.1063/1.1845395

MIJST
MIST International Journal of Science and Technology

Bank-Line Behaviour of the Main Rivers Located Within Sundarbans Using Digital Shoreline Analysis System

Md. Manjurul Anam[1], Abdullah-Al-Jabir[2], and G. M. Jahid Hasan[3*],

Department of Civil Engineering, Military Institute of Science and Technology (MIST), Dhaka, Bangladesh

emails: *[1]anam368027@gmail.com; [2]jishraq@gmail.com; and [*3]jahid@ce.mist.ac.bd*

ARTICLE INFO

Article History:

Received: 20th February 2021
Revised: 05th April 2021
Accepted: 07th April 2021
Published: 27th June 2021

Keywords:

Landsat images
Manual digitization
DSAS
ArcGIS
Bank-line movement
Rivers of Sundarbans

ABSTRACT

Sundarbans, the largest mangrove forest located over the GBM basin, has impacted lives of millions over the years. Standing against various natural disasters, rivers of Sundarbans have undergone major issues such as erosion-accretion of both the banks. The paper deals with a combination of remote sensing and Digital Shoreline Analysis System (DSAS), studying temporal behaviour of bank-lines along the main rivers of Sundarbans for the last three decades. The course of main rivers spanning from southwest Baleswar to west Bengal Bidyadhari within coverage of 10,000 sq. km. has been analyzed in this study. DSAS, the extension tool of ArcGIS, was used for monitoring the rate-of-change from multiple historic bank-line positions extracted from satellite images. Comparison of historic bank-lines between different rivers of Sundarbans was done based on Net Bank-line Movement (NBM) with an interval of five years. Finally, the results were presented graphically to get a better understanding of the bank-line behaviour. The study revealed that the western region of mangrove prevails eroding behaviour than the eastern region. Increased rates of riverward movement due to accretion was found from 2008-2013. These results are important for future monitoring and proper management within the coastal communities surrounding the mangrove forest.

1. INTRODUCTION

Bengal delta, extending offshore ward in the Bay of Bengal as a clinoform (sloping depositional surface) was formed during the last 11,000 years within the Bengal basin (Mikhailov and Dotsenko, 2007; Kuehl et al., 2005). With years of climate change, degrading of coastal areas will endanger lives to millions and coastal infrastructures. Such a situation can be more appalling for low-lying deltaic regions like Bangladesh which are less organized to cope-up with the risks related to climate change issues (Kanwal et al., 2019). The south-west coastal zone of Bangladesh which represents the largest mangrove forest, Sundarbans, which is ecologically fragile and climatically vulnerable, serves home to 4.5 million people. Such mangrove forest contributes to a variety of ecosystem services proved to be advantageous for the protection of shorelines from erosion caused by storms and waves and accelerating sediment accretions (Sathirathai and Barbier, 2001). Their exceptional root system with physical roughness helps in capturing and storing valuable quantities of sediment both from highland as well as oceanic origin (Rahman et al., 2011). Above all, mangrove morphology and sedimentation indicate the interaction between sea-level changes, sediment entrapment, and coastal processes (Souza Filho et al., 2006; McIvor et al., 2013; Gilman et al., 2007 etc).

Landforms within active coastal areas are dynamic in nature (Sheik and Chandrasekar, 2011). They are uninterruptedly modified by natural and man-made processes causing streams of Sundarbans to be threatened. Areas of Sundarbans are categorized by stream channels and creeks of changing widths, from a few meters to several kilometers (Sahana and Sajjad, 2019). Almost 85% of people living in Sundarbans are dependent on agriculture. Erosion-accretion can augment challenges to coastal habitats (e.g., Katz and Mushkin, 2013; Collins and Sitar, 2008; Moore and Griggs, 2002; Benumof et al., 2000; etc.) as well as river systems. Therefore, it is important to understand the extent of land- and river-ward retreat of riverbanks at different timescales (Katz and Mushkin, 2013; Esteves et al., 2011).

Application of Digital Shoreline Analysis System (DSAS) is one of the feasible tools which can be used in the analysis of changes over historical timescales. The DSAS

is an extension to ArcMap and is famous to generate measurements of transects either automatically or manually. These transects based on user-specified parameters develop metadata for calculating rates of changes and providing other useful statistical information (Thieler et al., 2009). Generally, DSAS is widely used in studying shoreline dynamics of coastal areas i.e., coasts of India, Italy, Turkey, USA, Vietnam etc (Hegde and Akshaya, 2015; Moussaid et al., 2015 etc). Since DSAS is effective for calculating changing rates incorporating an evidently identified attribute position at different times (Sheik and Chandrasekar, 2011; Cohen and Lara, 2003), it is capable to present the overall scenario with a better understanding of the trends and dynamics of river bank-lines as well. However, utilizing DSAS methodology, which is generally used for delineating shorelines, an initiative was taken in this study to investigate the changing trend of river bank-lines along the main rivers of the Sundarbans. According to the author's knowledge, so far, no study has been conducted to monitor the dynamics of river bank-lines using DSAS tool. It is anticipated that this advanced technique of GIS-based tool would represent an overall scenario of the landform conditions along the mangrove delta for an effective coastal zone management strategy against effects of sea-level rise and other effects due to changing climates.

2. STUDY AREA

The study area emphasizes the changing trends of bank-lines of eight main rivers located within Sundarbans namely - Baleswar, Pussur, Shibsa, Arpangasia, Bara Pangga, Harinbhanga, Raimangal, Bidyadhari (rivers are displayed in Figure 1). Among the rivers, the Bidyadhari River is located within the Indian part of Sundarbans whereas the remaining seven rivers exist in the Bangladesh part. Starting from the western part of Sundarbans, the Harinbhanga River falls along the India-Bangladesh border. Adjacent to this River, the Raimangal River is situated occupying the South 24 Parganas district of India along with the Satkhira District of Bangladesh. About 220 km southwest of Dhaka, the Arpangasia River is in the province of Khulna originated after the Kholpetua River. Bara Pangga River, the smallest River within the study area, lies at the end of the Arpangasia River. The other main important rivers are the Shibsa and Pussur River. The Shibsa River is about 100 km long and located within Khulna region. Inside the Sundarbans mangrove forest, the Shibsa River meets the Pussur River, and then split up again near Mongla, before merging the Bay of Bengal. Approaching towards the Bay of Bengal, at the downstream region lays the Hiron point tide station. Being distributaries of the Ganges, the Pussur River lies at the eastern part of Sundarbans right next to Baleswar River. The Baleswar River forms within part of the Bagerhat and Barguna District. Among all the above discussed rivers in the Bangladesh part, Baleswar, Pussur, Shibsa and Arpangasia are approximately 100 km long. Figure 1 depicts all the rivers located within the mangrove forest.

3. MATERIALS AND METHODS

A. Collection of Satellite Images

NASA initiated the Landsat program for the first time in early 1970 due to a lack of appreciation of terrain data. Within a decade, Landsat 1-3 were launched though they were not applicable for precise studies mainly because of poor resolution. Landsat 4 was launched in 1982 which was collecting data until 1993. Landsat 5 was launched in 1984 which delivered earth imaging data for nearly twenty-nine years and finally decommissioned in 2013. Landsat 7 was launched in 1999 and in late 2020 Landsat 7 was replaced by Landsat 9.

The basic data used in this study were based on Landsat images freely available for research purposes. The images provide information within the resolution of 30 m x 30 m, any object less than this scale remains undetectable. Images of the short-wave infrared band were selected for this study. Hence, band 5 of Landsat 4-5 (1.55-1.75 μm) (for the years - 1989, 1993, 1998); Landsat 7 (1.55-1.75 μm) (for the years - 2003, 2008); and Landsat 8 (0.85-0.88 μm) (for the years - 2013, 2018) were used for separating land and water interfaces. Thematic Mapper (TM) of Landsat 4-5 and Enhanced Thematic Mapper Plus (ETM+) of Landsat 7 are widely used datasets for land surface and water mapping (Masocha et al., 2018). Besides, Landsat 8 is equipped with Operational Land Imager (OLI) sensor which has the potential to extract land surface and water information (Wenbo et al., 2013). Many previous studies have observed the performance of water indices using Landsat 8 OLI sensor (Wenbo et al., 2013; Ji et al., 2015). All the Landsat images required for this study were collected from the United States Geological Survey web domain (http:// earthexplorer.usgs.gov).

B. Categorization of Images

Images with lesser cloud cover and clear visibility were selected during the initial screening process. Dry season images were preferred from November to March. For each year, two scenes (path/row – 137/45 and 138/45) of Landsat images were used to capture the entire Sundarbans as can be seen from Figure 1. Changes of river bank-lines in every year interval are not that effective as the changes are minor and not detectable for 30 m resolution image, for which images were taken at an interval of 5 years. Another interval i.e., 4 years also considered due to the unavailability of good quality images for a particular year.

C. Sorting of Images

As large tidal ranges are observed in the Bay of Bengal (Murty and Henry, 1983), it is required to ensure that the satellite images collected for a particular year represent almost identical tidal water level conditions for other year images. Unless all the collected images correspond to similar tidal conditions (i.e., all images acquired during either high tide or low tide), river bank-line change detection will be largely inaccurate since the rivers are located near the estuary mouth with a flat slope. With a view of avoiding such error, the tidal water levels of all the collected images were checked by noting the image acquisition date and time, and tidal water level records collected by the Bangladesh Inland Water Transport Authority (BIWTA) at that time. High tide condition was considered as the reference and collected images showing good agreement in terms of tidal water level condition.

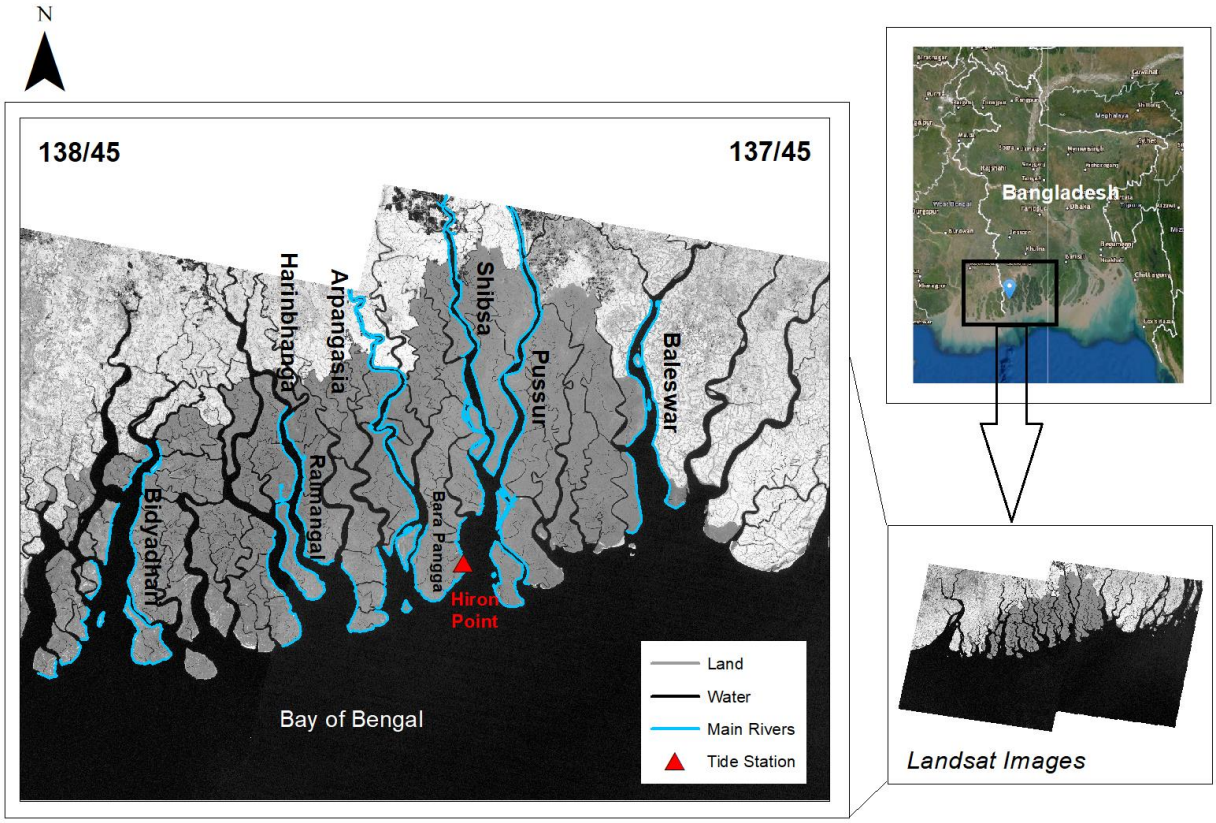

Figure 1: Main Rivers located within the Sundarbans where blue colour indicates riverbanks; black and grey colour indicates water and land area. Solid triangle indicates tide station

Table 1
Tidal water levels during the image acquisition date and times

Timeline	Path-Row	Landsat No	Acquisition Date	Acquisition Time GMT	Tide Level (m)	Tidal Condition	Reference Station
1989	137-45	5	2/21/1989	3:54 AM	2.1	High Tide	Hiron Pont
	138-45	4	1/19/1989	4:03 AM	1.8		
1993	137-45	5	11/12/1992	3:46 AM	2.5		
	138-45	5	1/22/1993	3:52 AM	1.9		
1998	137-45	5	2/14/1998	4:01 AM	1.5		
	138-45	5	3/9/1998	4:07 AM	1.9		
2003	137-45	7	1/19/2003	4:13 AM	2.3		
	138-45	7	11/23/2002	4:19 AM	2.0		
2008	137-45	5	11/24/2008	4:08 AM	2.2		
	138-45	7	12/25/2008	4:20 AM	2.3		
2013	137-45	7	2/15/2013	4:21 AM	1.5		
	138-45	7	2/22/2013	4:27 AM	1.8		
2018	137-45	8	1/20/2018	4:24 AM	1.6		
	138-45	8	2/28/2018	4:30 AM	2.5		

Images with low tide condition were discarded and replaced with new suitable satellite images of different periods. To accomplish this, a wide-ranging search of the USGS Earth Explorer interface was conducted for November to March whenever deemed necessary. This was done due to cloud-free and tide-synchronous images during dry months are not always available. Table 1 shows the tidal water level checks performed covering the study periods along with the Landsat numbers. Tide gauge station located at Hiron Point (operated by the BIWTA) was used to perform the water level checks. The location of the station is shown in Figure 1. Tidal water level check is done for both the scenes of Landsat (Path-Row: 137-45 and 138- 45). Thus, from 1989 to 2018, a total of 14 images were finally selected for analysis.

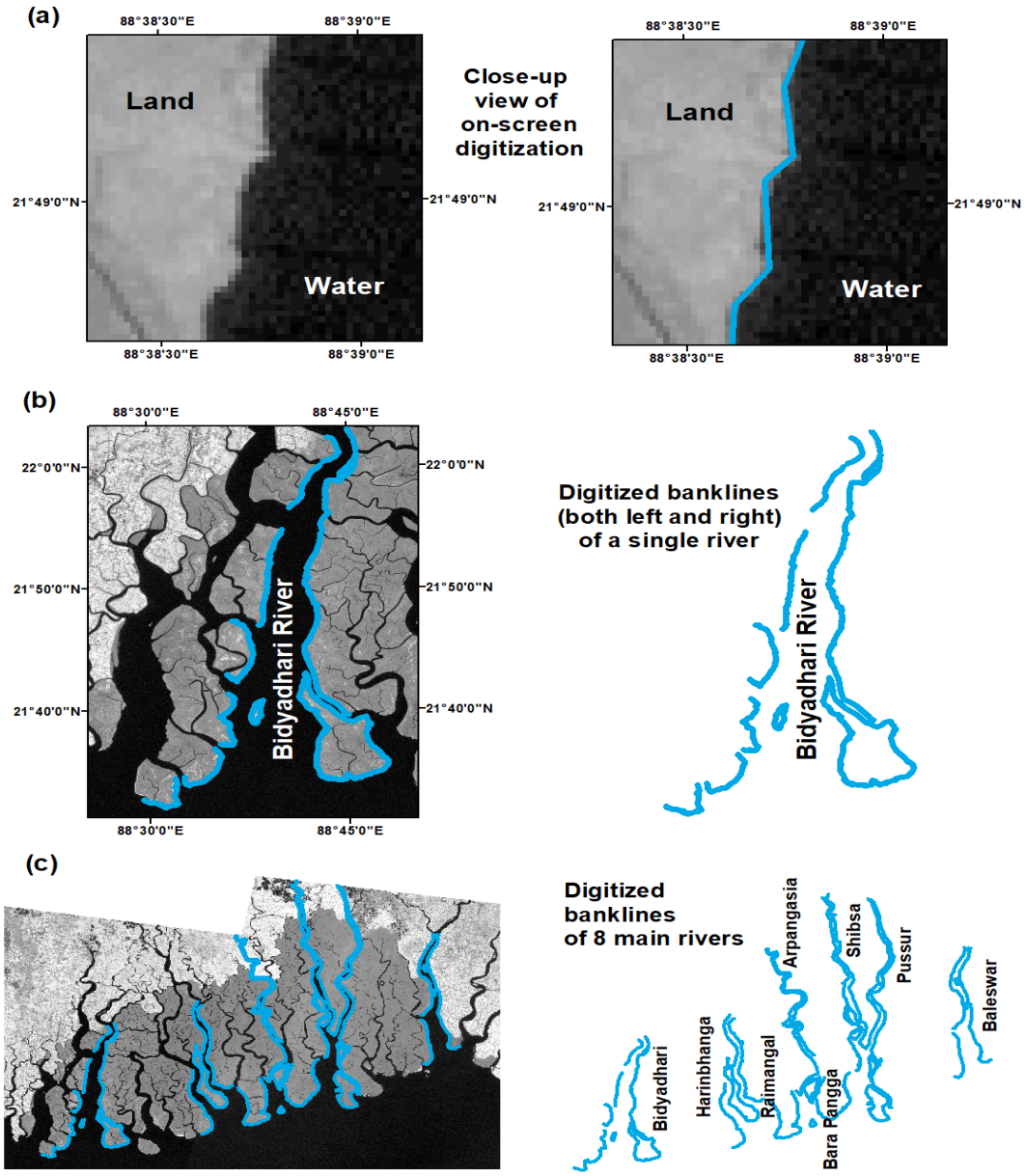

Figure 2: Manual digitization of riverbanks: (a) separation of land and water body by manual on-screen digitization, (b) digitized bank-lines of a sample river extracting from raw satellite image, and (c) digitized bank-lines of all the study rivers within Sundarbans

D. Digitization of River bank-Lines

Bank-lines can be delineated using several methods i.e., manual digitization, band rationing, density slicing, fuzzy-based classification, etc. Besides, there are several ways to digitize i.e., digitizing on-screen over an image, digitizing a hard copy of a map on a digitizing board, or using automated digitization by converting an image into different indexes. However manual digitization is one of the most common methods used for land-water boundary identification. Many previous studies performed using this method (Matin and Hasan, 2021; Nabi et al., 2016; Sarkar et al., 2012 etc). Practically, the manual digitization method seemed to be time-consuming and boring and may not highly effective when a huge number of images need to be analysed, but still proven to be the most accurate method. Since for this study the number of images is not huge, the manual digitization method was considered for bank-line delineation.

Images of selected bands (i.e., short wave infrared band) exhibit strong reflectance by soil and vegetation, and absorbance by water (i.e., Frazier and Page 2000; Kuleli 2010 etc) are used in this study. The river bank-lines of the main rivers of Sundarbans were digitized using on-screen manual method and explained pictorially in Figure 2. Marking the land-water boundary with proper utilization of polyline features of ArcGIS, complete digitization of the riverbanks (both left and right) was performed for all the year images. A total of 16 bank-lines were manually digitized for a single year Landsat scene. Shapefiles of riverbanks were generated with a projected coordinate system of WGS_1984_UTM_Zone_46N. A similar approach of image collection, sorting and digitization was used by Matin and Hasan (2021) for their study covering the entire coastline of Bangladesh.

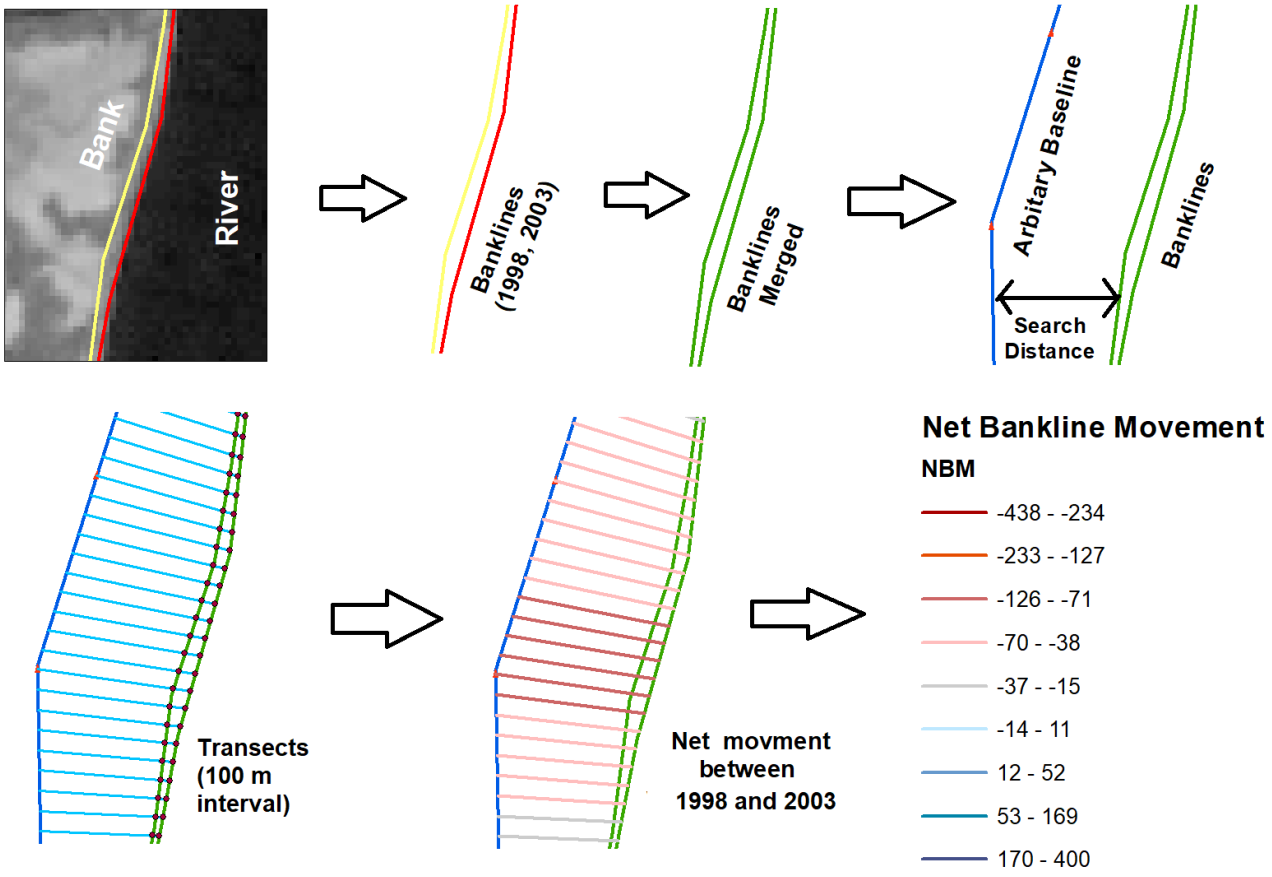

Figure 3: Digital Shoreline Analysis System (DSAS) utilized to determine the net movement between the bank-lines of 1998 and 2003

E. Bank-Lines Interpretation Using DSAS

DSAS enables a user to calculate statistics of rate-of-change from multiple historical bank-line positions. Generally, two versions of DSAS are available: the DSAS extension of the Environmental System Research Institute (ESRI)'s ArcGIS software and the web version of DSAS (Thieler et al., 2009). The web-based version was adopted in this study because of its faster performance. Records from previous shoreline studies carried out along the coastline showed successful application of DSAS i.e., Ellison and Zouh (2012) - Douala estuary, Cameroon; Appeaning Addo et al. (2008) - Accra, Ghana; Natesan et al. (2013) - Vedaranyam coast, Tamil Nadu; Kuleli (2010) - Mediterranean coast, Turkey; Hapke et al. (2009) - California coast, USA; To and Thao (2008) – Nam Dinh coast, Vietnam; Nguyen et al. (2015) - Kien Giang coast etc. However, none of them were observed to apply DSAS for analysing river bank-lines.

For using DSAS, firstly a baseline has to be considered along a river channel in such a way that the baseline should be almost perpendicular to the bank-line. The baseline acts as a reference line parallel to a bank-line, with respect to which the DSAS calculates the movement of different bank-lines. The DSAS requires the position of land and water body to be ascertained along the baseline for determining the movement of the bank-lines. The application of DSAS casts transects which intersect each bank-line to create a measurement point, and these measurement points calculate the changing rates of river bank-lines.

The DSAS was applied to the extracted bank-lines of the rivers of Sundarbans and explained in Figure 3. Transects shown in the figure represent the bank-line movement between two years via color ramps which are categorized into different ranges. All transects change into different colors according to the range or linear distance that the position of the bank-line changes on that location. Each transect represents the value of total bank-line movement of the location in which the transect is present. The positive values indicate accretion that is, riverward movement of the bank-lines. On the other hand, the negative values indicate erosion which is the landward movement of the bank-lines. The maximum distance between the baseline and the bank-line was set as 650 m (using trial and error, depending on the distance between the baseline and bank-line) and the distance between each transect was set to be 100 m. Finally, net bank-line movement (NBM) was calculated running the statistical option of the DSAS tool named Net Shoreline Movement (NSM). Net bank-line movement estimates the distance between the first and the last bank-lines. The rate of bank-line movement for both left and right banks was then analyzed graphically and as a sample movement of two rivers is displayed in Figure 4 and 5.

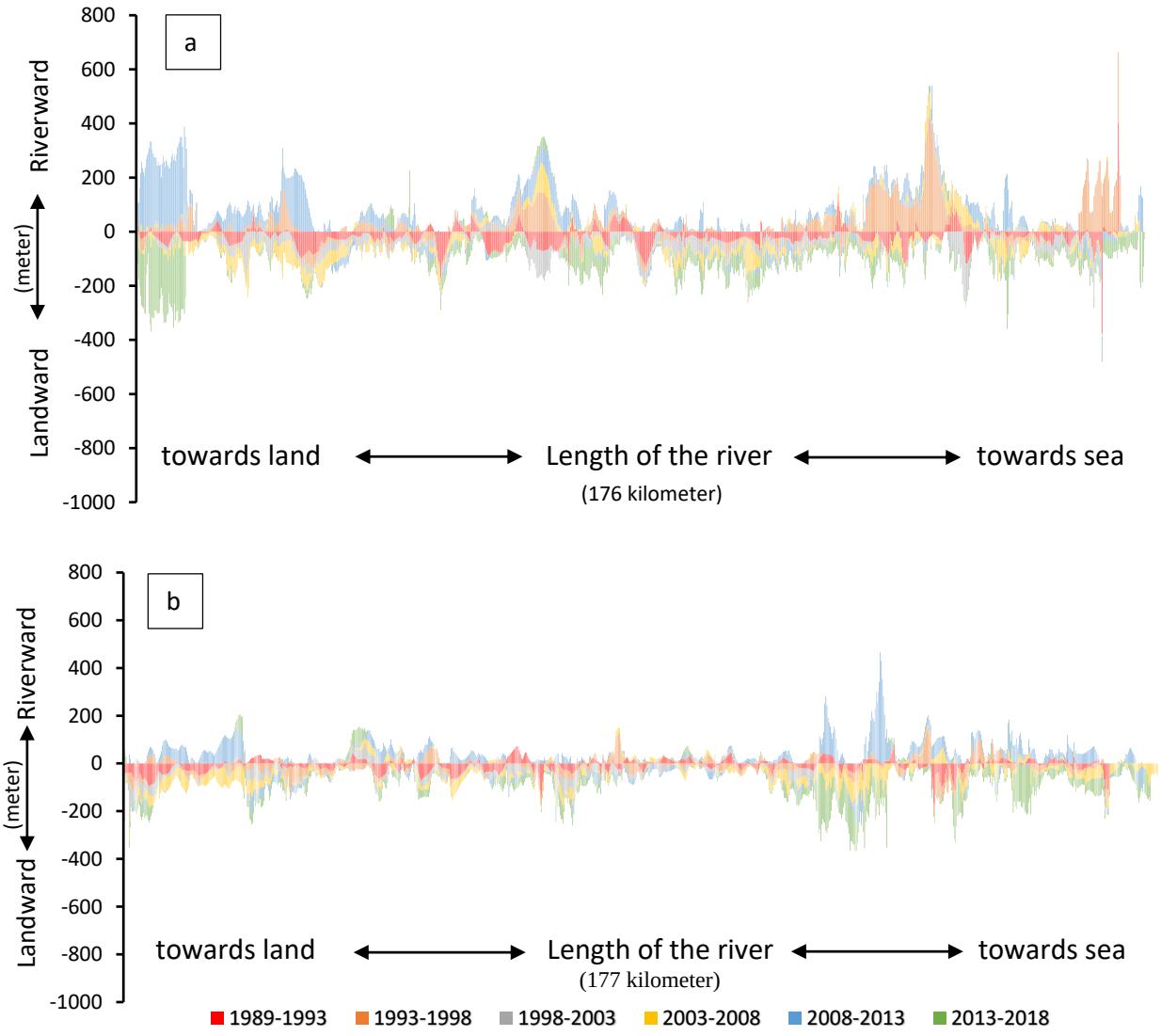

Figure 4: Graphical representation of net bank-line movement (a) left bank and (b) right bank of Pussur River from 1989 to 2018 utilizing NBM (Net Bank-line Movement) of DSAS toolbar in which negative values indicate erosion or landward movement and positive values for accretion or riverward movement

4. RESULTS AND DISCUSSION

The estimated net bank-line movement of the Pussur River is shown in Figure 4. From the figure, it can be observed that most of the regions of the left bank maintained a movement within 100 m (Figure 4a) during 1989-2018. During 1993-1998, a maximum riverward movement of more than 400 m is observed at a few locations. From 2008-2013, a portion in the upstream is faced riverward movement of more than 300 m which became totally opposite during 2013-2018. The highest amount of change that occurred to the right bank is around 500 m during 2008-2013 (Figure 4b). For the rest of the study periods, the movement remained almost identical except few locations during the 1990s.

Whereas the Arpangasia River (Figure 5) maintained a landward movement not greater than 50 m for almost all the locations during 1989-1993. From 1993-1998, the bank-line showed similar characteristics in most of the locations. Riverward movement is dominating than landward during 1989-1993. The density of bank-line movement is more with less intensity from 1989-2003 compared to the movements from 2003-2018 during which change is observed to occur in few locations but with large magnitude (Figure 5). Continuous and random movement of the bank-lines is observed for the right bank of Arpangasia River during the whole study period. During each interval, gentle movement of either landward or riverward is found. Figure 5b shows that the locations have undergone riverward movement during 1989-1993 which changes towards landward during the next 5 years which again became opposite for the next interval.

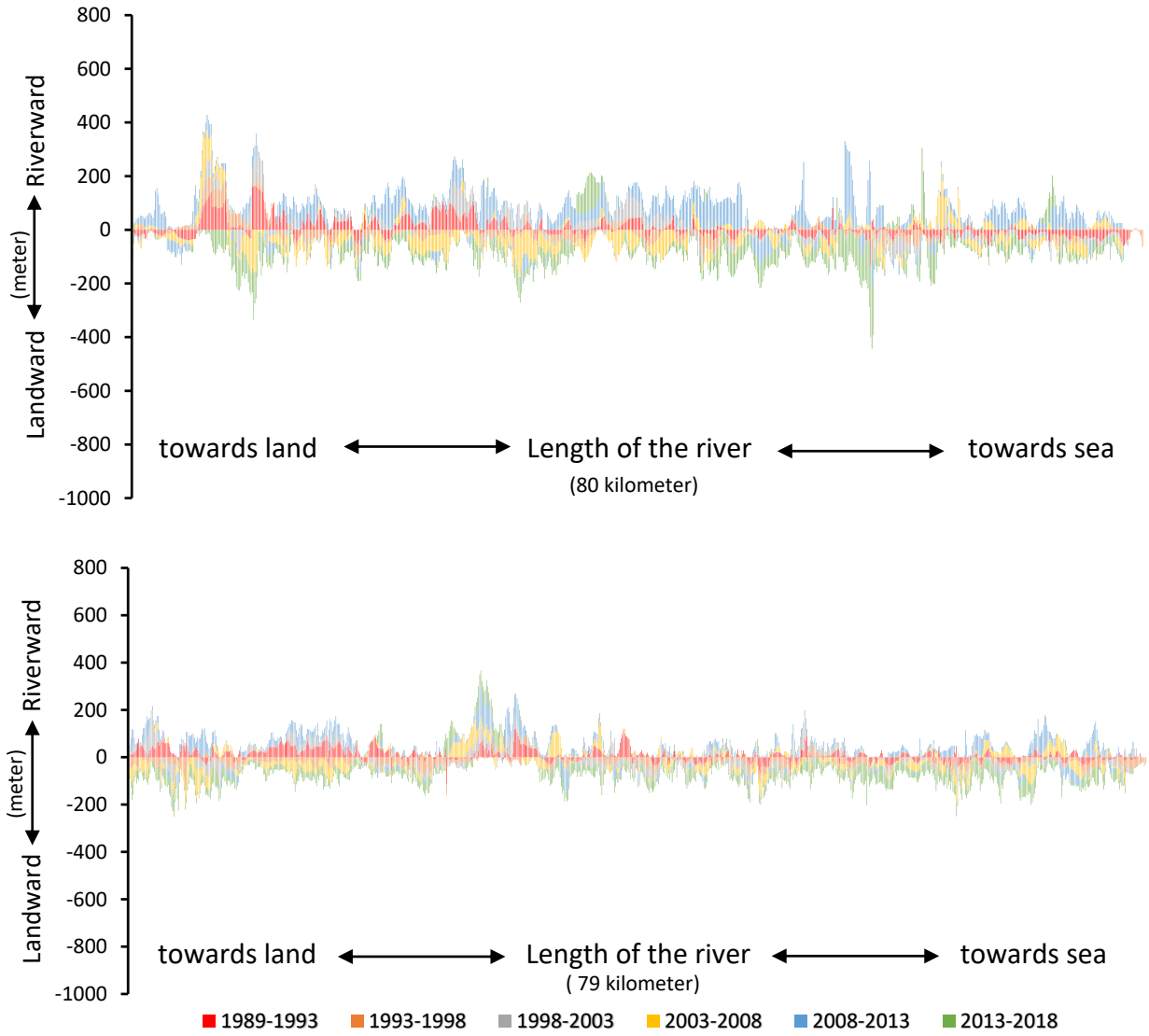

Figure 5: Graphical representation of net bank-line movement of left bank (upper panel) and right bank (lower panel) of Arpangasia River from 1989 to 2018 utilizing NSM (Net Shoreline Movement) of DSAS toolbar in which negative values indicate landward movement or erosion and positive values for riverward movement or accretion

Net bank-line movements are scrutinized more in the right bank than left banks of the Baleswar River from 1989 to 2018. Bank-lines shifting towards land are considered as land loss or erosion and towards river or water is considered as land gain or accretion. The highest riverward movement on the right bank is observed over 500 m whereas on the left bank observed 400 m. The highest landward movement marked about 600 m in left bank whereas in right bank observed about 400 m. Figure 6 illustrates the net bank-line movement of the Baleswar River from 1989 to 2018.

The banks of the Shibsa River had undergone random movement in almost all the locations along the channel length. Both the banks show non-sequential and non-uniform movements with similar characteristics during the study period (Figure 6). Though the riverbanks went through large changes for the whole period, they had undergone most alterations between 2008 and 2013.

The left bank of the Bidyadhari River has undergone continuous landward and riverward movement along the channel. Along most of the locations, the movement is observed to be less than 200 m which stands both for landward and riverward. But the bank-line severely changed near the coast where the Bay of Bengal lies. Particularly from 1993-1998 (Figure 6), the bank-line near the coast faced a large amount of riverward movement where a change of more than 400 m is observed. During the period 2013-2018, a riverward movement of more than 800 m occurred near the coast. But the observation has shown very little change along the entire channel during 2008-2013. The picture shows that the right bank of the river changed its position both landward and riverward for around 500 m in some regions during 1993-1998. Unlike the left bank of the river, the entire right bank went through random movement of its bank-line.

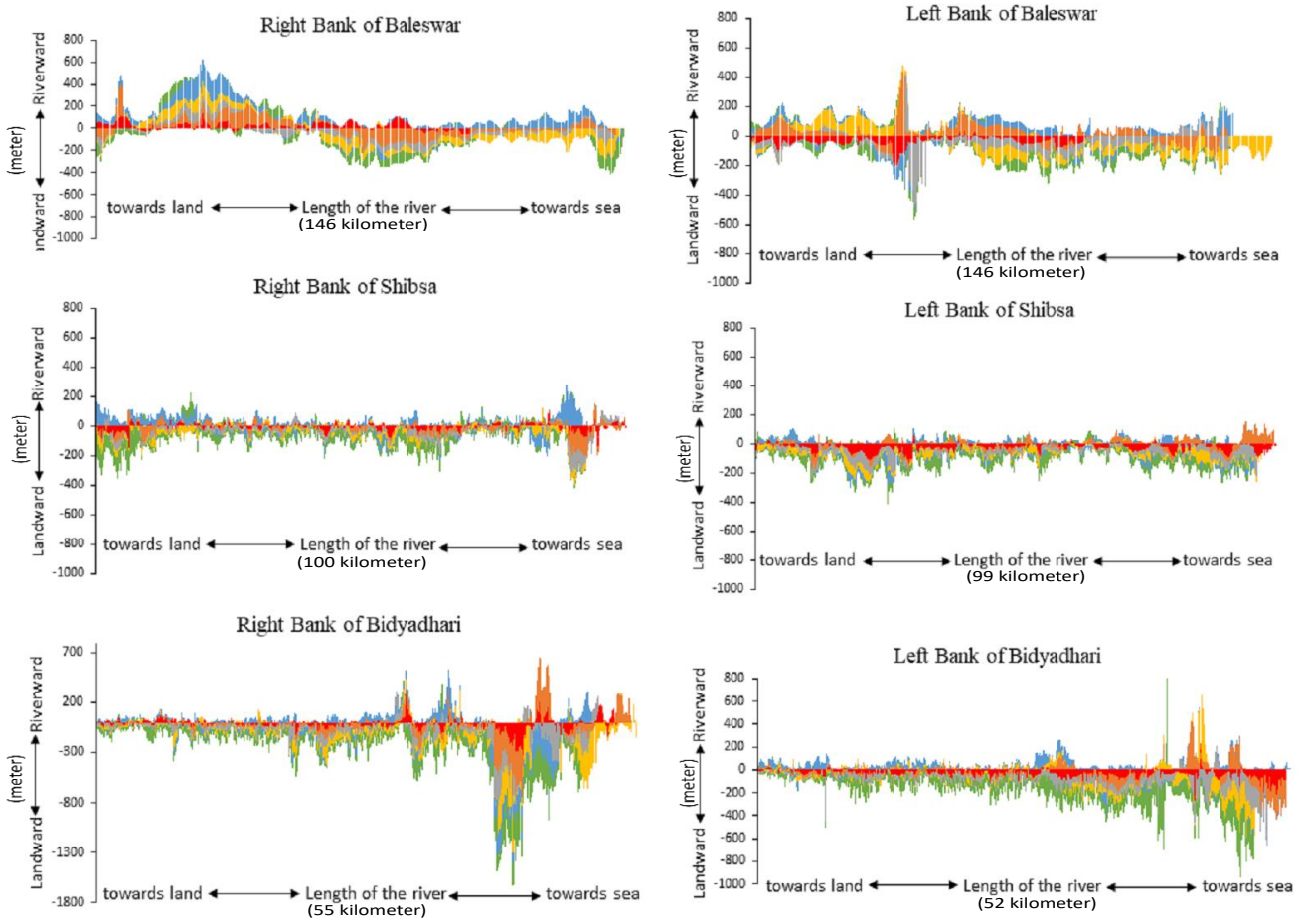

Figure 6: Graphical representation of net bank-line movement of Baleswar, Shibsa and Bidyadhari Rivers

The Bara Pangga River is a small river that absorbs the direct impact of the sea waves unlike other rivers whose coastal part goes through the force rather than the upstream part. As a result, both banks of the river underwent diverse alterations in every interval of the study period. Figure 7 shows that the riverbanks have mostly undergone landward movement. The riverward movement is observed to be much lesser compared to landward.

The left bank of the Harinbhanga River had a maximum landward movement near about 300 m and a maximum riverward movement, slightly more than 200 m. Though the maximum bank-line change is found near the coast, the left bank of the river underwent random changes for almost every location in each interval of the observation period. Figure 7 represents the random landward and riverward shifting of the riverbank along the channel. The graph shows that the right bank has undergone main changes along the bank-line near the coast i.e., at the downstream of the channel or the river mouth. During the year 1989-2003, the right bank maintained a balanced movement along the river which is found to be less than 100 m until reaches the coast. The bank-line showed almost a similar pattern during 2003-2018.

Except for very few locations, the landward and riverward movement is found to be almost identical to the River Raimangal. The left bank endures with a maximum riverward displacement of 310 m during 2008-2013 which is the highest for the bank-line considering the whole study period (Figure 7). The right bank of the Raimangal River resembled similar characteristics of the left bank. Being closer to the Bay of Bengal, the Raimangal River is found to experience continuous and random bank-line deformation during the study period along both the left bank and right bank.

Overall, the study highlights the highest average landward and riverward movement occurred to be within 120 m/year and 85 m/year respectively along the bank-lines for the rivers of Sundarbans. This indicates that the eroding rates are high among the rivers. Analysis reveals that the highest bank-line movement is less than 100 m/year observed more often in rivers like Shibsa, Arpangasia and Raimangal whereas Baleswar, Pussur, Bara Pangga and Harinbhanga within 150 m/year. Bidyadhari shows the highest rate of bank-line movement which is 320 m/year along the right bank. Increased rates of erosion at the downstream region could be one of the reasons for such a high rate. Even though other research also focused on monitoring shoreline change especially along the coast of Bangladesh using remotely sensed data (Khan and Hussain, 2018) or based on a combination of DSAS and remote sensing (Sarwar and Woodroffe, 2013), this is the first study using the application of DSAS for bank-line analysis along the main channels within the mangrove forest Sundarbans so far to the author's knowledge.

According to Brammer (2014), local small erosion has been observed along the south-western coastal region of Bangladesh. The rates are much less than the erosion rate of 200 m/year as reported by Vidal (2013) in the Sundarbans area which shows the quite similar result with respect to the present study except for the Bidyadhari River. Besides a geo-spatial approach based on the influence of erosion-accretion in Sundarbans concedes that Bulcherry and Dalhousi islands of Bidyadhari River were subjected to erosion since 1975. Uninhabited regions within the mangrove forest are more affected by erosion while most of the accretion occurred within the inhabited regions in the eastern part of the Sundarbans region (Sahana and Sajjad, 2019).

The aim of this study is to check the dynamic nature of river bank-lines using DSAS tool using the delineated bank-lines. This study successfully captured the scenarios of river- and land-ward movement of river bank-lines within a timescale of three decades. The obtained results are difficult to compare with other studies as no similar study was found covering the Sundarbans region.

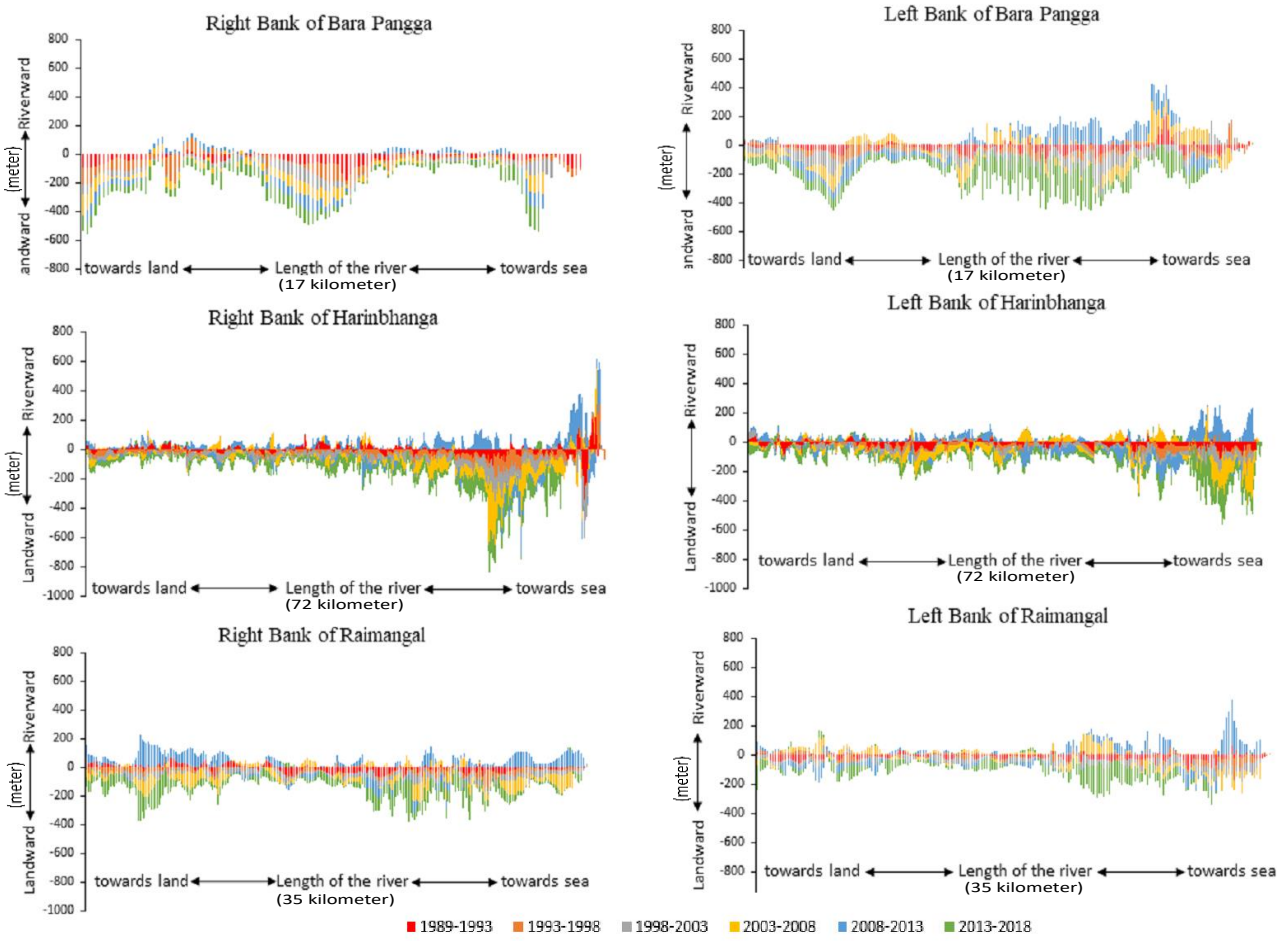

Figure 7: Graphical representation of net bank line movement of Bara Pangga, Harinbhanga and Raimangal Rivers

5. CONCLUSIONS

The present study has shown that the DSAS tool of GIS successfully extracted valuable information on the dynamics of river bank-lines in terms of landward and riverward retreats. Even though wide applications of DSAS have been observed for delineating shorelines especially, this is possibly the first study using DSAS for purpose of bank-line analysis. Results interpret that from 2013 to 2018 rates of erosion has dominated more compared to few other analyses. At the downstream of the rivers (proximity to coast) rates of erosion have increased rapidly during this period, especially near the open coast. From 2008 to 2013 rates of accretion dominated at a high amount all over the rivers compared to the next five years. Before the year 2000's rates of erosion-accretion were comparatively much less than after the year 2000. Sundarbans on the Indian side is eroding at a higher rate compared to the Bangladesh side.

This study furthermore can be helpful for future research works, although the findings are limited within high-resolution satellite images which would help to obtain results more precisely.

ACKNOWLEDGEMENTS

The authors would like to express their gratitude to the Department of Civil Engineering, Military Institute of Science and Technology (MIST), Dhaka, Bangladesh. The authors are also thankful to the editors and anonymous reviewers for providing insightful suggestions and comments to improve the manuscript.

REFERENCES

Appeaning Addo, K., Walkden, M., and Mills, J. P. (2008). 'Detection, measurement and prediction of shoreline recession in Accra, Ghana', *International Society for Photogrammetry and Remote Sensing*, 63(5), 543–558.

Benumof, B. T., Storlazzi, C. D., Seymour, R. J. and Griggs, G. B. (2000). 'The relationship between incident wave energy and sea cliff erosion rates: SanDiego County, California', *Journal of Coastal Research*, 17, 1162-1178.

Brammer, H. (2014). 'Bangladesh's dynamic coastal regions and sea-level rise', *Climate Risk Management*, 1, 51-62.

Cohen, M.C.L. and Lara R.J. (2003). 'Temporal changes of mangrove vegetation boundaries in Amazonia: application of GIS and remote sensing techniques', *Wetland Ecology Management*, 11(4), 23-231.

Collins, B. D. and Sitar, N. (2008). 'Processes of coastal bluff erosion in weakly lithified sands, Pacifica, California, USA', *Geomorphology*, 97, 483-501, doi: 10.1016/j.geomorph.2007.09.004.

Ellison, J. C. and Zouh, I. (2012). 'Vulnerability to climate change of mangroves: Assessment from Cameroon, Central Africa', *Biology*, 1, 617–638.

Esteves, L. S., William, J. J. and Brown, J. M. (2011). 'Looking for evidence of climate change impacts in the eastern Irish Sea', *Natural Hazards and Earth System Sciences*, 11, 1641-1656, doi: 10.5194/nhess-11-1641-2011.

Frazier, P. S. and Page, K. J. (2000). 'Water body detection and delineation with Landsat TM data', *Photogrammetric Engineering and Remote Sensing*, 66(12), 1461-1467.

Gilman, E., Ellison, J. C., and Coleman, R. (2007). 'Assessment of mangrove response to projected relative sea-level rise and recent historical reconstruction of shoreline position', *Environmental monitoring and assessment*, 124(1-3), 105-130.

Hapke, C.J., Reid, D. and Richmond, B. (2009). 'Rates and trends of coastal change in California and the regional behaviour of the beach and cliff system', *Journal of Coastal Research*, 25(3), 603-615.

Hegde, A.V. and Akshaya B.J. (2015). 'Shoreline transformation study of Karnataka Coast: Geospatial Approach', *Aquatic Procedia*, 4, 151-156.

Ji, L., Geng, X., Sun, K., Zhao, Y. and Gong, P. (2015). 'Target detection method for water mapping using Landsat 8 OLI/TIRS imagery', *Water*, 7(2), 794-817.

Kanwal, S., Ding, X., Sajjad, M., and Abbas, S. (2019). 'Three decades of coastal changes in Sindh, Pakistan (1989–2018): a geospatial assessment', *Remote Sensing*, 12(1), 8, https://doi.org/10.3390/rs12010008.

Katz, O. and Mushkin, A. (2013). 'Characteristics of sea-cliff erosion induced by a strong winter storm in the eastern Mediterranean', *Quaternary Research*, 80, 20-32, doi: 10.1016/j.yqres.2013.04.004.

Khan, E. and Hussain, N. (2018). 'Coastline dynamics and raising landform: a geo-informaticsbased study on the Bay of Bengal, Bangladesh', *The Indonesian Journal of Geography*, 50(1), 41-48.

Kuehl, S. A., Allison, M. A., Goodbred, S. L., and Kudrass, H. (2005). 'The Ganges–Brahmaputra Delta'. *In book: River Deltas – Concepts, Models, and Examples, Edited by Giosan L. and Bhattacharya J.*, 413–434.

Kuleli, T. (2010). 'Quantitative analysis of shoreline changes at the Mediterranean Coast in Turkey', *Environmental Monitoring and Assessment*, 167(1-4), 387-397.

Masocha, M., Dube, T., Makore, M., Shekede, M.D. and Funani, J. (2018). 'Surface water bodies mapping in Zimbabwe using landsat 8 OLI multispectral imagery: A comparison of multiple water indices', *Physics and Chemistry of the Earth*, Parts A/B/C 106, 63-67.

Matin, N. and Hasan, G.M.J. (2021). 'A quantitative analysis of shoreline changes along the coast of Bangladesh using remote sensing and GIS techniques', *Catena*, 201. https://doi.org/10.1016/j.catena.2021.105185.

McIvor, A. L., Spencer, T., Möller, I., and Spalding, M. (2013). 'The response of mangrove soil surface elevation to sea level rise', *Natural Coastal Protection Series: Report 3, Cambridge Coastal Research Unit Working Paper 42*, ISSN 2050-7941.

Mikhailov, V. N. and Dotsenko, M. A. (2007). 'Processes of delta formation in the mouth area of the Ganges and Brahmaputra rivers', *Water Resources*, 34(4), pp. 385–400.

Moore, L. J. and Griggs, G. B. (2002). 'Long-term cliff retreat and erosion hotspots along the central shores of the Monterey Bay National Marine Sanctuary', *Marine Geology*, 181(1-3), 265–283, doi: 10.1016/S0025-3227(01)00271-7.

Moussaid, J., Fora A.A., Zourarah B., Maanan M. and Maanan M. (2015). 'Using automatic computation toanalyze the rate of shoreline change on the Kenitra coast, Morocco', *Ocean Engineering*, 102(1), 71-77.

Murty, T. S., and Henry, R. F. (1983). 'Tides in the Bay of Bengal', *Journal of Geophysical Research: Oceans*, 88(C10), 6069-6076, doi: 10.1029/JC088iC10p06069.

Nabi, M.R., Rashid, M. S. and Hossain, M.I. (2016). 'Historical Bank-line Shifting Since 1760s: A GIS and Remote Sensing Based Case Study of Meghna River Plate of Rennell's Atlas', *International Journal of Scientific and Research Publications*, 6(12), 473-483.

Natesan, U., Thulasiraman, N., Deepthi, K. and Kathiravan, K. (2013). 'Shoreline change analysis of Vedaranyam coast, Tamil Nadu, India', *Environmental Monitoring and Assessment*, 185(6), 5099-5109.

Nguyen H. H., McAlpine C., Pullar D., Leisz S.J. and Galina G., (2015). 'Drivers of coastal shoreline change: case study of Hon Dat coast, Kien Giang, Vietnam', *Environmental Management*, 55(5), 1093-1108.

Rahman, A.F., Dragoni, D. and El-Masri, B., (2011). 'Response of the Sundarbans coastline to sea level rise and decreased sediment flow: a remote sensing assessment', *Remote Sensing of Environment*, 115(12), 3121-3128.

Sahana, M. and Sajjad, H., (2019). 'Assessing influence of erosion and accretion on landscape diversity in Sundarban Biosphere Reserve, Lower Ganga Basin: a geospatial approach'. *Quaternary Geomorphology in India, Springer*, 191-203, https://doi.org/10.1007/978-3-319-90427-6_10.

Sarwar, M.G.M. and Woodroffe, C.D. (2013). 'Rates of shoreline change along the coast of Bangladesh', *Journal of coastal conservation*, 17(3), 515-526.

Sathirathai, S. and Barbier E.B., (2001). 'Valuing mangrove conservation in southern Thailand', *Contemporary Economic Policy*, 19(2), 109-122.

Sheik, M. and Chandrasekar (2011). 'A shoreline change analysis along the coast between Kanyakumari and Tuticorin, India, using digital shoreline analysis system'. *Geo-spatial Information Science*, 14(4), 282-293.

Sarkar, A., Garg, R.D., and Sharma, N., (2012). 'RS-GIS based assessment of river dynamics of Brahmaputra river in India', *Journal of Water Resource and Protection*, 4, 63-72.

Souza Filho, P. W. M., Martins, E. do S. F., and Costa, F. R. (2006). 'Using mangroves as a geological indicator of coastal changes in the Bragança macrotidal flat, Brazilian Amazon: a remote sensing data approach', *Ocean and Coastal Management*, 49(7-8), 462-475.

Thieler, E. R., Himmelstoss, E. A., Zichichi, J. L., and Ergul, A. (2009). 'Digital Shoreline Analysis System (DSAS) version 4.0-An ArcGIS extension for calculating shoreline change', *US Geological Survey Report*, 2008-1278.

To, D.V. and Thao, P.T.P., (2008). 'A shoreline analysis using DSAS in Nam Dinh Coastal Area', *International Journal of Geoinformatics*, 4(1), 37-42.

Vidal, J. (2013). 'Tigers under threat from disappearing mangrove forest', *The Guardian*, accessed on 10 Dec 2020.

Wenbo, L., Du, Z., Ling, F., Zhou, D., Wang, H., Gui, Y., Sun, B. and Zhang, X. (2013). 'A comparison of land surface water mapping using the normalized difference water index from TM, ETM+ and ALI', *Remote Sensing*, 5(11), 5530-5549.

MIJST
MIST International Journal of Science and Technology

Geographical Information System Approach to Delineate the Watershed's Morphometric Parameters for Sustainable Hydrological Modeling of Barind Region, Bangladesh

Md. Ashikur Rahman[1*], M. H. Sazzad[2], and R. S. Rupom[3]

[1] Institute of Bay of Bengal & Bangladesh Studies, BSMR Maritime University Bangladesh, Dhaka-1216, Bangladesh
[2] Department of Urban & Regional Planning, Khulna University of Engineering & Technology, Khulna-9203, Bangladesh
[3] Department of Urban & Regional Planning, Rajshahi University of Engineering & Technology, Rajshahi-6204, Bangladesh

emails: *[*1]ro.ibbbs@bsmrmu.edu.bd; [2]planner.sazzad@gmail.com; and [3]rubayatshahriarrupom18@gmail.com;*

ARTICLE INFO

Article History:

Received: 03rd September 2020
Revised: 02nd March 2021
Accepted: 17th March 2021
Published: 27th June 2021

Keywords:

Geographical Information System
GIS
Remote Sensing
Watershed
Morphometric Parameter
Sustainable Hydrological Mode

ABSTRACT

Water is an important resource of the earth's surface and it is integral for all on this planet. The availability or the scarcity of water depends on the watershed characterizes that consider the basic, linear, and shape parameters of any waterbody. The objective of the study was to delineate 14 morphometric parameters in the Barind region (Dinajpur district, Bangladesh) for sustainable hydrological modeling. An ASTER-DEM of 30-meter resolution data, geographical information system (GIS), and Remote sensing technique were used for extracting drainage components of interest region. The whole study region was covered by the flow of the Purnovoba river, Jamuna river, Atrai river (part-1 and part-2). Research results found that the Purnovoba river had a high bifurcation ratio (0.9982) that defined hydrologically more disturbed than the other three watershed areas and it had a high stream frequency (0.8332) that denoted rocky having low infiltration capacity. Jamuna river had a low drainage density (0.7322) that defined more vegetation having higher permeability. Besides, the Jamuna river had the lowest no. of stream order that was insignificant in the steady runoff process and less prone to cause a flash flood. The research predicted that the availability of groundwater might decrease to Jamuna river in the future as it had the lowest basin area (217.42 sqr. km) and perimeter (114.90 km) and the basin surface slope would become gentle to Atrai river part-1 for the lowest length of overland flow (0.6072). Purnovoba river experienced the lowest form factor (0.2351) which indicated the most possibility for erosion. The elongated ratio of all basins was greater than 0.5 which considered all the shapes were more elongated. These findings will help for further modeling of an integrated watershed for sustainable hydrological models in the Barind region.

1. INTRODUCTION

Land and water resources both are vital elements of the earth as life depends on them. But these resources are being limited due to rapid population rises and other activities. Watershed management is a crucial part of the conservation and utilization of the natural resources in the water bodies (B.-W. Liu *et al.*, 2020; Rong *et al.*, 2019). Effective watershed management can play an important role in managing the damage runoff (Fu *et al.*, 2019), reducing the impact of sediment output and river erosion (Du *et al.*, 2016), increasing groundwater storage (Ghorbani Nejad *et al.*, 2017), and utilizing land and water resources (Ervinia *et al.*, 2019; Wada *et al.*, 2020). A watershed is a region that sustains all kinds of runoff of the stream, lake, or ocean. Watershed's morphometric modeling is commonly used for sustainable watershed management (Ahn & Kim, 2019; Alnahit *et al.*, 2020), resource protection (Wada *et al.*, 2020), and sustainable development (Prasannakumar *et al.*, 2013; Sujatha *et al.*, 2014) in any region. Morphometric analysis is an important method for hydrological research that provides the quantitative results of drainage basins (Choudhari *et al.*, 2018). Besides, morphometric analysis of watershed

includes the preparation of drainage map with the order of drainage streams, catchment area, and perimeter, stream order, and stream length (Alam *et al.*, 2020; Charizopoulos *et al.*, 2019). Three morphometric parameters such as basic parameters (Banerjee *et al.*, 2017; Choudhari *et al.*, 2018; Elsadek *et al.*, 2019; Gajbhiye *et al.*, 2014), linear parameters (Gajbhiye *et al.*, 2014; Patel *et al.*, 2012), and shape parameters (Ahmed *et al.*, 2010; Gajbhiye *et al.*, 2014; Panhalkar *et al.*, 2012; Patel *et al.*, 2012) are used to characterize the watershed. The basic parameters characterize the area, perimeter, basin length, stream order, stream length, maximum and minimum height, and slope. Basin length is considered as a straight-line interval from a basin mouth to the outlet point (Senter *et al.*, 2017; Soni, 2017). The linear parameters are analyzed for the stream order, stream length, mean stream length, and bifurcation ratio (Harsha *et al.*, 2020). The mean stream length is related to the drainage network and corresponds with its surface (Dragičević *et al.*, 2018; Pondari *et al.*, 2020). The shape parameters include the form factor, shape factor, elongation ratio, compactness coefficient, and circulatory ratio (Al-Assadi, 2020; Saha *et al.*, 2020). Though linear parameters have a substantial effect on erodibility, but the shape parameters have negative relationship on erodibility (Ratnam *et al.*, 2005).

Conducting watershed analysis and hydrological research for large drainage basins catchment areas through topographical maps or field observation are quite impossible but in small watersheds, it can be measured streamflow and water quality (Choudhari *et al.*, 2018; Harmel *et al.*, 2006). Recently, researchers used geospatial techniques like Geographical Information System (GIS) and Remote Sensing (RS) for sustainable watershed analysis and modeling. GIS and RS techniques have high efficiency and effectiveness for extraction of drainage components (Gong & Xie, 2009; Metz *et al.*, 2011), watershed development, and management (Ameri *et al.*, 2018; Chatterjee *et al.*, 2014; Okumura & Araujo, 2014). Nowadays GIS techniques are inexpensive, reliable, and fast way to calculate morphometric analysis (Balasubramanian *et al.*, 2017; Sreedevi *et al.*, 2009) and used for drainage pattern, topography, and subsurface material studies (Balasubramanian *et al.*, 2017; Chandniha & Kansal, 2017; Javed *et al.*, 2011; Withanage *et al.*, 2014). RS data offer accurate, timely, and real-time information about specific aspects such as watershed size and form, soil distribution, drainage characteristics, etc (Suresh *et al.*, 2004).

Elsadek. W. M. et al., 2019 have analyzed the morphometric characteristics to estimate the flood risk hazards of sub-watersheds using morphometric analysis in Qena watersheds. In their research, the shuttle radar topography mission (STRM) data are used to analyze the topography, modeling of surface processes, and flood risk zone. The calculation of hydrological parameters, extraction of topography map, drainage network, and the direction of the flow of floods are analyzed by GIS techniques (Elsadek *et al.*, 2019). Choudhari, P. P. et al., 2018 have analyzed the morphometric parameters and prioritization of sub-watersheds for groundwater potential and conservation structures for a watershed of the Mula river basin in the Puna district of Maharashtra, India. The prioritization of five watersheds of the Mula river is graded by computing morphological parameters where the lowest ranking is represented the top priority of soil erosion and less measure of conservation. In their research, the STRM data and GIS technique are used for estimating morphometric parameters of the Mula river basin (Choudhari *et al.*, 2018).

The present research contributes to delineate the 14 morphometric parameters in the Barind region where there is limited such research work in Bangladesh. The research findings will help for further modeling of an integrated watershed for sustainable hydrological models. Besides, it will help for solving hydrology-related problems such as irrigation, harvesting of surface water, cause of river erosion, surface stormwater runoff process, and water resource management in the Barind region.

2. MATERIALS AND METHODS

A. Study Area Profile

Watershed basin of Dinajpur region is located in between 25^0 10′ and 26^0 04′ North latitudes and between 88^0 23′ and 89^0 18′ East longitudes at the Northern part of Bangladesh (Figure 1). It is bounded by Thakurgaon and Panchagram districts on the North, Gaibandha and Joypurhat districts on the South, Nilphamari and Rangpur districts on the East and West Bengal state of India on the West. Geographically it is situated in the Barind region of Bangladesh. The Barind region is influenced by lower rainfall and higher temperature as compared to other regions of Bangladesh (Rashid *et al.*, 2013). Jamuna river, Purnovoba river, and Atrai river are major rivers that pass through the area of interest (AOI). The Dinajpur district experiences a hot, wet, and humid tropical climate. In Bangladesh, the Northern part is the steepest slope than the Southern region (Figure 2). In the AOI the water flow usually happens from the Northern to the Southern direction and it is occurred based on the slope of the land (Figure 3).

B. Data Description

Digital elevation model (DEM) generated from advanced spaceborne thermal emission and reflection radiometer (ASTER) data were used for this research (K. Liu *et al.*, 2020; Mokarram & Hojati, 2017; Poongodi & Venkateswaran, 2018) and they were collected from open topography website (https://opentopography.org/) (Figure 4). The numbers of Columns and rows of the raster data were 1107 and 1000 respectively. Spatial extents of the DEM were 26.05930 degree at the top, 25.22597 degree at the bottom, 88.38231 degree at the left, and 89.30481 degree at right. The pre-processed DEM image was used for extraction and quantification of watershed morphometric parameters. Districts and Upazilla boundary data were collected from the Survey of Bangladesh (SoB). Universal Transverse Mercator (UTM) projection system was used as spatial parameter and World Geodetic System (WGS) 1984 was used as a datum for the data preparation and mappng.

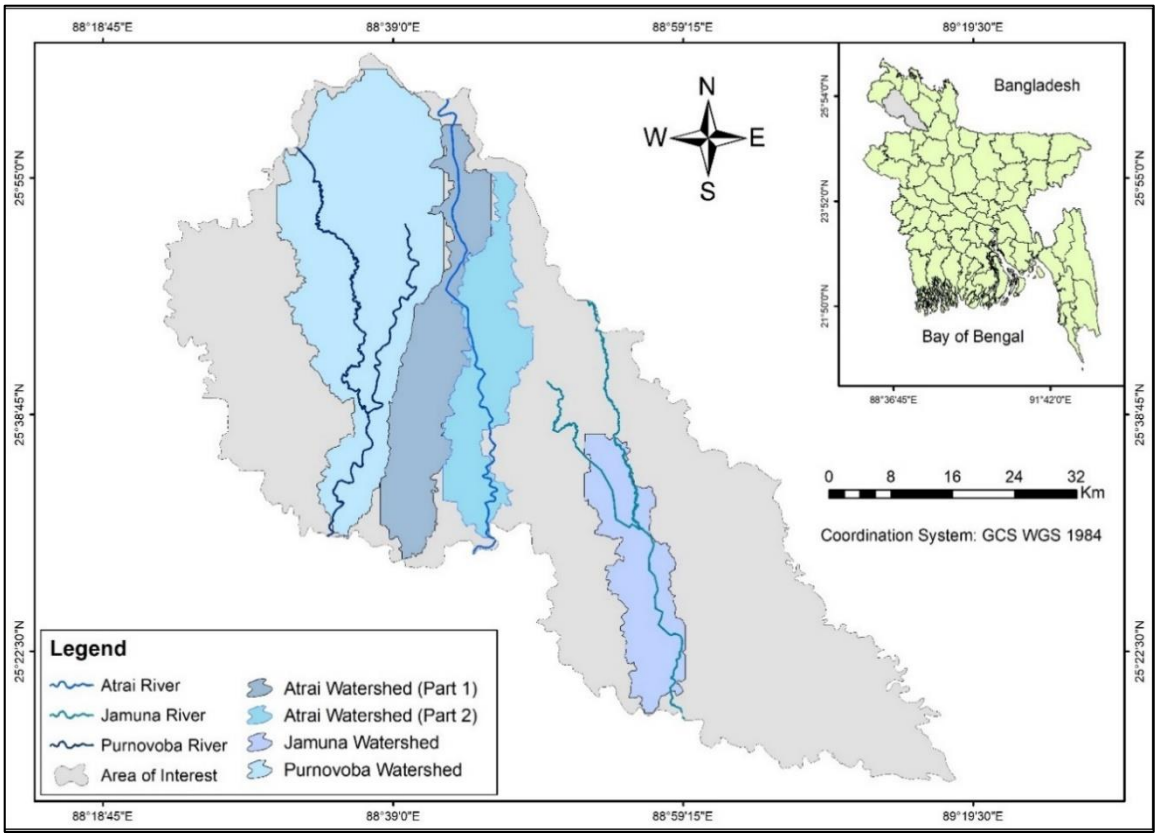

Figure 1: Study area map including major river and watershed in Dinajpur district, Bangladesh

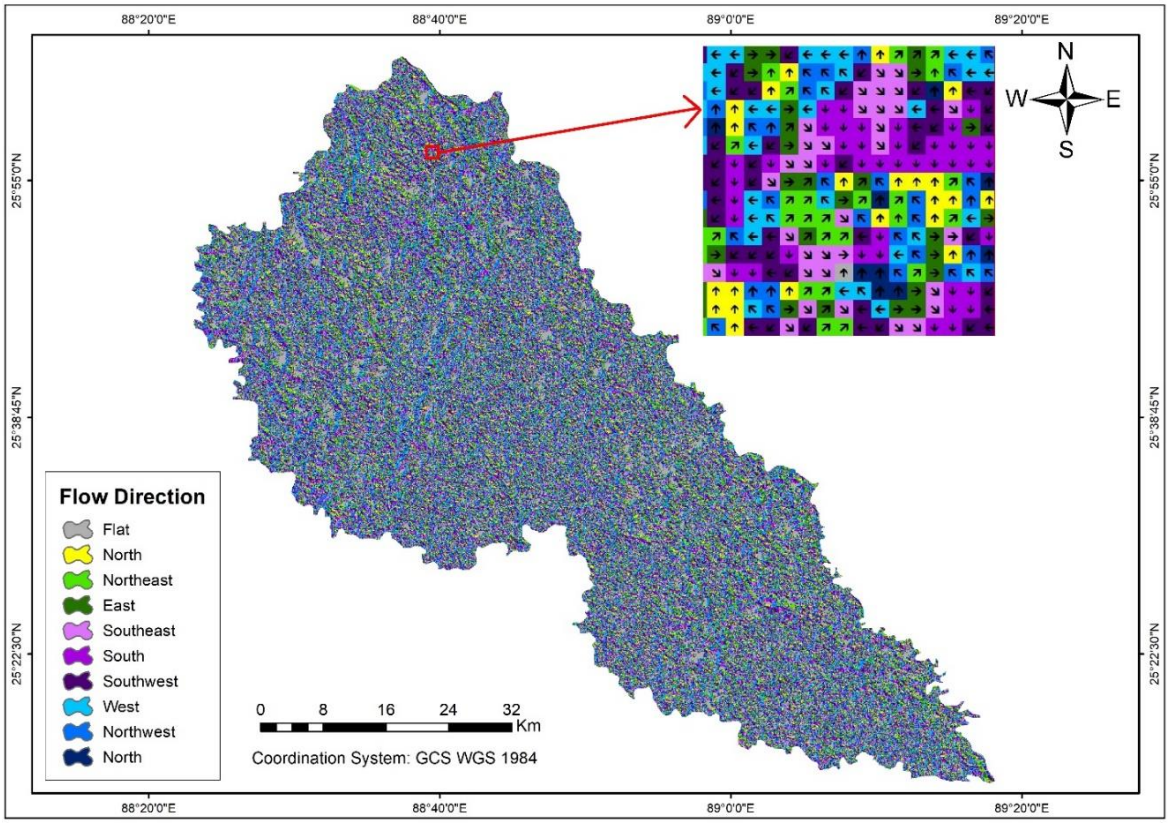

Figure 2: Flow direction of water in the AOI

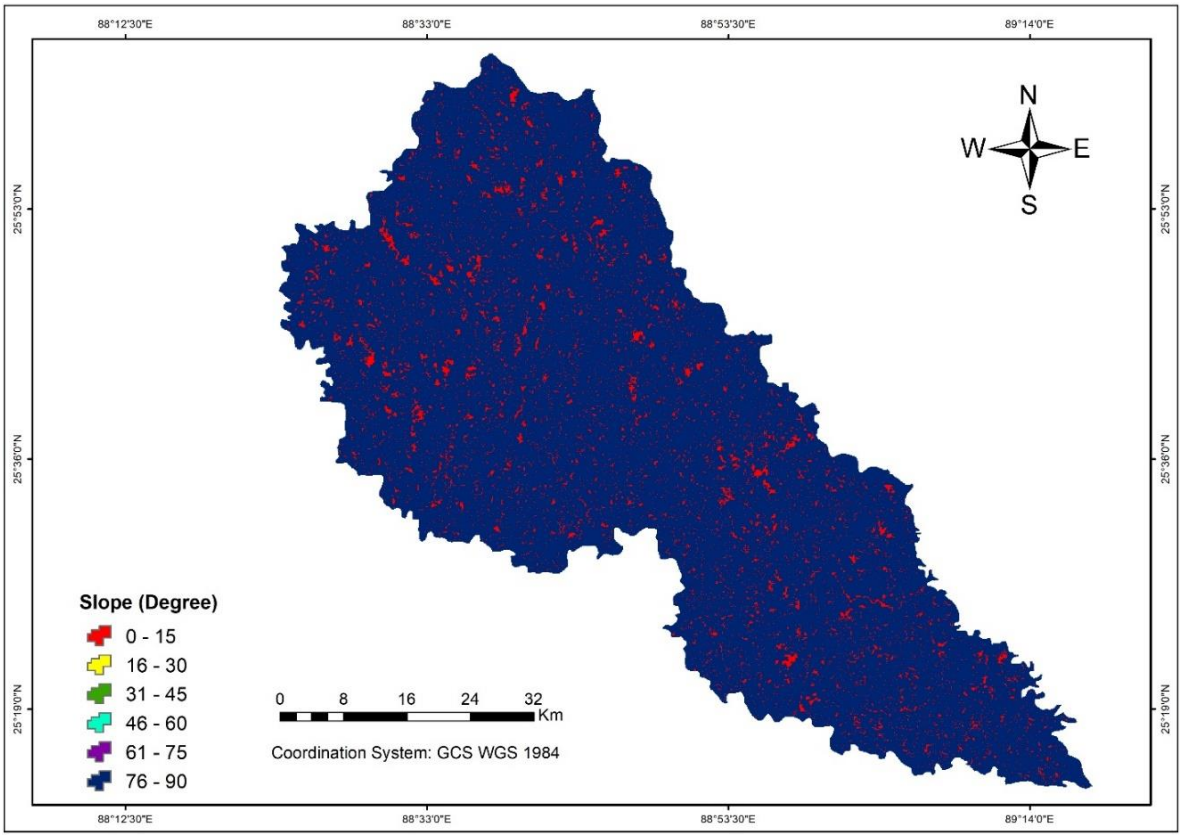

Figure 3: Slope aspect map of Study area

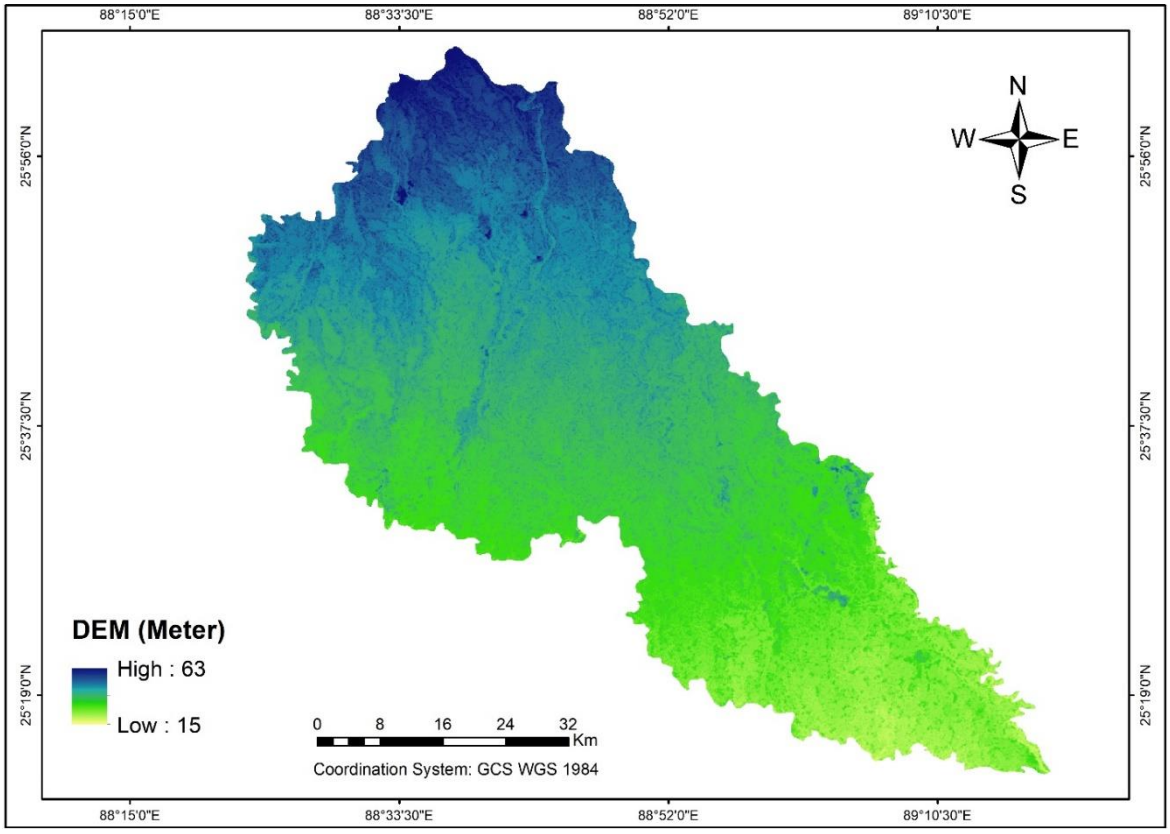

Figure 4: DEM map of Study area

C. *Morphometric Parameter Analysis Technique and Computation*

Watershed basin created stream orders like 1st, 2nd, 3rd, 4th, and 5th order stream depending on the flow characterizes. All the streams in a watershed area were delineated from DEM image using ArcGIS software v 10.7. Firstly, the collected DEM image was reconditioned by a commercial DEM developer, and based on AOI reconditioned DEM was extracted. Secondly, the Flow direction of the analyzed region was computed. Thirdly, the flow accumulation of DEM was computed. Fourthly, the stream network covering the AOI was defined and it was found in a grid format. Fifthly, these grid format data were taken to convert vector data format. Sixthly, stream order was extracted based on theory. Finally, some extreme outlet points were selected of the concerned river, and based on counting outlet points the watershed basins were delineated (Ameri *et al.*, 2018; Amiri *et al.*, 2019; Tykocki *et al.*, 2018).

The watershed of AOI was divided into four sub-watershed basins called Purnovoba river, Jamuna river, Atrai river part-1, and Atrai river part-2 (Figure 1). Five basic parameters, five linear parameters, and four shape parameters were analyzed in the present study. All these parameters were computed using some formulas showing in Table 1.

Table 1
The list of formulas for computation morphometric parameters in the research

No.	Parameter	Formulas	Reference
Basic parameter			
1	Area (A) (km^2)	ArcGIS computation	
2	The Perimeter of the basin (P) (km)	ArcGIS computation	
3	Stream order (u)	Hierarchical rank (ArcGIS computation)	(Strahler, 1964)
4	Stream Length (Lu) (km)	ArcGIS computation	
5	Basin Length (Lb) (km)	$L_b = 1.321 \times A^{0.568}$ ---------- (1) Where A = Basin area (km^2)	(Ratnam *et al.*, 2005)
Linear parameter			
6	Bifurcation ratio (Rb)	$R_b = N_u/N_u + 1$ ---------- (2) Where $N_u + 1$ = Segments no. of the next higher order	(Schumm, 1956)
7	Drainage density (Dd) (km/km^2)	$D_d = L_u/A$ ---------- (3) Where, L_u = Total stream length of all orders (km) and A = Area of the watershed (km^2)	(Horton, 1945)
8	Stream frequency (Fu) ($no./km^2$)	$Fu = N_u/A$ ---------- (4) Where, N_u = Total no. of steams of all orders and A = Area of the basin (km^2)	(Horton, 1945)
9	Texture ratio (T) ($no./km^2$)	$T = N_u/P$ ---------- (5) Where N_u = total no. of streams of all orders and P = Perimeter (km)	(Horton, 1945)
10	Length of overland flow, Lo (km)	$L_o = 1/2D_d$ ---------- (6) Where D_d = Drainage density	(Horton, 1945); (Schumm, 1956)
Shape parameter			
11	Form factor (Rf)	$R_f = A/L_b^2$ ---------- (7) Where, A = Basin area (km^2) and L_b = Basin length (km)	(Horton, 1945)
12	Shape factor (Bs)	$B_s = L_b^2/A$ ---------- (8) Where L_b = Basin length (km) and A = Area of the basin (km^2)	(Horton, 1945)
13	Elongation ratio (Re)	$R_e = 1.128\sqrt{(A/L_b)}$ ---------- (9) Where A = area of the basin (km^2) and L_b = Basin length (km).	(Schumm, 1956; Strahler, 1964)
14	Compactness coefficient (Cc)	$Cc = \frac{P}{2\sqrt{\pi A}}$ ---------- (10) Where P = Perimeter of the basin (km) and A = area of the basin (km^2)	(Horton, 1945)

3. RESULTS AND DISCUSSION

A. Area (A) and Perimeter of the Basin (P)

Area and perimeter were the basic parameters of a watershed basin and these were described in the way of the extent of the basin over a watershed region. The research focused on the area of four analyzed watersheds that were 699.664 km^2, 217.424 km^2, 244.047 km^2, and 298.788 km^2 for Purnovoba river, Jamuna river, Atrai river part-1, and Atrai river part-2 watershed basin area respectively. The minimum and maximum perimeters were 187199.00 km for Purnovoba river and 114.907 km for Jamuna river (Table 2). So, the availability of groundwater might decrease in the Jamuna river watershed region in the future as its basin area and perimeter were low.

B. Stream Order (u)

Higher stream order denoted the higher discharged rate and greater velocity of a stream while lower-order was described as opposite. The maximum stream order was demarked as 5th order stream and the minimum was demarked as 1st order. Analyzed results showed that there was a total of 1214 no of the stream (Table 2). Increasing the order decreased the number of streams. The 1st order stream contained the highest number of stream orders in the study area. The 5th order stream was found in the Purnovoba river watershed area which was denoted the main river stream (Figure 5d; Fig. 6a). The 1st to 4th order stream was found in both Atrai river part-1 and Atrai river part-2 (Figure 5a, b; Figure 6a). Only 1st, 2nd, and 3rd order streams were found in the Jamuna river watershed (Figure 5c; Figure 6a).

C. Stream Length (Lu)

The stream length of a watershed basin represented the travel distance and time of a stream. The total length of all streams was 1117.77 km in the study area (Table 2). The 1st order stream contained the highest length and the 5th order contained the lowest (Figure 6b). Among them, the Purnovoba river contained the highest distances (534.03 km) and carried a higher stream length that defined the area as hydrologically more active. As a result, the velocity of the stream was greater and it consequenced the erosion and sediment transport in the AOI. Figure 6c showed the Spider graph that showed the 1st order stream both in-stream order and stream length carried the highest value than other stream orders.

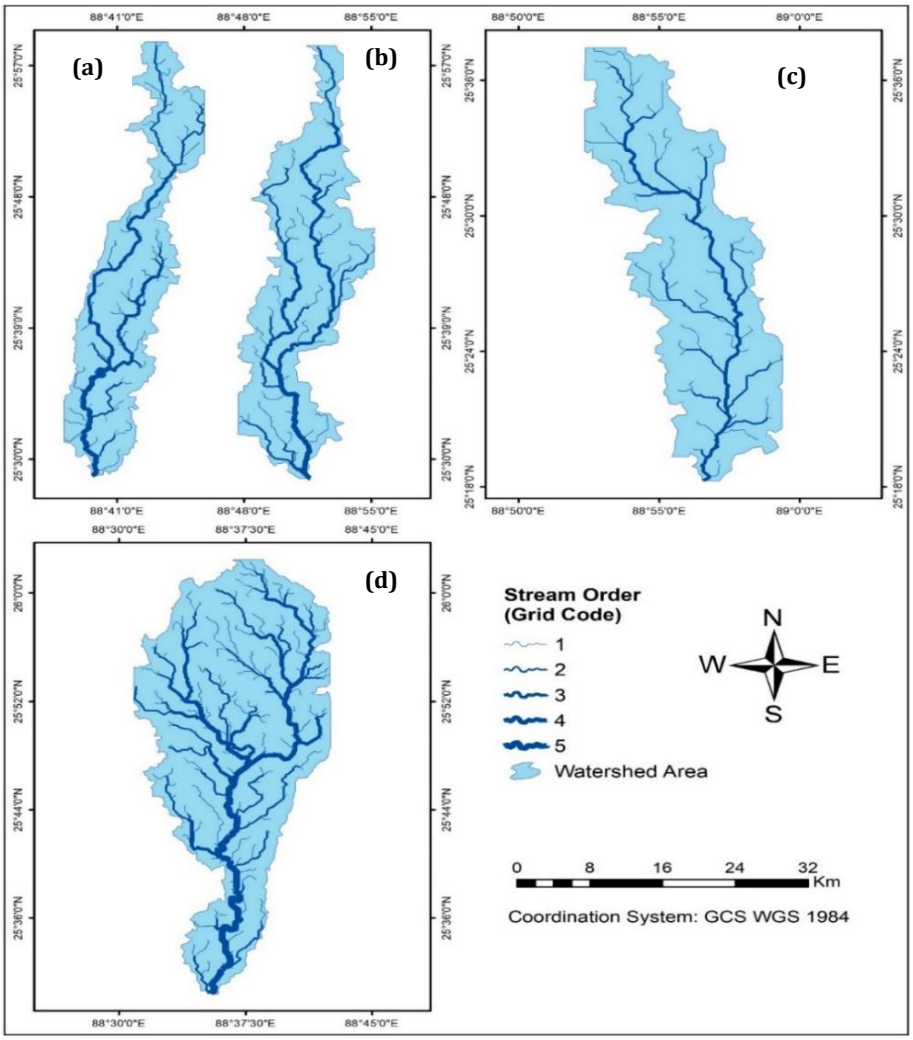

Figure 5: Map of the watershed and stream order of the research area (a) Atrai river part-1, (b) Atrai river part-2, (c) Jamuna river (d) Purnovoba river

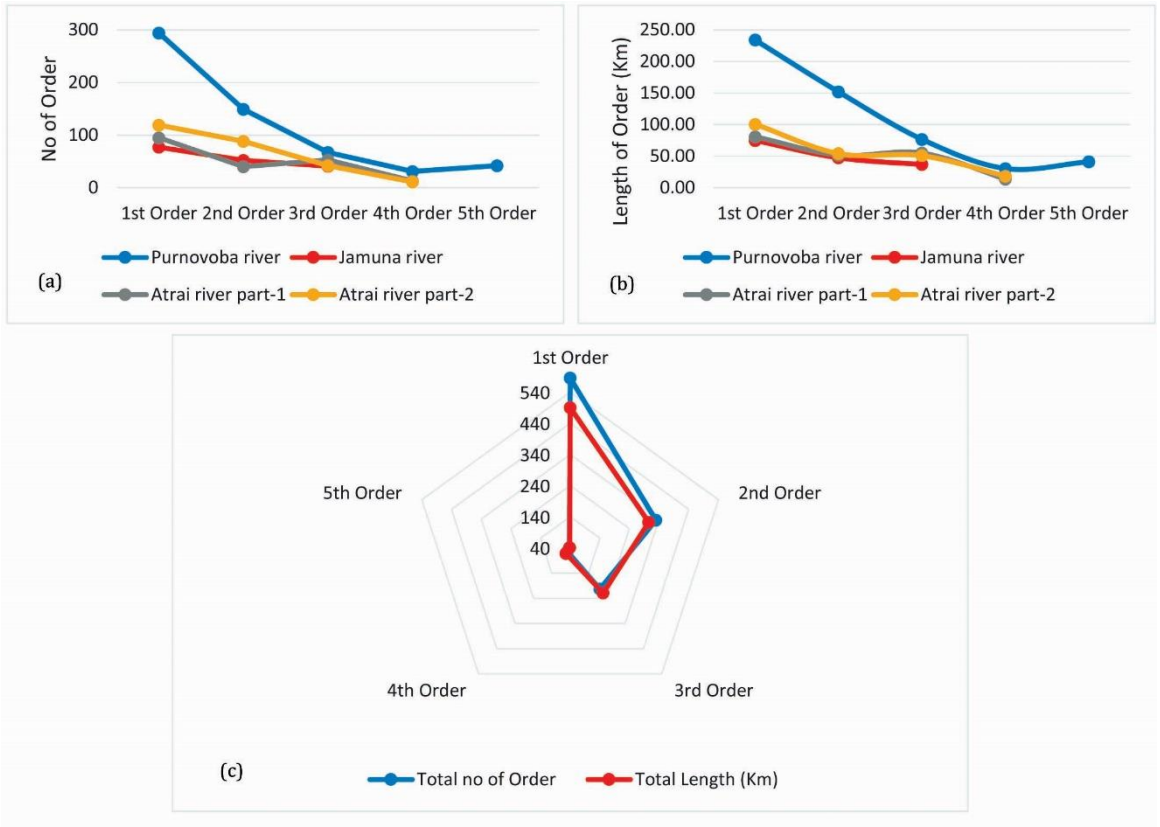

Figure 6: (a) Stream according to no. of order, (b) Stream according to the length of order, and (c) Spider graph of total no of order and total length

D. Basin Length (Lb)

Basin length was described as the shape of a basin. The geological structure of a watershed basin was dependent on the length of a basin. In the AOI the Atrai river (part-1 & part-2) contained the highest length of the basin (approximately 63.63 km). But in a single watershed area, the Purnovoba river was considered as the highest and more valuable basin length (Table 2). It was computed through equation (1).

E. Bifurcation Ratio (Rb)

Bifurcation ratio was the foremost parameter linking the hydrological regime in a basin. A high bifurcation ratio suggested the flash flooding during the storm events when the early hydrograph peak was potential. In the study, the maximum bifurcation ratio was 0.9982 and the minimum was 0.2919 (Table 3). Purnovoba river was found with a higher ratio and the Jamuna river was found with a lower ratio. While the mean bifurcation ratio was 0.51969 and at 95% confidence level it was 0.51779 (Table 4). It was computed through equation (2). The bifurcation ratio was predicted that the Purnovoba river was hydrologically more disturbed than the other three watershed areas. While Atrai river and Jamuna river watershed were delayed to happen any flash flood.

F. Drainage Density (Dd)

Drainage density was the total length of all the streams in the watershed. It helped to determine the permeability and porosity of the watershed and it conveyed the indicator of landform elements in stream-eroded topography. It was derived using equation (3). Low drainage density led to coarse drainage texture while high drainage density led to fine drainage texture. Drainage density was related to the vegetation, permeability, and development of the basin. Here the mean drainage density was found 0.76681 (Table 4) while the Atrai river part-1 showed higher drainage density, it defined the fine drainage texture and it carried low resistant or permeable subsoil material (Table 3). So, it had low vegetation and less permeable capacity. On the other hand, the Jamuna river had low drainage density and so it had high resistant or permeable subsoil material (Figure 7).

G. Stream Frequency (Fs)

Stream frequency was defined as computing the unit area that contained the total number of stream segments of all orders. It was extracted by equation (4). Stream frequency was related to permeability, infiltration, and capacity of relief of a watershed. Besides, there is a contradictory relationship between the stream frequency and the number of streams. The present study forecasted the Stream frequency of Purnovoba river, Jamuna river, Atrai river part-1, and Atrai river part-2 watershed were 0.8332, 0.2429, 0.2872, and 0.3716 respectively (Table 3), and the mean stream frequency was 0.43378 (Table 4). As the Purnovoba river carried the highest stream frequency It described the watershed area as rocky and with low infiltration capacity (Figure 7d). On the other hand, the Jamuna river carried the lowest stream frequency (Figure 7c). As a result, it was covered with more vegetation with higher permeability and it was less prone to cause flash floods than other watershed areas.

Table 2
Computation of basic parameters of watershed

Watershed	Area (km²)	Perimeter (km)	Total no of stream order	Stream Length (km)	Basin length (km)
Purnovoba river	699.66	187199.00	583.00	534.03	54.55
Jamuna river	217.42	114.90	170.00	159.21	28.08
Atrai river part-1	244.04	146.61	201.00	200.95	29.99
Atrai river part-2	298.78	166.67	260.00	223.58	33.64
Total	1459.92	187627.20	1214.00	1117.77	146.27

Table 3
Computation of linear parameters of watershed

Watershed	Bifurcation ratio	Drainage density	Stream frequency	Texture ratio	Length of overland flow
Purnovoba river	0.9982	0.7632	0.8332	0.0031	0.6550
Jamuna river	0.2919	0.7322	0.2429	1.4794	0.6828
Atrai river part-1	0.3441	0.8234	0.2872	1.3709	0.6072
Atrai river part-2	0.4452	0.7482	0.3716	1.5598	0.6681

H. Texture Ratio (Tr)

Texture ratio was influenced by infiltration capacity. There were five different texture classes: very coarse (less than 2), coarse (2 to 4), moderate (4 to 6), fine (6 to 8), and very fine (greater than 8) (Altaf *et al.*, 2013). This texture was related to the soil type, infiltration capacity of the watershed basin. It was computed through equation (5). The study ascertained that the minimum texture ratio was 0.0031 for the Purnovoba river, the maximum texture ratio was 1.5598 for the Atrai river part-2 (Table 3), and the average ratio was 1.10335 (Table 4). All the watershed regions apprehended very coarse texture and so the infiltration capacity was decreased.

I. Length of Overland Flow (Lo)

Length of overland flow was considered as the traveling distance of a stream over the earth's surface before meeting with the main channel. It was considered the most significant hydrological parameter of the watershed. Besides, the hydrographic development was related to the length of overland flow. The study found that the lengths of overland flow were 0.6072, 0.6681, 0.6550, and 0.6828 for Atrai river part-1, Atrai river part-2, Purnovoba river, and Jamuna river respectively (Table 3). It was computed through equation (6). This result forecasted that the slope became gentle for the watershed basin of Atrai river part-1.

J. Form Factor (R_f)

The basins containing high form factors had high peak flows of shorter duration. On the other hand, elongated watershed regions with low form factors had lower peak flows of longer duration. It was computed through equation (7) and the results were displayed in Table 5. Considering the range of form factor 0 to 1, the maximum and minimum value of form factor defined the possibility of erosion. As the Purnovoba river had the lowest form factor (0.2351), so it had the most possibility for erosion. On the other hand, the Jamuna river watershed contained the highest form factor and it had less possibility for erosion. The mean form factor of the AOI was 0.26151 (Table 7).

K. Shape Factor (Bs)

If the basin area was circular it had more response to watershed after a storm event. Basin with high shape factor intended to shortest basin lag time and low shape factor intended to longest basin lag time. In the present study, the Purnovoba river watershed was engaged in high shape factor and it was considered as shortest basin lag time (Table 5). Consequently, it provided more responses after a storm event. It was computed through equation (8).

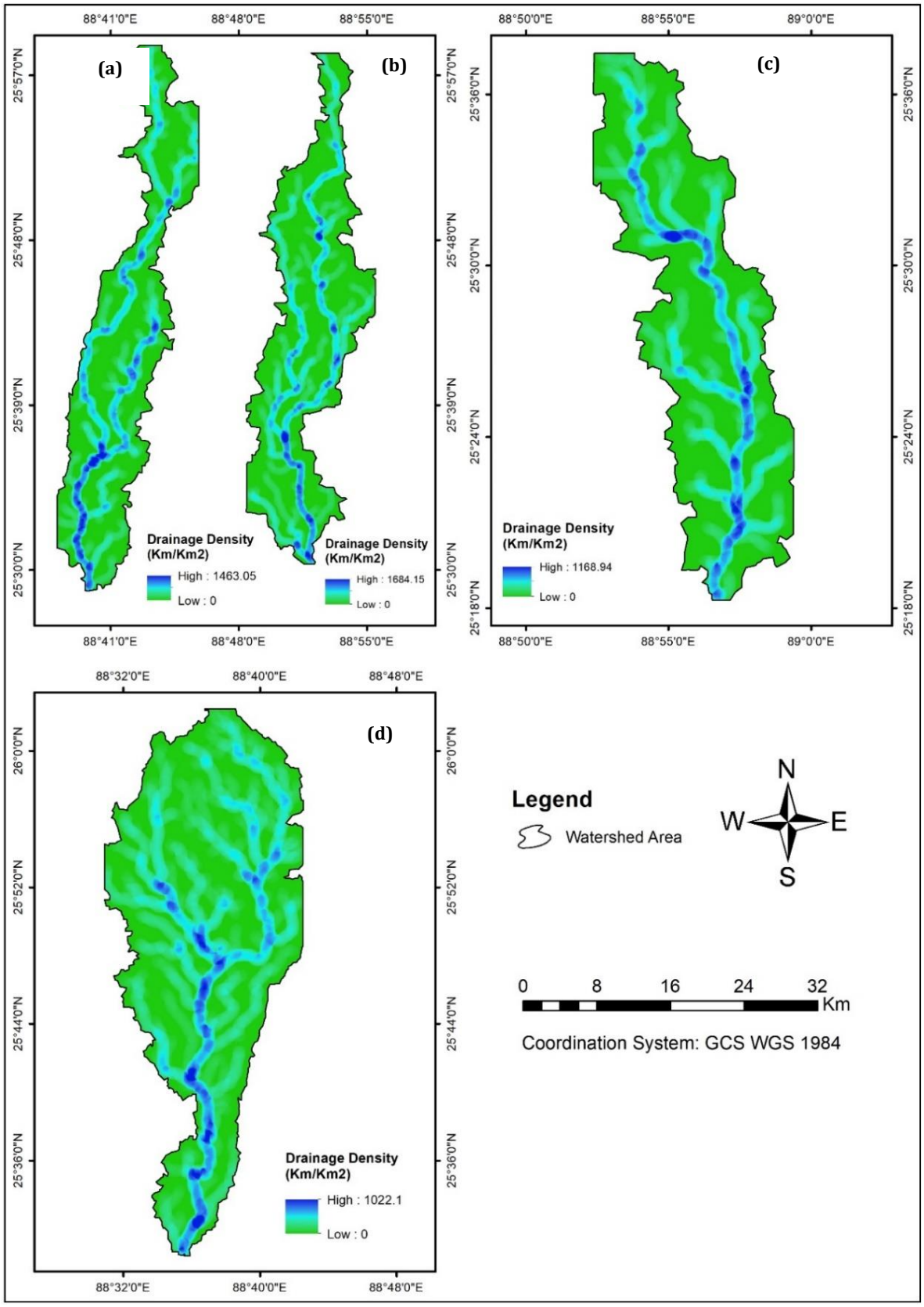

Figure 7: Map of drainage density of the research area (a) Atrai river part-1, (b) Atrai river part-2, (c) Jamuna river (d) Purnovoba river

Table 4
Statistical parameter analysis of linear aspects

Statistical parameter	Rb	Dd	Fs	Tr	Lo
Mean	0.51969	0.76681	0.43378	1.10335	0.65333
Standard Error	0.1627	0.0199	0.13581	0.36878	0.01638
Median	0.39469	0.75578	0.32944	1.42519	0.66164
Standard Deviation	0.3254	0.0398	0.27161	0.73756	0.03275
Sample Variance	0.10589	0.00158	0.07377	0.544	0.00107
Kurtosis	3.20087	2.18059	3.20087	3.7776	1.90909
Skewness	1.7773	1.41366	1.7773	-1.9346	-1.3095
Range	0.70719	0.09115	0.59028	1.55677	0.07559
Minimum	0.2911	0.73226	0.24297	0.00311	0.60723
Maximum	0.99829	0.82341	0.83326	1.55989	0.68282
Sum	2.07877	3.06722	1.73512	4.41338	2.61332
Count	4	4	4	4	4
Confidence Level (95.0%)	0.51779	0.06334	0.43219	1.17363	0.05212

Table 5
Computation of shape parameters of watershed

Watershed	Form factor	Shape factor	Elongation ratio	Compact co-efficient
Purnovoba river	0.2351	4.2531	4.0397	1996.9
Jamuna river	0.2756	3.6281	3.1384	2.1988
Atrai river part-1	0.2713	3.6855	3.2177	2.6481
Atrai river part-2	0.2639	3.7883	3.3615	2.7208

L. Elongation Ratio (Re)

The elongation ratio was related to the shape of the watershed basin and a standard was developed to demarcate the shape of an analyzed basin (Table 6). It was computed through equation (9). The elongation ratio of the experimented watershed basin was shown in (Table 5) and the results narrated that the basins were more elongated (Table 6). The mean elongation ratio was 3.43937 (Table 7).

M. Compactness Co-efficient (Cc)

The compactness coefficient explained the relationship between the area of a basin and the circular shape of that basin. Table 5 showed the coefficient factor where all the basins were above 1 that expounded the basin shapes were more deviation from the circular shape. Table 6 showed the elongation ratio range with its basin shape. Here the mean value of the compactness coefficient was 501.3 which examined that the shape of the interested watershed basin largely deviated from the circular shape (Table 7). It was computed through equation (10).

Table 6
Basin shape by elongation ratio

Elongation Ratio	Basin Shape
>0.5	More Elongated
0.5-0.7	Elongated
0.7-0.8	Less Elongated
0.8-0.9	Oval
0.9-1.0	Circular

Table 7
Statistical parameters analysis of shape aspects

Statistical parameters	Rf	Bs	Re	Cc
Mean	0.26151	3.8388	3.43937	501.126
Standard Error	0.00912	0.14204	0.20538	498.603
Median	0.26765	3.73697	3.28964	2.68452
Standard Deviation	0.01824	0.28408	0.41076	997.206
Sample Variance	0.00033	0.0807	0.16873	994420
Kurtosis	2.58127	2.8806	2.95976	4
Skewness	-1.6043	1.68828	1.71033	2
Range	0.04051	0.62505	0.90129	1994.74
Minimum	0.23512	3.6281	3.13846	2.19886
Maximum	0.27563	4.25315	4.03974	1996.94
Sum	1.04604	15.3552	13.7575	2004.5
Count	4	4	4	4
Confidence Level (95.0%)	0.02903	0.45204	0.65361	1586.78

4. CONCLUSIONS

The Barind region, Dinajpur district was selected for its special geographical character like its undulating topography having impenetrable and low productive soils. About 14 sub-parameters were analyzed and these sub-parameters were categorized into three parameters like basic, linear, and shape parameter. Under the basic parameter, the Purnovoba river had the highest area and maximum perimeter. Besides, the Purnovoba river was found a higher discharged rate and greater velocity of the stream as it contained the higher stream order (5^{th} order). On the other hand, the Jamuna river had only 3^{rd} order and stream length was only 159.21 km. The aftermath ascertained that the Jamuna river was considered as a lower discharged rate and fewer velocity of the stream. As the basin length described the geological structure of any watershed region Atrai river (part-1 & part-2) contained the highest length of basin. The bifurcation ratio of the Purnovoba river indicated the lack of structural control over the formation of drainage patterns and it was hydrologically more disturbed than other watersheds. In the study, the Atrai river part-1 was found a higher drainage density. The higher drainage density described the low vegetation and less permeable capacity. Jamuna river was considered as a lower drainage density that had high permeable subsoil material. Permeability, infiltration, and capacity of relief of any watershed depended on stream frequency. As the Purnovoba river had a higher stream frequency, it was rocky and low infiltration capacity. On the other hand, the Jamuna river was covered with more vegetation with higher permeability and less prone to cause flash floods. As the texture ratio was related to soil type or texture class and infiltration capacity of the watershed basin, the Purnovoba river resulted in decreasing infiltration capacity which decreased the availability of groundwater. In the study area, the length of overland flow resulted that the slope became gentle to Atrai river part-1. Under the shape parameter, the Jamuna river had a high form factor that defined the high peak flows with shorter duration and the Purnovoba river had a low form factor that defined the lower peak flows with longer duration. Measuring the shape factor, Purnovoba river contained a high shape factor with the shortest basin lag time and Atrai river part-2 contained a low shape factor with the longest basin lag time. As the value of elongation ratio was >1, all the watershed basins were considered as the deviation of the circular form. These findings will help for further modeling of an integrated watershed for sustainable hydrological and hydrograph models in the Barind region of Bangladesh. Besides, it will help the policymakers, planners, geographers, environmentalists, and many more who use GIS and RS techniques for solving hydrology-related problems such as irrigation, harvesting of surface water, cause of river erosion, surface stormwater runoff process, and water resource management.

ACKNOWLEDGEMENTS
The authors would like to thank the Survey of Bangladesh (SoB) and Bangladesh Meteorological Department for assisting this research by sharing the data-sets, . The authors are also thankful to the Dept. of URP at KUET, Khulna,

Dept. of URP at RUET, Rajshahi, and IBBBS at BSMRMU, Dhaka for providing the the software and lab assistances.

REFERENCES

Ahmed, S., Chandrashekarappa, K., Raj, S., Nischitha, V., & Kavitha, G. (2010). Evaluation of morphometric parameters derived from ASTER and SRTM DEM—a study on Bandihole sub-watershed basin in Karnataka. Indian society of remote sensing, 38(2), 227-238.

Ahn, S.-R., & Kim, S.-J. (2019). Assessment of watershed health, vulnerability and resilience for determining protection and restoration Priorities. Environmental Modelling & Software, 122, 103926.

Al-Assadi, K. H. F. (2020). Analyzing the morphometric characteristics of Wadi Mezal basin using geographical information systems. Groundwater for Sustainable Development, 100436.

Alam, A., Ahmed, B., & Sammonds, P. (2020). Flash flood susceptibility assessment using the parameters of drainage basin morphometry in SE Bangladesh. Quaternary International.

Alnahit, A. O., Mishra, A. K., & Khan, A. A. (2020). Quantifying climate, streamflow, and watershed control on water quality across Southeastern US watersheds. Science of The Total Environment, 139945.

Altaf, F., Meraj, G., & Romshoo, S. A. (2013). Morphometric analysis to infer hydrological behaviour of Lidder watershed, Western Himalaya, India. Geography Journal, 2013.

Ameri, A. A., Pourghasemi, H. R., & Cerda, A. (2018). Erodibility prioritization of sub-watersheds using morphometric parameters analysis and its mapping: A comparison among TOPSIS, VIKOR, SAW, and CF multi-criteria decision making models. Science of the Total Environment, 613, 1385-1400.

Amiri, M., Pourghasemi, H. R., Arabameri, A., Vazirzadeh, A., Yousefi, H., & Kafaei, S. (2019). Prioritization of flood inundation of Maharloo Watershed in iran using morphometric parameters analysis and TOPSIS MCDM model. In Spatial modeling in GIS and R for earth and environmental sciences (pp. 371-390): Elsevier.

Balasubramanian, A., Duraisamy, K., Thirumalaisamy, S., Krishnaraj, S., & Yatheendradasan, R. K. (2017). Prioritization of subwatersheds based on quantitative morphometric analysis in lower Bhavani basin, Tamil Nadu, India using DEM and GIS techniques. Arabian Journal of Geosciences, 10(24), 552.

Banerjee, A., Singh, P., & Pratap, K. (2017). Morphometric evaluation of Swarnrekha watershed, Madhya Pradesh, India: an integrated GIS-based approach. Applied Water Science, 7(4), 1807-1815.

Chandniha, S. K., & Kansal, M. L. (2017). Prioritization of sub-watersheds based on morphometric analysis using geospatial technique in Piperiya watershed, India. Applied Water Science, 7(1), 329-338.

Charizopoulos, N., Mourtzios, P., Psilovikos, T., Psilovikos, A., & Karamoutsou, L. (2019). Morphometric analysis of the drainage network of Samos Island (northern Aegean Sea): Insights into tectonic control and flood hazards. Comptes Rendus Geoscience, 351(5), 375-383.

Chatterjee, S., Krishna, A., & Sharma, A. (2014). Geospatial assessment of soil erosion vulnerability at watershed level in some sections of the Upper Subarnarekha river basin, Jharkhand, India. Environmental earth sciences, 71(1), 357-374.

Choudhari, P., Nigam, G. K., Singh, S. K., & Thakur, S. (2018). Morphometric based prioritization of watershed for groundwater potential of Mula river basin, Maharashtra, India. Geology, Ecology, and Landscapes, 2(4), 256-267.

Dragičević, N., Karleuša, B., & Ožanić, N. (2018). Improvement of Drainage Density Parameter Estimation within Erosion Potential Method. Paper presented at the Multidisciplinary Digital Publishing Institute Proceedings.

Du, H., Dou, S., Deng, X., Xue, X., & Wang, T. (2016). Assessment of wind and water erosion risk in the watershed of the Ningxia-Inner Mongolia Reach of the Yellow River, China. Ecological Indicators, 67, 117-131.

Elsadek, W. M., Ibrahim, M. G., & Mahmod, W. E. (2019). Runoff hazard analysis of Wadi Qena Watershed, Egypt based on GIS and remote sensing approach. Alexandria Engineering Journal, 58(1), 377-385.

Ervinia, A., Huang, J., Huang, Y., & Lin, J. (2019). Coupled effects of climate variability and land use pattern on surface water quality: An elasticity perspective and watershed health indicators. Science of The Total Environment, 693, 133592.

Fu, X., Hopton, M. E., Wang, X., Goddard, H., & Liu, H. (2019). A runoff trading system to meet watershed-level stormwater reduction goals with parcel-level green infrastructure installation. Science of The Total Environment, 689, 1149-1159.

Gajbhiye, S., Mishra, S., & Pandey, A. (2014). Prioritizing erosion-prone area through morphometric analysis: an RS and GIS perspective. Applied Water Science, 4(1), 51-61.

Ghorbani Nejad, S., Falah, F., Daneshfar, M., Haghizadeh, A., & Rahmati, O. (2017). Delineation of groundwater potential zones using remote sensing and GIS-based data-driven models. Geocarto international, 32(2), 167-187.

Gong, J., & Xie, J. (2009). Extraction of drainage networks from large terrain datasets using high throughput computing. Computers & Geosciences, 35(2), 337-346.

Harmel, R., Cooper, R., Slade, R., Haney, R., & Arnold, J. (2006). Cumulative uncertainty in measured streamflow and water quality data for small watersheds. Transactions of the ASABE, 49(3), 689-701.

Harsha, J., Ravikumar, A., & Shivakumar, B. (2020). Evaluation of morphometric parameters and hypsometric curve of Arkavathy river basin using RS and GIS techniques. Applied Water Science, 10(3), 1-15.

Horton, R. E. (1945). Erosional development of streams and their drainage basins; hydrophysical approach to quantitative morphology. Geological society of America bulletin, 56(3), 275-370.

Javed, A., Khanday, M. Y., & Rais, S. (2011). Watershed prioritization using morphometric and land use/land cover parameters: a remote sensing and GIS based approach. Geological Society of India, 78(1), 63.

Liu, B.-W., Wang, M.-H., Chen, T.-L., Tseng, P.-C., Sun, Y., Chiang, A., & Chiang, P.-C. (2020). Establishment and Implementation of Green Infrastructure Practice for Healthy Watershed Management: Challenges and Perspectives. Water-Energy Nexus.

Liu, K., Song, C., Ke, L., Jiang, L., & Ma, R. (2020). Automatic watershed delineation in the Tibetan endorheic basin: A lake-oriented approach based on digital elevation models. Geomorphology, 107127.

Metz, M., Mitasova, H., & Harmon, R. (2011). Efficient extraction of drainage networks from massive, radar-based elevation models with least cost path search. Retrieved from

Mokarram, M., & Hojati, M. (2017). Morphometric analysis of stream as one of resources for agricultural lands irrigation using high spatial resolution of digital elevation model (DEM). Computers and Electronics in Agriculture, 142, 190-200.

Okumura, M., & Araujo, A. G. (2014). Long-term cultural stability in hunter–gatherers: a case study using traditional and geometric morphometric analysis of lithic stemmed bifacial points from Southern Brazil. Archaeological Science, 45, 59-71.

Panhalkar, S., Mali, S., & Pawar, C. (2012). Morphometric analysis and watershed development prioritization of Hiranyakeshi Basin in Maharashtra, India. International journal of environmental sciences, 3(1), 525-534.

Patel, D. P., Dholakia, M. B., Naresh, N., & Srivastava, P. K. (2012). Water harvesting structure positioning by using geo-visualization concept and prioritization of mini-watersheds through morphometric analysis in the Lower Tapi Basin. Indian society of remote sensing, 40(2), 299-312.

Pondari, S., Dandabathula, G., Bera, A., Nagamani, P., & Amminedu, E. (2020). Characterization of drainage network of Brahmaputra river basin in Indian sub-continent using geospatial technologies. Science, Technology and Environment Informatics, 8(01), 583-594.

Poongodi, R., & Venkateswaran, S. (2018). Prioritization of the micro-watersheds through morphometric analysis in the Vasishta Sub Basin of the Vellar River, Tamil Nadu using ASTER Digital Elevation Model (DEM) data. Data in brief, 20, 1353-1359.

Prasannakumar, V., Vijith, H., & Geetha, N. (2013). Terrain evaluation through the assessment of geomorphometric parameters using DEM and GIS: case study of two major sub-watersheds in Attapady, South India. Arabian Journal of Geosciences, 6(4), 1141-1151.

Rashid, M. B., Islam, M. B., & Sultan-Ul-Islam, M. (2013). Causes of acute water scarcity in the Barind Tract, Bangladesh. Economic and Environment Geology, 4(1), 5-14.

Ratnam, K. N., Srivastava, Y., Rao, V. V., Amminedu, E., & Murthy, K. (2005). Check dam positioning by prioritization of micro-watersheds using SYI model and morphometric analysis—remote sensing and GIS perspective. Indian society of remote sensing, 33(1), 25.

Rong, Q., Cai, Y., Su, M., Yue, W., Yang, Z., & Dang, Z. (2019). A simulation-based bi-level multi-objective programming model for watershed water quality management under interval and stochastic uncertainties. Environmental Management, 245, 418-431.

Saha, A., Joseph, J., & Ghosh, S. (2020). Climate controls on the terrestrial water balance: Influence of aridity on the basin characteristics parameter in the Budyko framework. Science of The Total Environment, 139863.

Schumm, S. A. (1956). Evolution of drainage systems and slopes in badlands at Perth Amboy, New Jersey. Geological society of America bulletin, 67(5), 597-646.

Senter, A. E., Pasternack, G. B., Piegay, H., Vaughan, M. C., & Lehyan, J. S. (2017). Wood export varies among decadal, annual, seasonal, and daily scale hydrologic regimes in a large, Mediterranean climate, mountain river watershed. Geomorphology, 276, 164-179.

Soni, S. (2017). Assessment of morphometric characteristics of Chakrar watershed in Madhya Pradesh India using geospatial technique. Applied Water Science, 7(5), 2089-2102.

Sreedevi, P., Owais, S., Khan, H., & Ahmed, S. (2009). Morphometric analysis of a watershed of South India using SRTM data and GIS. Geological Society of India, 73(4), 543-552.

Strahler, A. N. (1964). Handbook of applied hydrology. Quantitative geomorphology of drainage basins and channel networks. New York, NY: Mc-Graw Hill Book Company, 39-76.

Sujatha, E. R., Selvakumar, R., & Rajasimman, B. (2014). Watershed prioritization of Palar sub-watershed based on the morphometric and land use analysis. Mountain Science, 11(4), 906-916.

Suresh, M., Sudhakar, S., Tiwari, K., & Chowdary, V. (2004). Prioritization of watersheds using morphometric parameters and assessment of surface water potential using remote sensing. Indian society of remote sensing, 32(3), 249-259.

Tykocki, T., du Plessis, J., & Wynne-Jones, G. (2018). Analysis of morphometric parameters in cervical canal stenosis on neutral and dynamic magnetic resonance imaging. World neurosurgery, 114, e317-e322.

Wada, C. A., Pongkijvorasin, S., & Burnett, K. M. (2020). Mountain-to-sea ecological-resource management: Forested watersheds, coastal aquifers, and groundwater dependent ecosystems. Resource and Energy Economics, 59, 101146.

Withanage, N., Dayawansa, N., & De Silva, R. (2014). Morphometric analysis of the Gal Oya river basin using spatial data derived from GIS. Tropical Agricultural Research, 26(1), 175-188.

MIJST
MIST International Journal of Science and Technology

Effect of Admixture on Physical and Mechanical Properties of Recycled Brick Aggregate Concrete

Md. Jahidul Islam[1*], Md. Shahjalal[2], Md. Mehedi Hasan[3], and Zarin Tasnim Chowdhury[4]

Department of Civil Engineering, Military Institute of Science and Technology (MIST), Dhaka, Bangladesh

emails: *[1]mjislam@ce.mist.ac.bd; [2]shahjalal@ce.mist.ac.bd; [3]mehediopu74@gmail.com; and [4]zarintasnimch117@gmail.com*

ARTICLE INFO

Article History:

Received: 18th January 2021
Revised: 25th March 2021
Accepted: 31th March 2021
Published: 27th June 2021

Keywords:

Recycled Brick Aggregate
Chemical Admixture
Compressive Strength
Tensile Strength
High-Temperature Exposure

ABSTRACT

With the increasing population of the world, the rate of development of infrastructure is increasing day by day; which has placed a massive demand for natural aggregates. Besides, huge amount of demolished construction wastes are generated all over the world which creates pressure on the environment as well as landfills. Therefore, it is necessary to find a sustainable solution to adopt these C&D wastes as an alternative to natural aggregates for construction purposes. Therefore, the objective of the present study is to explore the influence of superplasticizers while adopting recycled brick aggregate (RBA) in the sustainable concrete application as a coarse aggregate. Six different mixes are considered with 100% replacement of recycled brick aggregate and three diverse water-cement (w/c) ratios, such as 0.40, 0.45, and 0.50. To improve the workability and mechanical characteristics of concrete a superplasticizer is used as an admixture. Fresh properties of concrete, compressive strength at normal and high temperatures, flexural strength and splitting tensile strength are presented. The results indicate that addion of superplasticizer improves slump values and reduces air voids of concrete. Although strengths of RBA concrete are lesser than the virgin brick aggregate concrete, they are still satisfactory in the application for structural concrete and can be also significantly improved by incorporating admixture. Finally, this research will help to recycle the brick aggregate instead of dumping it as waste in a landfill.

1. INTRODUCTION

The concrete industry is facing towering challenges to meet up the consumption of natural resources such as natural stone and sand because of the growing demand for production and utilization of concrete all over the world. Every year almost 17.5 billion tons of concrete are produced worldwide which equals 2.5 tons of concrete per person per year (Barcelo, 2013; Mehta, 2009). To meet this demand almost 10 to 12 billion tons of aggregates are used all over the world per year (Smith, 2010). Aggregates are generally collected by mining stone quarries and staving river gravels. In near future, stone quaries will dry up and sources for natural aggregate will be exhausted.

A large amount of demolished construction waste is generated from the repair work of old infrastructures. Almost 2–3 billion tons of demolished concrete is estimated globally which is 30% to 40% of total solid wastes (C&D Waste Management Guide, 2016; Rodríguez-Robles et al., 2015). In many parts of the world, these wastes are dump into landfills. Therefore, it is necessary to release this pressure on land sites as well as to find the alternative of natural aggregates for construction purposes. One of the possible solutions is to reuse them in such a way where these C&D wastes cannot affect the environment. Various research has been conducted to reuse the alternative materials like recycled stones and crumb rubber (Hossain et al., 2019; Shahjalal et al., 2019; Shahjalal et al., 2021), FRP scrap aggregate (Alam et al., 2013), Poly-Ethylene Terephthalate (PET) (Islam et al., 2018; Islam et al., 2016), brick (Islam et al., 2020) recycled brick (Mohammed et al., 2015), etc.

Many of the old structures in Bangladesh are constructed with bricks that are now out of their service and the brick aggregates obtained from these demolished structures can be used in new structures as coarse aggregate. Sustainable construction has gotten much attention among researchers to design and construct sustainable, resilient, and environmentally friendly structures. Therefore, it is

essential to identify the properties of these recycle waste materials before using them in structural concrete.

Mohammed et al. (2015) collected recycled brick aggregate from various building sites of different ages. From their study they found that up to 50% replacement of virgin first-class brick aggregates (FBA) by recycled brick aggregates (RBA), there is very little change in compressive strength of concrete. It was also found that about 20.7 MPa to 31 MPa concrete can be made easily with RBA and the workability of concrete made with RBA is lower than the concrete prepared with FBA. Another study found that for the w/c ratio of 0.45 and 0.55, the average strength of RBA concrete was 24.7 MPa and 20.4 MPa, respectively which is very close to the available design strength of concrete used in Bangladesh for various structures (Mohammed et al., 2013b). Mohammed and Hasnat (2014) found no significant difference in modulus of rapture and splitting tensile strength of RBA concrete compared with virgin FBA concrete.

Mohammed et al. (2013a) tried to improve the workability of recycled aggregate concrete (RAC) where aggregates were coated with cement paste; and found that the application of coating over the RCA can improve the workability of concrete and reduce the absorption capacity of aggregate. In the case of mechanical properties, like compressive and splitting tensile strengths, and Young's Modulus of concrete, a benefit of the coating was found for w/c of 0.55; but not found any significant improvement for w/c ratio of 0.45.

The durability properties of RAC can be strongly influenced by the higher water absorption capacity and porosity of RCA. Kou et al. (2011) studied the pore size distribution and long-term mechanical properties of recycled aggregate concrete (RAC). It was observed that the porosity of RBA had a higher value compared to the crushed new brick aggregates and had a higher water requirement when used as aggregate in concrete. It was also found that the porosity and compressive strength had an inverse relationship for RBA concrete.

It is conceivable to obtain comparatively higher compressive strength from RAC than natural aggregate concrete (NAC); and the properties of RAC can be significantly improved by using superplasticizers admixture and silica fume (Ajdukiewicz & Kliszczewicz, 2002). Ajdukiewicz and Kliszczewicz (2002) found that with an application of admixtures RAC of 80 MPa was achievable from NAC of 60 MPa.

Kou et al. (2014) worked with the effects of high temperature (300ºC, 500ºC, and 800ºC) exposure of RBA concrete. Before exposure the concrete to high temperature, the NAC showed lower capillary absorption capacity and higher compressive strength than that of RBA concrete. After exposure to 300ºC, though the mechanical properties of all concrete (NAC and RBA concrete) improved, the capillary absorption capacity increased. On the other hand, it was seen that after exposure to 500ºC and 800ºC the NAC suffered higher deteriorations than RAC for all the tested properties especially the splitting tensile strength as well as the capillary absorption capacity. The authors concluded that the RCA suffered fewer degradations in mechanical and durability properties than that of NCA at high temperatures.

In Bangladesh, many of the old infrastructures are constructed with brick aggregate which is now out of their services. A large amount of recycled brick aggregate will be generated in the future. So, it will be a great challenge to manage these huge demolished recycled brick concrete. From the literature, it is seen that using recycled aggregate can reduce the strength of concrete.Thus using admixture can play a significant role to improve this strength. One of the prime objectives of this study is to improve recycled aggregate concrete strength without increasing the cement content through addition of admixture. Besides, the mechanical behavior of recycled brick aggregate at high temperatures should also be investigated. Though the effect of admixtures, such as superplasticizers and high-temperature exposure on the physical and mechanical properties of concrete with recycled stone aggregate has been studied extensively, there are very limited studies yet to be reported on the physical and mechanical properties of concrete with recycled brick aggregate and superplasticizers subjected to elevated temperature exposure. Therefore, in the present study physical and mechanical behavior of RBA is studied while incorporating admixture and compare them with FBA as well as RBA concrete without admixture.

2. EXPERIMENTAL INVESTIGATION

A. Materials

The materials used for concrete mixtures include virgin first-class brick aggregate (FBA), recycled brick aggregate (RBA), natural fine aggregate (NFA), Portland composite cement (PCC), and admixture. The RBA was collected from the demolished brick concrete blocks of a 30 years old residential building shown in Figure 1. Then the collected blocks were broken manually into three particular sizes such as 25 mm to 19.5 mm, 19.5 mm to 9.5 mm, and 9.5 mm to 4.75 mm which was ensured by sieving them with a sieve shaker. After crushing into pieces, the aggregates were mixed as 5% retained on 19.5 mm, 60% retained on 9.5 mm, and 35% retained on 4.75 mm seive as per ASTM (ASTM C33/C31M, 2018). The gradation of brick chips and NFA were selected in such a manner that they fall within the ASTM lower and upper limits (ASTM C33/C31M, 2018). The particle distribution plot of brick chips and NFA is presented in Figure 2. All the physical and mechanical properties of aggregates are summarized in Table 1. As shown in the table, the absorption capacity of RBA is higher than the FBA. Furthermore, mechanical properties, such as Los Angeles abrasion (LAA) value, aggregate crushing value (ACV), and aggregate impact value (AIV), for RBA is lower than the FBA indicating inferior aggregate quality.

Portland Composite Cement (PCC), specified as BDS EN 197-1:2010, CEM II/B-M (S-V-L) 42.5 N, is the most common type of cement used in Bangladesh. It is relatively cheaper than Ordinary Portland Cement (OPC) and easily available in local market. Therefore, in the present study PCC is adopted as the binding material for concrete. The

physical and chemical and physical properties of PCC were determined. The major chemical compounds of PCC are CaO – 64.82%, Al_2O_3 – 4.74%, SiO_2 – 20.60%, Fe_2O_3 – 3.28%, and LOI – 1.73%. Specific gravity and normal consistency of PCC are 2.95 and 26.7%, respectively. The admixture used in this study is a synthetic polymer-based high range water reducing superplasticizer following ASTM C494 (2019). This admixture is used to reduce the amount of mixing water while maintaining control on the extend of set retardation.

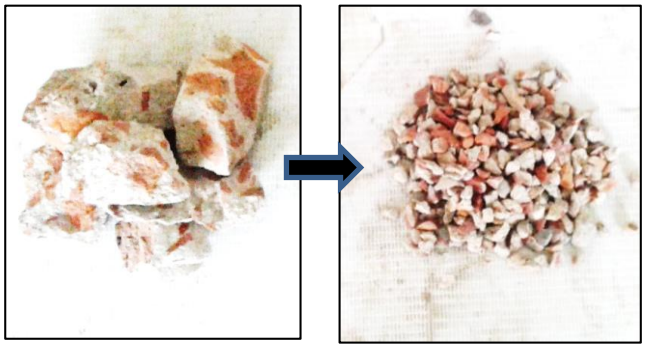

Figure 1: Demolished brick concrete block and recycled brick aggregates

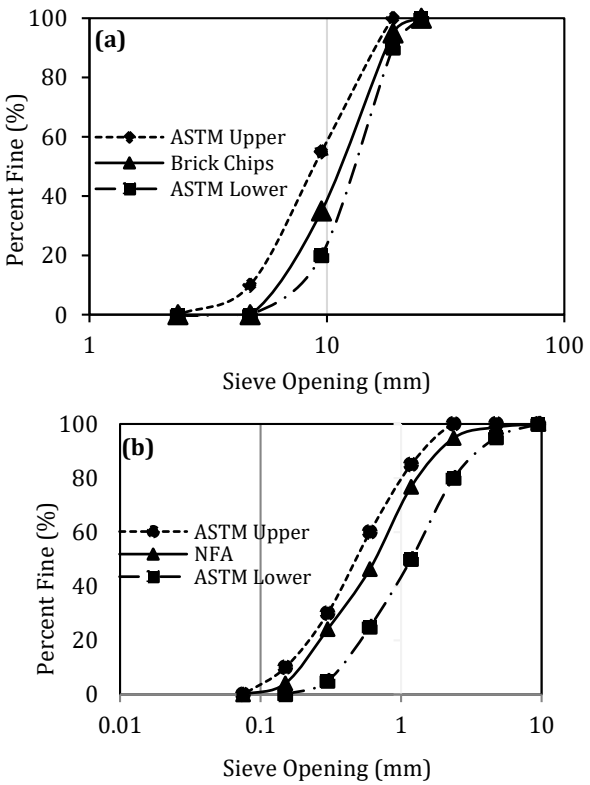

Figure 2: The gradation curve of (a) brick aggregate and (b) NFA

B. Mixture Proportions

Seven variant concrete mixtures were produced for this study. Among them, six of the mixtures were prepared with recycled brick aggregate (RBA) and the rest was made with virgin first-class brick aggregate (FBA). Water-cement (w/c) ratios of 0.40, 0.45, and 0.50 were considered for RBA, and w/c ration of 0.50 is considered for virgin FBA, as a control mix, to compare the results. Among the six mixtures of RBAs, three of them were with admixture and the other three were without admixture. The mix proportions of the seven different mixes are summarized in Table 2. Each mix design is designated with a unique name for ease in referencing within the text. For example, Batch name $RB_{40}A$ indicates that the coarse aggregate used in this mixture is RBA, 40 means the w/c ratio is 0.40 and 'A' is designated for admixture. The other batches are named in the same manner. On the other hand, FB_{50} means that the coarse aggregates used in this mixture are FBA, and 50 means the w/c ratio is 0.50.

Table 1
Properties of FBA, RBA and NFA

Variables	FBA	RBA	NFA
SSD Specific Gravity	2.08	1.98	2.37
OD Specific Gravity	1.96	1.82	2.32
Absorption Capacity (%)	14.55	18.74	1.87
Fineness Modulus	7.05	7.05	2.55
Unit Weight-Loose (kg/m³)	958	999	1476
Unit Weight-Compact (kg/m³)	1022	1055	1557
Void % (Loose)	45.9	38.7	40.1
Void % (Compact)	43.2	37.2	35.7
LAA value (%)	37	43.5	-
ACV (%)	30	40	-
AIV (%)	36	44	-

C. Specimens

A total of 126 cylinders (200 mm height × 100 mm diameter) were prepared to determine different properties of concrete. The compressive strength was determined after 7 days, 28 days, and 56 days at normal temperature and to determine the change of compressive strength in high temperature two different temperatures are used (400ºC and 600ºC). After 28 days the concrete cylinder samples were exposed to higher temperatures of 400ºC and 600ºC with the help of an electric oven. It took the oven about 10 minutes to reach the peak temperatures and then the samples were kept at a constant temperature for an hour. After an hour the oven was turned off and samples were then cooled down. Once the sample was cool down to room temperature the compressive strength test was done. The splitting tensile strength of concrete was determined at 28 days.

To determine the flexural strength of concrete, a total of 21 beams with a sample size of 100 mm × 100 mm × 500 mm were prepared. The test was done at 28 days. A vibrator was used to compact the fresh concrete in molds. After casting, the specimens were kept in a controlled room for 24 hours, and then demolded. After demolding, the specimens were cured in a water curing tank at a constant temperature (23 ± 1ºC) for 28 days except for samples that were tested at 7 days.

Table 2
The proportion of water, cement, aggregates, and admixture for a cubic meter of concrete

Batch Code	W/C Ratio	Water (kg)	Cement (kg)	FBA/ RBA (kg)	NFA (kg)	Admixture (l)
FB_{50}	0.50	205	410	675†	720	-
RB_{40}	0.40	205	513	675	643	-
RB_{45}	0.45	205	456	675	686	-
RB_{50}	0.50	205	410	675	720	-
$RB_{40}A$	0.40	185	513	675	685	1.29
$RB_{45}A$	0.45	185	456	675	729	1.11
$RB_{50}A$	0.50	185	410	675	765	0.92

Note: †FBA

D. Testing Procedure

Slump value test and air content test of fresh concrete samples were determined according to ASTM C143 (2015) and ASTM C231 (2017), respectively. The compressive strength test, as shown in Figure 3(a), was performed according to ASTM C39 (2018) and the loading rate was kept at 0.25 ± 0.05 MPa/s. The splitting tensile strength test was conducted following ASTM C496 (2014) and the flexural strength of the concrete prisms was perfomred following ASTM C78 (2016). The flexural strength test was performed at the one third point with a displacement rate of 0.15 mm/min. The tests set up for different tests are shown in Figure 3.

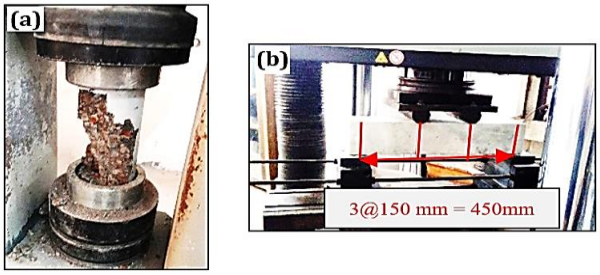

Figure 3: Test setup for (a) compression test (b) flexural test

3. RESULTS AND DISCUSSIONS

The effects of using RBA, on fresh and mechanical properties of concrete, such as workability, air content, compressive strength at room temperature and high temperature, splitting tensile and flexural strengths are presented in this section.

A. Fresh Concrete Properties

The slump values and air content of vaious combinations of concrete mixes are shown in Figure 4. Comparing between FB_{50} and RB_{50} it is observed that RBA concrete showed a slightly lower slump value (112 mm) than that of virgin FBA concrete (115 mm) due of its higher surface roughness and absorption capacity. Furthermore, slump values were increased with the increase in w/c ratio and with the incorporation of admixture into the concrete mix. On the other hand, the fresh air content value had an inverse relation with the w/c ratio. The lower w/c ratio concrete showed the higher air content and it decreased when the admixture was added into the concrete by improving the flowablity of concrete. $RB_{50}A$ showed the highest slump value (124 mm) and lowest air content value (1.97%).

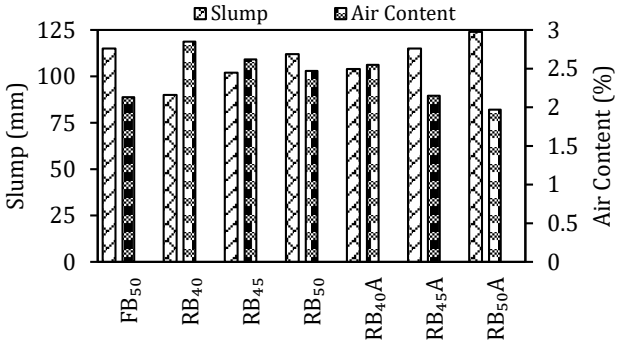

Figure 4: Sump value and air content of different concrete mixtures

B. Compressive Strength

The compressive strength of hardened concrete at 7, 28, and 56 days is presented in Figure 5. Overall, it is seen that the compressive strengths were increased by almost 36% and 46% at 28 days and 56 days compared to 7 days. For the w/c ratio of 0.5, it is observed that the compressive strength of RBA concrete (RB_{50}) was decreased by 8.8% compared to virgin FBA concrete (FB_{50}) at 28 days. This may happen because of the mortar attached on the surface of the aggregate which may weaken the interfacial transition zone (ITZ) and have a weaker bond between the virgin cement mortar matrix and existing mortar on the aggregate surface. This behavior is consistent with the previous studies (Arabiyat et al., 2021; Hossain et al., 2019; Mohammed et al., 2015). After adding admixture with this RBA concrete of the same w/c ratio ($RB_{50}A$), the compressive strength was increased by 5.2% compared to the control mix (FB_{50}). When there was no admixture in RBA concrete, the compressive strength was decreased with the increasing w/c ratios. For the three different w/c ratios (0.40, 0.45, and 0.50), the compressive strengths varied from 41.40 MPa to 47.55 MPa. After adding admixture this range varied from 47.72 MPa to 52.94 MPa. This incremental trend is also observed for compressive strengths at 7 days and 56 days. All the compressive strengths of RBA concrete were more than 40 MPa which is enough for structural concrete. The failure pattern of concrete cylinders subjected to compressive load is presented in Figure 6 (a & b). Most of the concrete cylinders showed cone and shear failure.

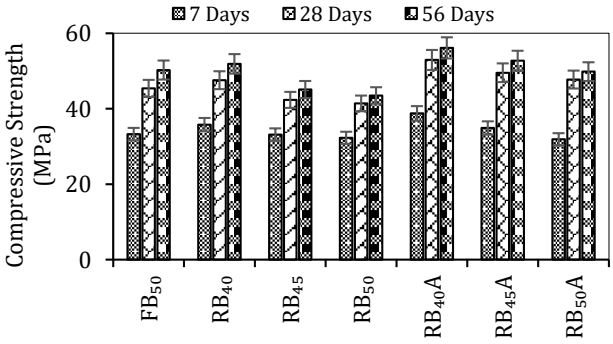

Figure 5: Variation in compressive strength of various combinations of concrete at different ages

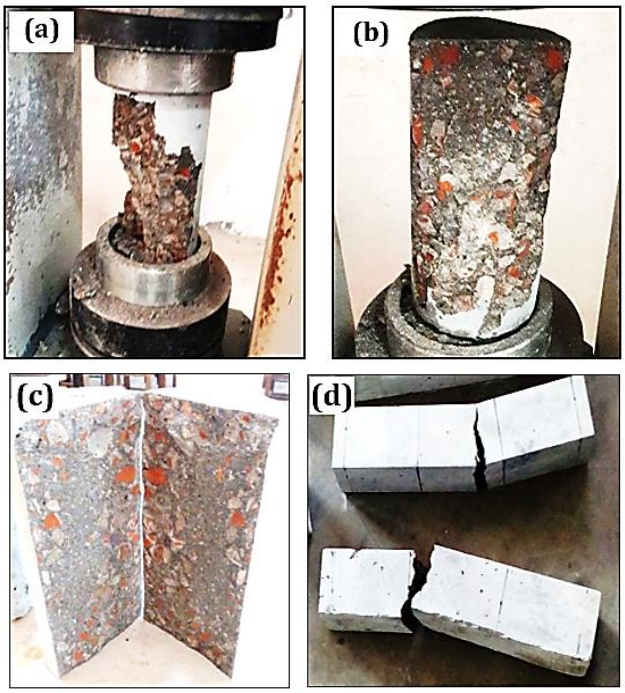

Figure 6: Failure pattern of the concrete cylinder under (a & b) compressive strength test (c) splitting tensile strength test (d) beam flexural strength test

C. Effect of Temperature on Compressive Strength

Effect of high temperature on compressive strength of concete was studied. Concrete goes through mineralogical changes when subjected to heat. Around 250ºC to 350ºC temperature suffered damage because of the pore water pressure development. Furtheremore, at about 600ºC reinforcements in reinforced concrete become half of its room temperature strength. Therefore, in the present study two tempartures were selected for high temperature study, that is 400ºC and 600ºC.

The compressive strengths of concrete at 28 days after subjected to 0ºC, 400ºC and 600ºC temperature is presented in Figure 7. After exposed to 400ºC, the compressive strengths of RBA concrete without admixture were decreased by 10.1%, 12.8%, and 14.4% for the w/c ratio of 0.40, 0.45, and 0.50, respectively compared to concrete compressive strength at room temperature; whereas, for 600ºC exposure compressive strength were reduced by 26.3%, 24.7%, and 32.2%, respectively. On the other hand, for RBA concrete with admixture after exposed to 400ºC, the compressive strengths were decreased by 17.1%, 18.2%, and 21.4% for the w/c ratio of 0.40, 0.45, and 0.50, respectively; whereas, for 600ºC exposure compressive strengths were reduced by 27.2%, 32.3%, and 29.8%, respectively. Reduction of compressive strength at 400ºC temperature was higher for RBA with admixtures. However, at 600ºC temperature, it became consistent with RBA without admixture.

D. Splitting Tensile Strength

The splitting tensile strengths of different concrete mixes are shown in Figure 8. The tensile strengths were decreased with increasing w/c ratio. For the w/c of 0.5, the tensile strength of RBA concrete was decreased by 7.8% compared to virgin FBA concrete but it was increased by 15.3% after adding admixture with it. For the w/c ratio of 0.40, the tensile strength was 2.77 MPa which was increased to 3.42 MPa after adding admixture into it; and for the 0.45 w/c ratio this strength was 2.61 MPa and 3.31 MPa without admixture and with admixture, respectively. For all cases of RBA concrete without admixture, the tensile strength was more than 2.45 MPa. It can be concluded that the tensile strengths are slightly decreased for RBA concrete and it can be easily compensated by adding admixture.

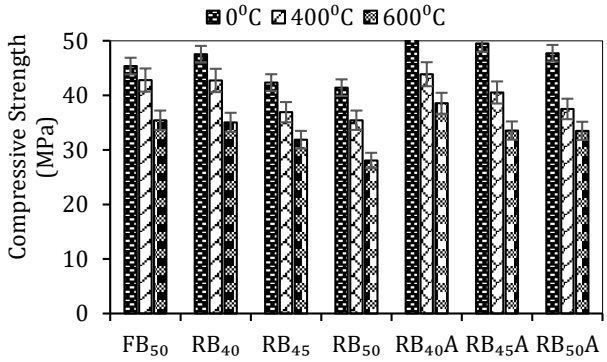

Figure 7: Compressive strengths at high temperature

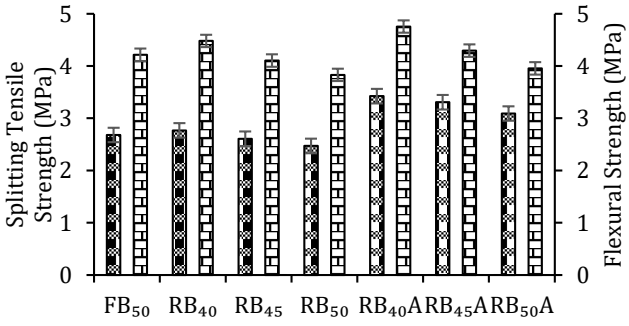

Figure 8: Variation in splitting tensile strength and flexural strength of different concrete mixtures at 28 days

E. Flexural Strength

The flexural strength of concrete of different batches is presented in Figure 8. The flexural strength shows a similar pattern to splitting tensile strength. Comparing between the same w/c ratio (0.50) concrete composed with virgin brick aggregate (FB_{50}) and recycled brick aggregate (RB_{50}) it is seen that the flexural strength was decreased almost 9.1% for RBA. The recycled brick aggregate had a low water absorption capacity compare to the FBA which results in a higher free water in the concrete mixture which weakens the ITZ. The same pattern was also observed in previous studies (Hossain et al., 2019). However, Mohammed and Hasnat (2014) found almost no decernable changes in flexural strength of the recycled brick aggregate and first-class brick aggregate concrete. Reducing the w/c increases the flexural strength as observed from the test results. For the w/c ratio of 0.40 and 0.45, these strengths were 4.48 MPa and 4.11 MPa which were more than the w/c ratio of 0.5 (3.83 MPa) for recycled brick. The addition of the admixture also increased the flexural strength of concrete. After adding admixture, the strengths were 4.76 MPa, 4.30 MPa, and 3.96 MPa which were 6.1%, 4.6%, and 3.3% more compared to the combinations without admixture.

F. Comparison of Strength Properties with the Standard Codes

Studies show that there is a strong correlation between compressive strength and splitting tensile strength or flexural strength of concrete. To predict these strengths there exist various guidelines and equations. In this section, design recommendations from the ACI, CSA, Euro-code (EC2), fib, and available equations given by various researchers are used to predict the splitting tensile and flexural strengths of the concrete specimens which is illustrated in Table 3 and Figure 9. Then these predicted values are paralleled with the experimental results shown in Figure 10. From the ratio between theoretical and experimental values, it can be predicted whether the existing guidelines over-estimate or under-estimate the experimental results of recycled bricks. The ratio between theoretical and experimental values is greater than 1 means over-estimate while less than 1 means under-estimate the experimental result. It can be seen that all the equations show an over-prediction.

Table 3
Splitting tensile strength and module of rupture

Splitting tensile strength	ACI 318 (2014)	$f_{t,sp} = 0.556\sqrt{f'_C}$; where $f_{t,sp}$ is splitting tensile strength (MPa) and f'_C is the compressive strength of concrete (MPa).
	fib2010 (fib, 2010)	$f_t = 0.3(f'_C)^{\frac{2}{3}}$; where f_t is tensile strength (MPa). and f'_C is compressive strength (MPa).
	EC2 (EN 1992-1-1, 2005)	$f_t = \alpha_{sp}\, f_{t,sp}$; where EC2 recommends the value of α_{sp} as 0.9
	Mohammed et al. (2015)	$f_t = 0.50\sqrt{f'_C}$; where f_t is tensile strength (MPa).
Modulus of rupture	ACI 318 (2014)	$f'_r = 0.62\sqrt{f'_c}$; where f_r is the modulus of rupture (MPa) and f'_C is in MPa.
	fib2010 (fib, 2010)	$f'_r = \frac{0.3((f'_C)^{\frac{2}{3}})}{\alpha_{fl}}$; where, $\alpha_{fl} = \frac{0.06h_b^{0.7}}{1+0.06h_b^{0.7}}$ and h_b = depth of beam (mm); f'_C is in MPa
	CSA A23.3-14 (2014)	$f'_r = 0.6\lambda\sqrt{f'_c}$; where $\lambda = 1.0$ for normal density concrete and f'_C is in MPa.
	Akhtaruzzaman and Hasnat (1983)	$f_r = 0.69\sqrt{f'_C}$; where f_r and f'_C is in MPa.
	Carasquillo et al. (1981)	$f_r = 0.97\sqrt{f'_C}$; where where f_r and f'_C is in MPa.
	Mohammed and Hasnat (2014)	$f_r = 0.95\sqrt{f'_C}$; where where f_r and f'_C is in MPa.

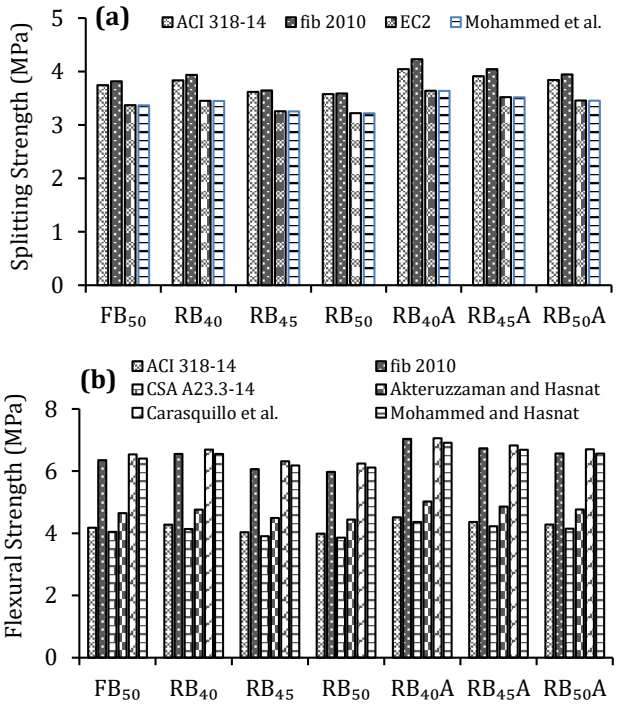

Figure 9: Comparison of (a) splitting tensile strength, and (b) flexural strength of concrete with different equations

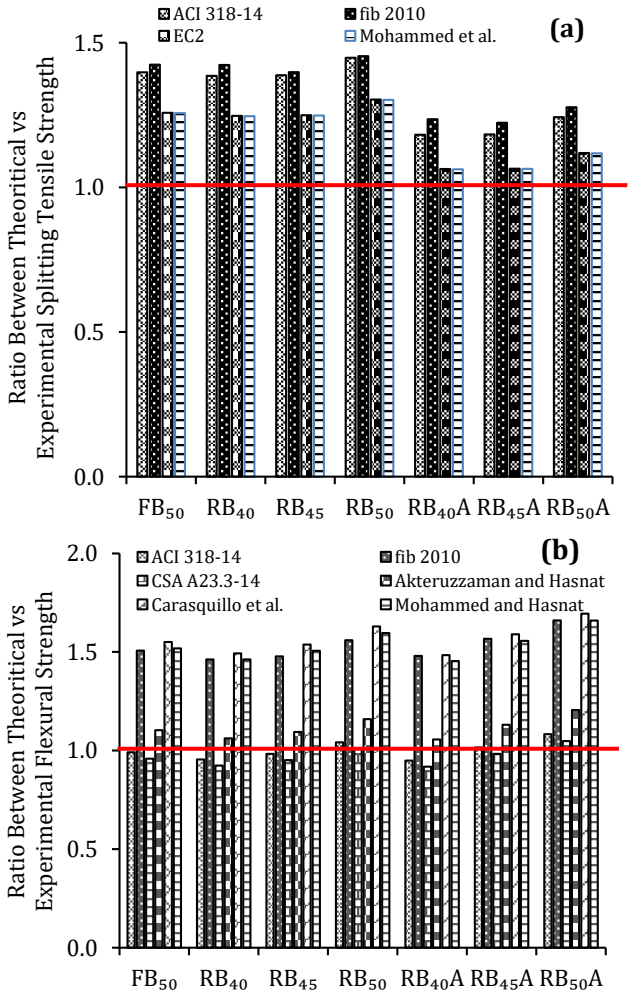

Figure10: Ratio between theoretical and experimental values of (a) splitting tensile strength, and (b) flexural strength using available equations

4. CONCLUSIONS

From the experimental program carried out in the present study, the following conclusions can be drawn:

- The slump values and air content of all RBA concrete without admixture show lower slump values and higher air content values than that of the control mix which can be improved by incorporating water-reducing superplasticizer into RBA concrete.
- The compressive strengths of RBA concrete are slightly decreased compared to virgin FBA concrete for all ages up to 8.8%. After adding admixture with this RBA concrete this disadvantage can be improved up to 16.7%. It is possible to make more than 40 MPa concrete with RBA aggregate which can be easily used in any structural member.
- The compressive strengths of concrete at 600ºC are decreased by almost 15.6% compared to 400ºC. Though the compressive strengths are decreased at high temperature (600ºC), they are still more than 28 MPa without admixture and more than 33 MPa with admixture.
- For RBA concrete, the splitting tensile strengths show more than 2.45 MPa. The tensile strengths are slightly (7.8%) decreased for RBA concrete compared to virgin FBA concrete and it can be easily compensated by adding admixture into the concrete.
- The flexural strength is decreased by almost 9.1% for recycled brick compared to virgin FBA concrete. After adding admixture into the RBA concrete, the flexural strengths are increased by 6.1%, 4.6%, and 3.3% compared to the combinations without admixture for the w/c ratio of 0.40, 0.45, and 0.50, respectively.
- The available design guidelines and equations over-predict the splitting tensile and flexural strengths of recycled brick concrete. Extensive investigation is needed for predicting the actual behavior of recycled brick aggregate.

DECLARATION OF COMPETING INTEREST

The authors declare that there are no conflict of interest.

ACKNOWLEDGEMENTS

This study was funded by the Military Institute of Science and Technology (MIST) and work was carried out at the Concrete Laboratory of Civil Engineering Department, MIST, Dhaka, Bangladesh.

REFERENCES

ACI 318-14. (2014). Building Code Requirements for Structural Concrete and Commentary. American Concrete Institute.

Ajdukiewicz, A., & Kliszczewicz, A. (2002). Influence of recycled aggregates on mechanical properties of hs/hpc. Cement & Concrete Composites, 24, 269–279.

Akhtaruzzaman, A., & Hasnat, A. (1983). Properties of Concrete Using Crushed Brick as Aggregates. Concrete International, 5(2), 58-63.

Alam, M. S., Slater, E., & Billah, A. H. M. M. (2013). Green concrete made with rca and frp scrap aggregate: Fresh and hardened properties. Journal of Materials in Civil Engineering, 25, 1783-1794.

Arabiyat, S., Abdel Jaber, M. t., Katkhuda, H., & Shatarat, N. (2021). Influence of using two types of recycled aggregates on shear behavior of concrete beams. Construction and Building Materials, 279, 122475. doi:https://doi.org/10.1016/j.conbuildmat.2021.122475

ASTM C33/C31M. (2018). Standard Specification for Concrete Aggregates. ASTM International, West Conshohocken, PA.

ASTM C39. (2018). Standard Test Method for Compressive Strength of Cylindrical Concrete Specimens. ASTM International, West Conshohocken, PA.

ASTM C78/C78M. (2016). Standard Test Method for Flexural Strength of Concrete (Using Simple Beam with Third-Point Loading). ASTM International, West Conshohocken, PA.

ASTM C143. (2015). Standard Test Method for Slump of Hydraulic-Cement Concrete. ASTM International, West Conshohocken, PA.

ASTM C231. (2017). Standard Test Method for Air Content of Freshly Mixed Concrete by the Pressure Method. ASTM International, West Conshohocken, PA.

ASTM C494/C494M. (2019). Standard Specification for Chemical Admixtures for Concrete. In ASTM International (pp. West Conshohocken, PA).

ASTM C496. (2014). Standard Test Method for Splitting Tensile Strength of Cylindrical Concrete Specimens. ASTM International, West Conshohocken, PA.

Barcelo, L. (2013). A path towards more sustainable cement. ACI fall convention, Phoenix, USA, 24.

C&D Waste Management Guide. (2016). Minimizing construction & demolition waste. . Department of Health, Office of Solid Waste Management, Honolulu, HI.

Carrasquillo, R. L., Nilson, A. H., & Slate, F. O. (1981). Properties of High-Strength Concrete Subjected to Short-Term Loads. ACI Journal Proceedings, 78(3), 171-178.

CSA A23.3-14. (2014). Design of Concrete Structures. Canadian Standards Association.

EN 1992-1-1. (2005). Eurocode 2–Design of Concrete Structures–Part 1–1: General Rules and Rules for Buildings. Thomas Telford, London, UK.

fib. (2010). fib Model Code for Concrete Structures. International Fedaration for Structural Concrete.

Hossain, F. M. Z., Shahjalal, M., Islam, K., Tiznobaik, M., & Alam, M. S. (2019). Mechanical properties of recycled aggregate concrete containing crumb rubber and polypropylene fiber. Construction and Building Materials, 225, 983–996.

Islam, M. J., Dipta, I. A., & Rahat, M. (2018). Investigation of recycled poly-ethylene terephthalate (PET) as partial replacement of coarse aggregate in concrete. Journal of Civil Engineering (IEB), 46(1), 11-20.

Islam, M. J., Meherier, M. S., & Islam, A. K. M. R. (2016). Effects of waste pet as coarse aggregate on the fresh and harden properties of concrete. Construction and Building Materials, 125, 946-951.

Islam, M. J., Rahman, J., Nawshin, S., & Islam, M. M. (2020). Comparative Study of Physical and Mechanical Properties of Machine and Manually Crushed Brick Aggregate Concrete. MIST International Journal of Science and Technology, 8(1). doi:10.47981/j.mijst.08(01)2020.188(01-09)

Kou, S. C., Poon, C. S., & Etxeberria, M. (2011). Influence of recycled aggregates on long term mechanical properties and pore size distribution of concrete. Cement & Concrete Composites, 33, 286–291.

Kou, S. C., Poon, C. S., & Etxeberria, M. (2014). Residue strength, water absorption and pore size distributions of recycled aggregate concrete after exposure to elevated temperatures. Cement & Concrete Composites, 53, 73–82.

Mehta, P. K. (2009). Global concrete industry sustainability. ACI Concr. Int., 32(2), 45-48.

Mohammed, T. U., & Hasnat, A. (2014). Modulus of rupture of concrete made with recycled brick aggregate. The 6th International Conference of Asian Concrete Federation, Seoul, Korea.

Mohammed, T. U., Hasnat, A., Awal, M. A., & Bosunia, S. Z. (2013a). Recycling of brick aggregate concrete :An extended study on some key issues. Third International Conference on Sustainable Construction Materials and Technologies, Japan.

Mohammed, T. U., Hasnat, A., Awal, M. A., & Bosunia, S. Z. (2013b). Recycling of brick aggregate concrete: Physical and mechanical properties. Third International Conference on Sustainable Construction Materials and Technologies, Japan.

Mohammed, T. U., Hasnat, A., Awal, M. A., & Bosunia, S. Z. (2015). Recycling of brick aggregate concrete as coarse aggregate. Journal of Materials in Civil Engineering, 27(7).

Rodríguez-Robles, D., García-González, J., Juan-Valdés, A., Morán-Del Pozo, J. M., & Guerra-Romero, M. I. (2015). Overview regarding construction and demolition waste in spain. Environ. Technol., 36(23), 3060-3070.

Shahjalal, M., Hossain, F. M. Z., Islam, K., Tiznobaik, M., & Alam, M. S. (2019). Experimental study on the mechanical properties of recycled aggregate concrete using crumb rubber and polypropylene fiber. CSCE Annual Conference, Canada.

Shahjalal, M., Islam, K., Rahman, J., Ahmed, K. S., Karim, M. R., & Billah, A. H. M. M. (2021). Flexural response of fiber reinforced concrete beams with waste tires rubber and recycled aggregate. Journal of Cleaner Production, 278, 123842. doi:https://doi.org/10.1016/j.jclepro.2020.123842

Smith, J. T. (2010). Recycled concrete aggregate – A viable aggregate source for concrete pavements. (PhD), University of Waterloo, Canada.

MIJST
MIST International Journal of Science and Technology

Comparing the Potentiality of Propane, Propanol and Octane Fuel Using in SI Engine Based on Energy-Exergy Analysis

Md Mizanuzzaman Mizan

Bangladesh Military Academy (BMA), Bhatiary, Bangladesh

email: *mizan_zaman@yahoo.com*

ARTICLE INFO

Article History:

Received: 28th August 2020
Revised: 23rd April 2021
Accepted: 25th April 2021
Published: 27th June 2021

Keywords:

Potentiality
Energy
Irreversibility
Exergy
Combustion
Friction
efficiency

ABSTRACT

From the beginning of IC engine era, it is trying to improve the performance and efficiency of internal combustion engine. In this study, numerically analysis on combustion of Propane, Propanol and Octane in SI engine have been done thoroughly and presented to assess the potentiality and highlighted the comparison. For this analysis thermodynamic engine cycle model is developed for numerical analysis. Mathematical models considering fundamental equation and empirical relation are implemented in a single cylinder 4 stroke spark ignition engine (system) with the help of FORTRAN 95 to find out heat losses, friction losses, output parameter etc. Single cylinder four-stroke spark-ignition (SI) engine is considered as system. In this study, different working parameters like 8 and 12 compression ratios with three different rpm 2000, 4000 & 6000 are considered for simulation. This study shows the different comparisons of energy-exergy content (%), as example of exhaust gas 35.08 & 17.82, 37.02 & 19.22, 37.79 & 19.79 for Octane (at compression ratio 8 and 2000, 4000, 6000 rpm) etc., which explains the potentiality content and the potentiality losses in different process like combustion, mixing of gases etc. It also shows for the fuel propane and propanol in similar way with changing different operating conditions. Maximum inside cylinder temperature, 1st law and 2nd law efficiencies were determined for the fuels with respect to different compression ratio and engine speed.

1. INTRODUCTION

Nowadays it is a great concern about the energy conservation and its efficient uses. The reserve of fuels is reducing day by day so need to find out alternative source or efficient conversion techniques. Alternative fuels also known as 'cleaner fuel' is great concern in this regard. With better combustion technique alternative fuels burns efficiently and give less emission than conventional fuels (Moran & Shapiro, 2000). Alternative fuels are inherently cleaner than petroleum derived fuels. Alternative fuels usually are less harmful to the environment and greater suitable than conventional fuels. By the using of advanced emission control technologies, it was found that the efficient burn of alternative fuels and less harmful ingredients released from incomplete combustion. Advanced combustion and emission control technology requires combustion data with certain degree of detailing. But for better combustion technique and conversion technology, it requires combustion data or properties for alternative fuel. Generation of experimental data is very expensive, and therefore more emphasis is given, now-a-days, on modelled results for combustion of non-conventional fuels.

Propane normally is a gas at normal temperature and pressure (NTP) and becomes liquid (after compression) during transport. Propane uses as a fuel in different purposes. There is also a possibility to use as refrigerant in air conditioning system.

After diesel and petrol, the large amount of heat energy is produced by the complete combustion of propane. Also, propane is known as a cleaner fuel and produces lower emission to the environment. So as a result, the propane is becoming the third fuel after petrol and diesel to use as a vehicle fuel.

Comparing with the traditional fuel propane is an abundance of supply, can be stored at low pressure, offers good safety and low cost. Propanol considering as primary alcohol is less toxic and less volatile than propane. Propanol producing

less amount of undesirable CO and unstable HC during combustion process than gasoline fuel (Eduardo & Fernando, 2017).

The performance of an internal combustion engine has been ascertained by the calculated energy value with the help of the first law of thermodynamic. Energy cannot be destroyed but transformed one form to another. But now it was found first law of thermodynamic alone cannot explain the all phenomenon of combustion process accurately (Kumar et al., 2015). It cannot identify the actual potentiality of the fuel because of its limitations like not considering the energy losses due to irreversible process like combustion, heat transfer, mixing of gases etc. so with the help of 1st law of thermodynamics alone the potentiality losses due to different process/ sources cannot be identified, as a result it hinders the further improvement of the total process/ system. For this reason, the 2nd law of thermodynamics has been extensively used in the field of IC engines. During a process or a system analysis in terms of the 2nd law of thermodynamics is named exergy or availability analysis. Exergy analysis for IC engine system and process proves to be very convenient because it highlights the essential information about the irreversibility as well as exergy losses in the process or system. So, the thermodynamic efficiency can be measured, gray areas can be specified and thus processes or systems can be designed and functioned to be in efficient way (Moran & Shapiro, 2000). So, exergy calculation based on 2nd law of thermodynamics considered in this study to overcome this issue. Exergy analysis is an appropriate tool for scientists and academics to investigate the thermodynamic processes and systems. The 2nd law of thermodynamics states that energy has quality and quantity as well. By introducing exergy, it provides an alternative mean of evaluating and comparing processes and systems realistically. Again, the various thermodynamics data for alternative fuels like propane and propanol is not available in various operating conditions of SI engine. So, considering all the issues the present study highlighted the potentiality as well as the sources of potentiality losses including different thermodynamic data for propane, propanol, and octane fuel during the combustion in SI engine.

Exergy is explained the maximum theoretical work as when a system with specific process comes to the equilibrium condition with the reference environment. System and process contain the amount of exergy depends on the degree of systems quality or possible system utility, its capability to execute work. Nowadays the exergy calculation technique became commonly used in the estimation, calculation, design, model and performance calculation of thermodynamic process and system.

As the exergy of a system contain fuel is diminished during irreversible processes, the total fuel energy cannot be transformed to useful work even during complete combustion. In view of this exergy destruction, exergetic efficiency offers more realistic measures for calculating the effectiveness of the energy conversion system during combustion.

Based on exergy analysis produces an exact amount of real performance styles the perfect, and undoubtedly indicates the reasons and the sources of systems potentiality reduces. Exergy calculation can contribute in refining and improving design (Hakan, et. al., 2018 & Juan, et. al. 2018). However, potentiality of propane, propanol and octane fuel in SI engine is still in research investigation, in particular, in terms of energy-exergy analysis. Therefore, exergy analysis technique is applied in this process like compression, combustion, and expansion phases of spark ignition engine.

2. METHODOLOGY

FORTRAN 95 programming language is used as a based program to write the simulation software considering all the necessary governing equation. Module wise programming for different process like compression, combustion, expansion, heat transfer, friction etc. has been done to calculate the various results due to different engine conditions. Key parameters and boundary conditions are also shown in Table 1 and 2.

In this study, a two-zone thermodynamic-based combustion model was developed for Energy – Exergy analysis of internal combustion engine (SI). By using FORTRAN 95 the governing equations with boundary conditions are numerically solved considering 0.1 degree CA as unit time step. After the power stroke the estimation for a process in a cycle stops when the exhaust valve opens and P_e and T_e are noted to compute the temperature at the beginning of the cycle, T_{IVC} and residual gas fraction, f. The computation process is repeated with assessed values of residual mass fraction and temperature at inlet valve closed until converged solution is attained.

A. Basic Equations of SI Engine Cycle

The cylinder volume is the function of crank angle (θ). The governing equation (1) of volume is as follows (Ferguson & Kirkpatrick, 2001):

$$V(\theta) = \frac{V_D}{R_C - 1} + \frac{V_D}{2}\left[\left(\frac{2L_C}{L_S}\right) + 1 - cos\,\theta - \sqrt{\left(\frac{2L_C}{L_S}\right)^2 - \sin^2\theta}\,\right] \quad (1)$$

where, the displacement volume can be expressed as $V_D = \frac{\pi}{4}B^2L_S$, where, B, L_s, R_c and L_c are bore, stroke length, compression ratio and connecting rod length, respectively.

The infinitesimal change of pressure in cylinder, dp can be explained by Eq. (2) (Ferguson & Kirkpatrick, 2001):

$$dP(\theta) = -KP(\theta)\left[\frac{dV(\theta)}{V(\theta)}\right] + (k-1)\left[\frac{\delta Q_{net}(\theta)}{V(\theta)}\right] \quad (2)$$

where, the specific ratio, $k = C_p/C_v$ and $\delta Q_{net}(\theta) = \delta Q_{fuel} - \delta Q_{loss}(\theta)$.

From the 1st law of thermodynamics, it is noted that

$$\delta Q_{net}(\theta) = dU(\theta) + \delta w(\theta) \quad (3)$$

where, $\delta w = PdV$ and $dU = mC_v dT$ assuming $PV = mRT$ for ideal gas.

The reference data used in this study is stated in Table 1 (Rakopoulos, 1993).

Table 1
Engine specification (Haq & Morshed, 2013; Rakopoulos, 1993)

Bore dia	Stroke length	Connecting rod length	Start of Combustion	Combustion duration	Compression ratio
76.3 mm	111.1 mm	160.0 mm	330^0	60^0	7

B. Wiebe Function as Fuel Burn Profile

Considering the ideal spark ignition engine cycle, air-fuel mixture inside the cylinder never burns instantly rather it requires some time and follows a profile or curve which can be explained by the Wiebe function (Heywood, 1988):

$$y_b(\theta) = \begin{cases} 1 - exp[-a(\theta - \theta_s/\Delta\theta_b)^b] \;\; if\; \theta_s \le \theta \le \theta_s + \Delta\theta_b \\ 0 \qquad\qquad\qquad\qquad\qquad if\; \theta < \theta_s, \theta > \theta_s + \Delta\theta_b \end{cases} \quad (4)$$

where, $y_b(\theta)$ is the burnt mass fraction at a CA, θ is the combustion start (CA), $\Delta\theta_b$ is the duration of combustion, a is Wiebe efficiency factor and b is Wiebe form factor.

C. Energy Analysis

Total heat release from the air-fuel mixture combustion, δQ_{fuel}can be written as:

$$\delta Q_{fuel}(\theta) = Q_{LHV}.y_s.dy_b.(1-f) \quad (5)$$

where,

$$y_s = \frac{(F/A)_s}{(F/A)_s+1} \quad (6)$$

The heat losses from the gases to the cylinder walls, δQ_{loss}, can be determined with a Newtonian convection Eq (7):

$$\delta Q_{loss}(\theta) = h_g(\theta).A_w(\theta).[T(\theta) - T_w].\frac{d\theta}{2\pi N} \quad (7)$$

Cylinder area A_w (θ) is sum of the cylinder wall, cylinder head and piston head area expressed as:

$$A_w(\theta) = A_{wall} + A_{head} + A_{piston}$$
$$= 2V_D\left[\frac{1}{L_s} + \frac{1}{B}\left\{\left(\frac{2L_c}{L_s}\right) + 1 - cos\theta - \sqrt{(2L_c/L_s)^2 - sin^2\theta}\right\}\right] \quad (8)$$

The instantaneous heat transfer coefficient, $h_g(\theta)$ can be determined by Woschni correlation (Ferguson & Kirkpatrick, 2001) as:

$$h_g(\theta) = 3.26[P(\theta)]^{0.8}.\left[U_g(\theta)\right]^{0.8}.B^{-0.2}.[T(\theta)]^{-0.55} \quad (9)$$

where, U_g is the characteristic gas velocity and proportional to mean piston speed during different process of cycle. When pressure rises during combustion then gas velocities also increase. As a result, value of U_g is calculated by mean piston speed, $\overline{U}_p = 2NL_s$ & cylinder pressure, (P-P_m). Hence,

$$U(\theta) = 2.28\overline{U}_p + 0.00324T_0\left[\frac{V(\theta)}{V_D}\right]\left[\frac{P(\theta)-P_m(\theta)}{P_0}\right] \quad (10)$$

where, motoring pressure P_m is obtained by using the motor for movement of the piston considering without combustion or heat release and its value is calculated as: (Stone, 1999):

$$P_m(\theta) = P_0\left[\frac{V_0}{V(\theta)}\right]^{1.3} \quad (11)$$

For the clearance volume of inside cylinder there must be some residual exhaust remained after the exhaust stroke. Fresh air-fuel mixture mixed with this left residual exhaust. As a result, temperature of the air-fuel mixture increases and volumetric efficiency decreases. The residual gas fraction, f, is defined as the ratio of the mass after exhaust stroke (residual gas mass) and the mass when the piston at bdc after the intake stroke. The residual gas fraction, f, can be calculated as (Ferguson & Kirkpatrick, 2001):

$$f = \frac{1}{R_c}\left[\frac{P_e}{P_{EVC}}\right]^{\frac{1}{k}} \quad (12)$$

For unthrottled engine, considering P_e = atmospheric pressure. Hence, temperature at the beginning of the cycle, T_{IVC} is correlated with the residual gas fraction, f can be calculated as (Ferguson & Kirkpatrick, 2001):

$$T_{IVC} = (1-f).T_i + f.T_e.\left[1 - \left(1 - \frac{P_i}{P_e}\right)\left(\frac{k-1}{k}\right)\right] \quad (13)$$

Now the efficiency of the cycle is defined to compare different engine and estimate different improvements effects from the perspective of either the first or the second law of thermodynamics (Rakopoulos, 1993; 2006). The 1st law efficiency which is energy-based is defined as (Sezer & Bilgin, 2008; Mizanuzzaman, 2017):

$$\eta_{I,ind} = \frac{Energy\ out\ (as\ Indicated\ work, W_{ind})}{Energy\ in\ (m_f\ Q_{LHV})} \quad or$$

$$\eta_{I,brk} = \frac{Brake\ work, W_{brk}}{m_f\ Q_{LHV}} \quad (14)$$

In this study, brake thermal efficiency is used as 1st law efficiency.

D. Equilibrium Chemical Composition and Thermodynamic Properties

In this analysis, the chemical formula of fuel is considered as $C_\alpha H_\beta O_\gamma N_\delta$. Actual reaction of air (atmospheric condition) and fuel at equilibrium condition by volume is shown as (Ferguson & Kirkpatrick, 2001):

$$\epsilon\ \overbrace{C_\alpha H_\beta O_\gamma N_\delta}^{fuel} + \overbrace{0.21O_2 + 0.79N_2}^{air}$$
$$= \nu_1 N_2 + \nu_2 O_2 + \nu_3 CO + \nu_4 H_2 + \nu_5 CO_2 + \nu_6 H_2O + \nu_7 H + \nu_8 O + \nu_9 NO + \nu_{10} OH$$

The coefficients $\nu_i\ (i = 1,2,3\ldots.)$ that describes the product composition, ϵ is the molar fuel-air ratio and can be calculated by $\epsilon = 0.21/(\alpha+0.25\beta-0.5\gamma)$. By using atom balance and equilibrium constant, number of mole numbers and mole fraction of 10 specified products can be estimated. NASA polynomials are also used to find out the specific heat ratio and Gibbs free energy. Then all other

thermodynamic properties like entropy, enthalpy, internal energy etc. can be estimated easily.

E. Exergy Analysis

Exergy in a system or total exergy can be divided into two parts such as thermomechanical exergy and chemical exergy (Wark, 1995). Hereafter,

$$EX_{tot} = EX_{tm} + EX_{ch} \quad (15)$$

When a system goes through reversible process to reach the environment state (P0, T0), then the work obtained from the system & environment is called the thermomechanical exergy. This is the condition of restricted dead state condition. Here mixing and chemical reaction of the composition of system & environment was not considered. In this restricted dead state condition, there is a scope to mixing and chemical reaction of the composition of system and the environment. If this chemical reaction occurs through reversible process, then additional work obtained from the system and environment is called as chemical exergy. And at equilibrium condition this is called unrestricted dead state condition (Kuntesh, et. al., 2017).

Thermomechanical and chemical exergy can be defined as (Wark 1995):

$$EX_{tm} = u + P_0 v - T_0 s - \sum_{i=1}^{n} y_i \mu_{i,0} \quad (16)$$

$$EX_{ch} = \sum_{i=1}^{n} y_i \left(\mu_{i,0} - \mu_{i,00}\right) \quad (17)$$

Here $\mu_{i,0}$ is defined as the chemical potential of *i* species at restricted dead state condition and $\mu_{i,00}$ is defined as the chemical potential of *i* species at unrestricted dead state condition.

The chemical exergy in a system can be divided as the following equations:

$$EX_{ch} = EX_{diffusion} + EX_{reactive} = EX_{diffusion} + EX_{oxidation} + EX_{reduction} \quad (18)$$

Normally exergy in a system like internal combustion engine (SI) uses or losses as work, heat transfer, exhaust gas from cylinder and destructed causes of combustion of air-fuel mixture (irreversibility). Here equations (19-21) show the fuel exergy and exergy uses as work and loses as heat transfer:

Fuel exergy:

$$EX_{fuel} = -(\Delta g)_{T_0, P_0} \quad (19)$$

Exergy transfer as work:

$$EX_w = \int \delta w = \int P dv \quad (20)$$

Exergy transfer as heat:

$$EX_Q = \int (1 - T_0/T) \delta q \quad (21)$$

In the present study the following definition is used for second law efficiency (Sezer & Bilgin, 2009; Mizanuzzaman, 2018):

$$\eta_{II} = \frac{Exergy\ out\ (as\ work)}{Maximum\ extractable\ exergy\ (as\ work)} = \frac{W_{ind}}{W_{max}} = \frac{W_{ind}}{W_{ind}+I} \quad (22)$$

With the above discussion it can be concluded that the second law efficiency provides a better thoughtful of performance than the first law efficiency. Moreover, the second law efficiency stresses both exergy losses due to the dealing with irreversibility to improve performance.

F. Friction Calculation

For estimating the efficiency of a Spark Ignition engine, friction calculation is one of the requirements. Friction is a totally irreversible process. It will reduce the exergy of a system as well as the potentiality to do the work. There are several ways to calculate the friction. All governing equation and calculation described in ref (Bishop, 1964; Mizanuzzaman, 2012; Mizanuzzaman, 2013), the total friction is occurred in various parts in SI engine, that is:

$$Total\ Friction\ Loss = Friction\ losses\ in\ (piston + valve\ train + crank\ shaft + pumping + accessory)$$

3. RESULTS AND DISCUSSION

Energy and exergy analysis together gives a better result regarding the performance of a system. Recently exergy analysis became popular and essential tools for simulation and performance analysis of an internal combustion engine (SI).

The energy-exergy distribution for stoichiometric propane, propanol and octane fueling with efficiency in different processes of spark ignition engine at three different speeds have been shown in Figures 1 & 2. Furthermore, maximum inside cylinder temperature has been shown in Figure 3. Energy balance calculation does not consider the exergy losses due to irreversibility and degradation of its quality. But this irreversibility can play an important role in further performance improvement design.

Engine speed variations have been given few important observations. Heat transfer from the cylinder becomes less due to less time for it by increasing engine speed. So, at higher engine speed the remaining energy makes the exhaust temperature increasing because of higher loss of exhaust energy. Again, at higher engine speed provides lower heat transfer exergy losses and higher exhaust exergy to atmosphere. Few important parameters like adiabatic temperature, *LHV*, maximum temperature & pressure of three fuels are also validated (Haq & Morshed, 2013; Simeon & Kiril, 2012). However, work done, and work potential are comparable in various speeds and compression ratio shown in Table 2.

Table 2
Energy-Exergy Distribution (%)

Fuel	R_c	rpm	Energy work	Energy heat	Energy exhaust	Energy friction	Energy unaval	1st law η	Exergy work	Exergy heat	Exergy exhaust	Exergy friction	Exergy unaval	2nd law η
C_3H_8	8	2000	36.56	16.01	35.08	3.66	8.70	36.56	36.03	13.37	17.82	3.61	29.18	57.59
		4000	37.69	11.84	37.02	5.99	7.47	37.69	37.14	9.90	19.22	5.90	27.84	60.72
		6000	38.11	10.20	37.79	9.20	4.70	38.11	37.55	8.53	19.79	9.06	25.07	65.03
	12	2000	39.12	19.32	30.08	4.13	7.36	39.12	38.55	16.01	14.40	4.07	26.97	61.24
		4000	41.00	13.92	32.38	6.43	6.27	41.00	40.41	11.55	16.00	6.34	25.70	64.52
		6000	41.71	11.81	33.30	9.69	3.50	41.71	41.10	9.80	16.65	9.55	22.90	68.86
C_3H_8O	8	2000	35.88	15.32	34.22	3.54	11.05	35.88	35.04	12.63	17.01	3.46	31.87	54.71
		4000	36.95	11.31	36.08	5.79	9.88	36.95	36.08	9.34	18.33	5.65	30.60	57.70
		6000	37.34	9.74	36.93	8.89	7.20	37.34	36.47	8.04	18.86	8.69	27.94	61.78
	12	2000	38.47	18.45	29.34	3.99	9.75	38.47	37.57	15.10	13.73	3.90	29.70	58.27
		4000	40.25	13.27	31.54	6.22	8.71	40.25	39.31	10.87	15.24	6.07	28.51	61.42
		6000	40.92	11.25	32.42	9.37	6.04	40.92	39.96	9.21	15.84	9.15	25.83	65.53
C_8H_{18}	8	2000	35.95	15.44	34.01	3.55	11.05	35.95	35.08	12.74	16.95	3.46	31.77	54.81
		4000	37.04	11.40	35.88	5.80	9.87	37.04	36.14	9.42	18.27	5.66	30.50	57.81
		6000	37.44	9.81	36.63	8.92	7.20	37.44	36.53	8.11	18.81	8.70	27.85	61.90
	12	2000	38.51	18.59	29.14	4.00	9.76	38.51	37.58	15.22	13.67	3.91	29.63	58.34
		4000	40.32	13.37	31.35	6.23	8.73	40.32	39.34	10.96	15.18	6.08	28.44	61.50
		6000	40.99	11.33	32.23	9.40	6.05	40.99	40.00	9.29	15.79	9.17	25.76	65.62

Figure 1 shows the amount of energy and exergy in different process for propane is a little different than other fuels. Because of modest molecular structure and better mixing and combustion propane air mixture combustion produced a bit less generation of irreversibility. At present study, due to high combustion temperatures, maximum exergy contained in fuel is lost due to transfer of heat and as exhaust gases. Considering octane and propanol, propane showed moderately better results as of lower exergy loss (exergy unavailable) with irreversibility and higher work exergy. Work exergy and heat transfer for propanol were similar trend of conventional octane fuel. Few important observations by using three different fuels such as propane, propanol and octane are as follows:

At 2000 rpm, fuel energy of 35.88 to 36.56% is converted to useful work, and at 6000 rpm the energy percentages of 37.34 to 38.11% is converted to useful work at compression ratio 8.

At 2000 rpm, fuel energy losses are 15.32 to 16.01% and 9.74 to 10.20% at 6000 rpm, respectively due to heat transfer. On the other hand, at 6000 rpm, associated fuel exergy losses are 8.04 to 8.53% and 12.63 to 13.37% at 2000 rpm, respectively at compression ratio 8.

At 2000 rpm, fuel energy of 34.01 to 35.08% is lost with exhaust gases, whereas, at 6000 rpm, 36.63 to 37.79% losses are found. Similarly, exergy losses are found as 16.95 to 17.82% at 2000 rpm and 18.81 to 19.79% at 6000 rpm, respectively with exhaust gases at compression ratio 8.

Energy losses are found as 3.54 to 3.66% due to friction at 2000 rpm and 8.89 to 9.2% at 6000 rpm, respectively at compression ratio 8. It is noted that exergy losses with friction are nearly same as energy losses. However, fuel exergy is demolished of 29.18 to 31.87% at 2000 rpm because of irreversibility and 25.07 to 27.94% at 6000 rpm when compression ratio is 8.

It is found that as engine speed increases, the work output, energy/exergy exhaust loss and friction loss are increased. But at the same time losses for heat transfer and irreversibility's (when considering exergy of fuel) are decreased.

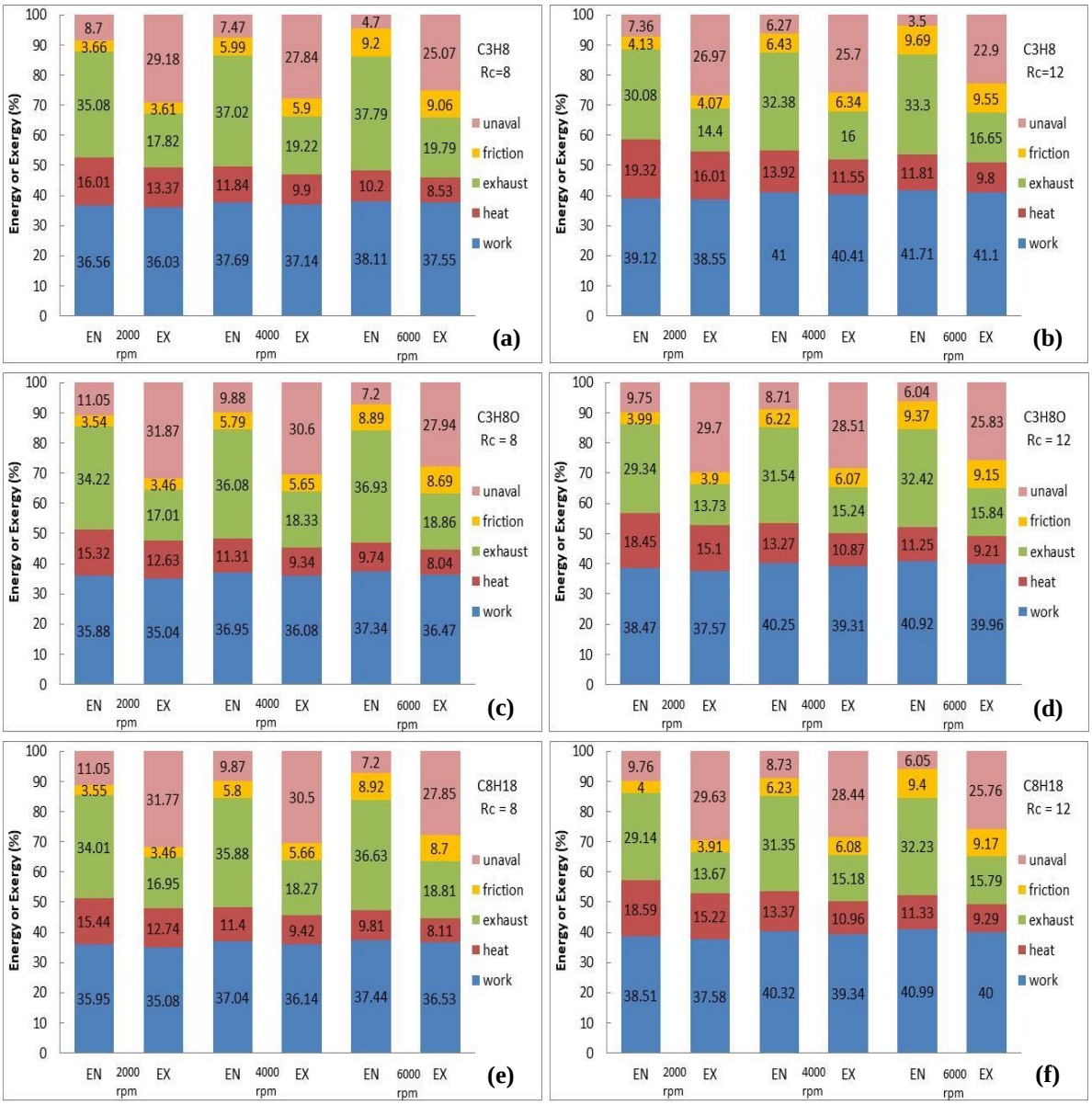

Figure 1: Energy and Exergy distribution for Propane, Propanol and Octane (stoichiometric condition) at different rpm and compression ratios, (a) C3H8, Rc=8; (b) C3H8, Rc=12; (c) C3H80, Rc=8; (d) C3H80, Rc=12; (e) C8H18, Rc=8; (f) C8H18, Rc=12

Figure 2 indicates the 1st and 2nd law efficiencies, depending on compression ratio and rpm. Trend of 1st and 2nd law efficiencies are usual and similar trend for compression ratio and rpm. It is found that 1st law efficiency for propane is slightly greater than other two fuels with various engine rpm and compression ratios. 1st law efficiency for octane and propanol is nearly same for different engine speed and compression ratios. 1st law efficiency found increased for all the fuels while increasing engine speed and compression ratios. For similar trend of first law efficiency, second law efficiency also found increased for all fuels while increasing engine speed and compression ratio. Propanol and octane show the similar trend and value for second law efficiency. Figure 3 shows the comparison of maximum inside cylinder temperature at different rpm and compression ratios. It was found that maximum temperature increases with increasing rpm but decreasing when compression ration increases. For propane, total irreversibility (friction plus unavailable exergy) is minimum or less than other two fuels and this value also increase with rpm but slightly decrease with compression ratio. There is a more scope to reduce the total irreversibility and so to increase the performance for propanol and octane. Normally compression ration increases the potentiality of the gases or liquid used in SI engine, at the same time it also increases the 1st law and the 2nd law of thermodynamics. In this study it was found that the potentiality of propane is greater than the octane and propanol. It is also found that with considering the concept of irreversibility, the potentiality of gases or liquid losses during combustion and mixing of gases inside the cylinder. Similarly, another finding is that by increasing the rpm, the exergy-energy of gases or liquid decreases by heat transfer and it also increases the irreversibility as well as the incompleteness of combustion. In this study it is also found that the cylinder temperature made by propane is maximum than octane and propanol.

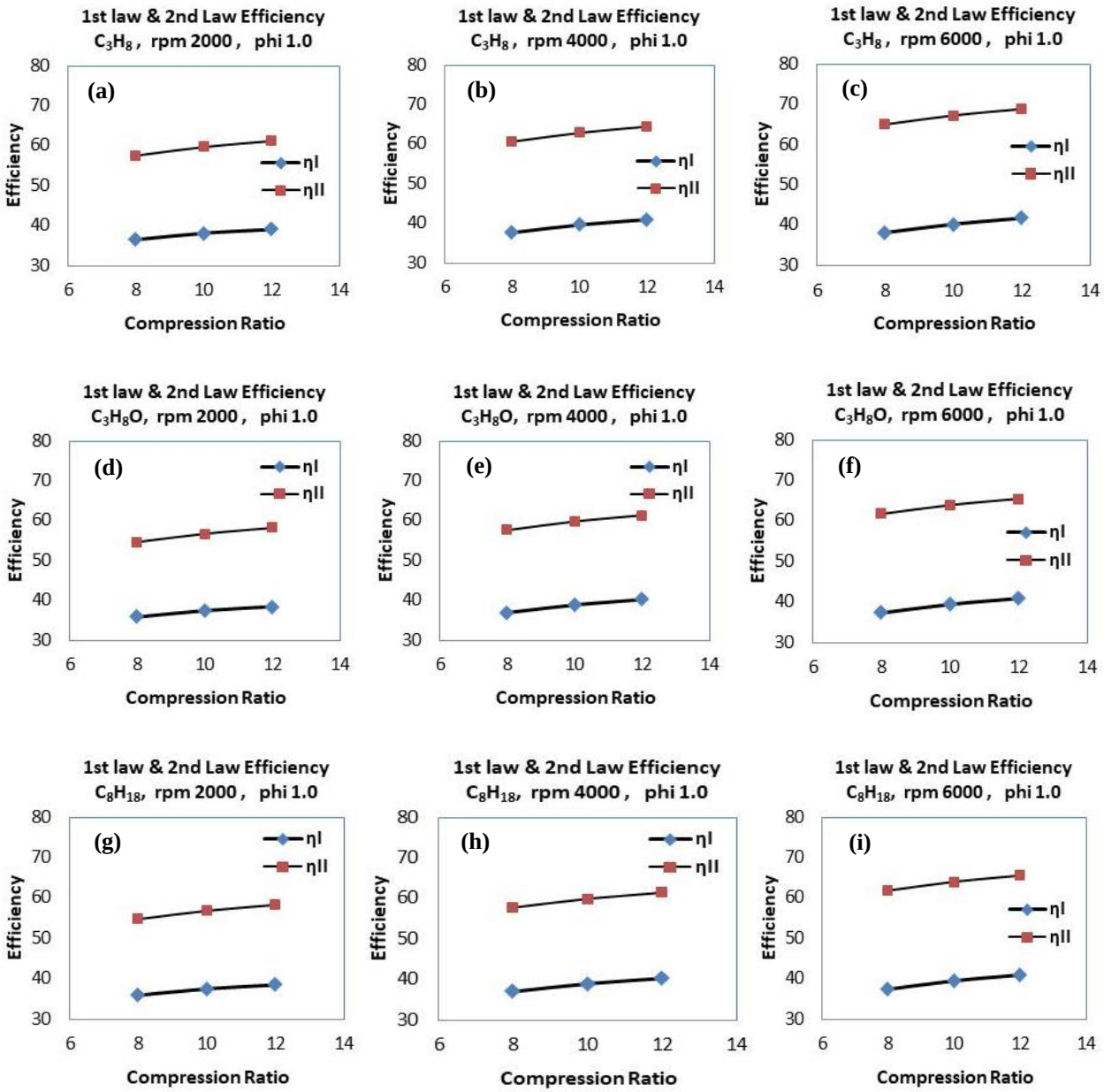

Figure 2: 1st law and 2nd law efficiency of Propane, Propanol, and Octane at different rpm and compression ratios, (a) to (i)

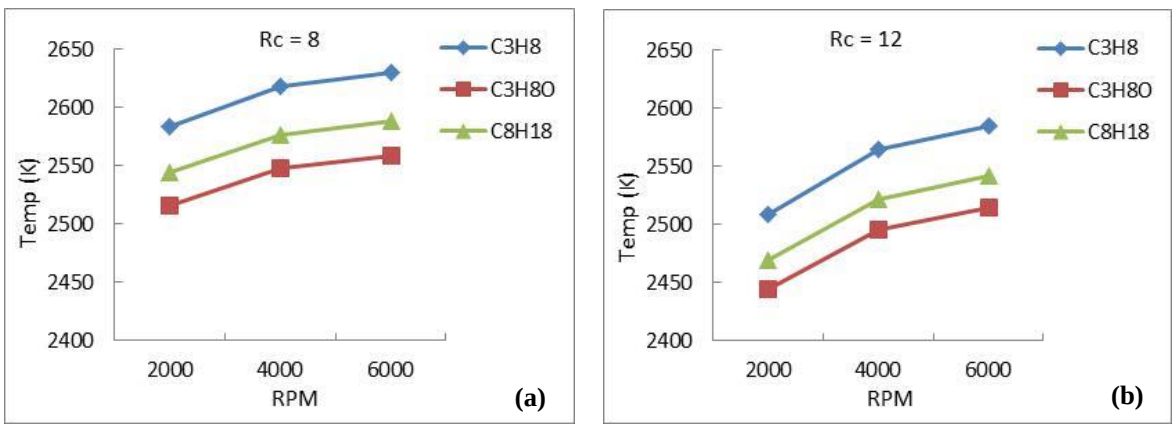

Figure 3: Comparison of maximum inside cylinder temperature for propane, propanol and octane at different rpm and compression ratio (considering stoichiometric mixture), (a) Rc = 8, and (b) Rc = 12

4. CONCLUSIONS

Energy and exergy analysis of SI engine are the important thermodynamic tools for finding better energy distribution. Irreversible process reduces the exergy of a system and leads to the inefficiency of the system. It is because of mainly for combustion process. The exhaust gas and heat transfer are also causing for exergy losses but in decreasing order. It is found that energy and exergy analysis together give a better and more accurate answer for the comparison of different fuels. However, the specific conclusions from the present study are:

a. At 2000 rpm, 35.88 to 36.56% of energy contained with fuel is converted to useful work, and the figure changes to 37.34 to 38.11% in case of 6000 rpm at compression ratio of 8.
b. Energy loss is found due to heat transfer from 15.32 to 16.01% and 9.74 to 10.20% at 2000 and 6000 rpm, respectively. However, associated exergy losses are found as 12.63 to 13.37% and 8.04 to 8.53% at 2000 and 6000 rpm, respectively at compression ratio of 8.
c. Energy loss with exhaust is found as 34.01 to 35.08% and 36.63 to 37.79% at 2000 and 6000 rpm, respectively. Consecutively, exergy loss with exhaust is 16.95 to 17.82% and 18.81 to 19.79% at 2000 and 6000 rpm, respectively at compression ratio of 8.
d. Energy loss due to friction is found as 3.54 to 3.66% and 8.89 to 9.2% at 2000 and 6000 rpm, respectively, at compression ratio of 8. Exergy losses with friction are found nearly as the same value as energy losses. Similarly, exergy contained with fuel is destroyed due to irreversibility as 29.18 to 31.87% and 25.07 to 27.94% at 2000 and 6000 rpm, respectively, at compression ratio of 8.

The outcomes of present study provide the significance of energy-exergy based analyses to identify the potentiality of individual fuel and the sources of work potential losses in different process in the spark ignition engine.

5. NOMENCLATURES

EX_{ch}	Chemical Exergy (kJ/kg-mix)
EX_Q	Exergy associated with heat transfer (kJ/kg-mix)
EX_{tm}	Thermomechanical Exergy (kJ/kg-mix)
$\left(\frac{F}{A}\right)_s$	Stoicchiometric fuel-air ratio
EX_{fuel}	Fuel Exergy (kJ/kg-mix)
EX_w	Exergy associated with work interaction (kJ/kg-mix)
y_s	Fuel mass fraction in stoichiometric mixture
R_c	Compression Ratio
N	Engine Speed, rpm
Δg	Change of Gibbs energy (kJ/kg-mix)
$\mu_{i,0}$	Chemical potential restricted equilibrium with environment
$\mu_{i,00}$	Chemical potential unrestricted equilibrium with environment
T_w	Cylinder wall temperature
L_c	Connecting rod length
L_s	Stroke length
f	Residual gas fraction
V_D	Displacement volume
I	Total Irreversibility

ACKNOWLEDGEMENTS

The author would like to express his gratitude to the Bangladesh Military Academy (BMA), Bhatiary, Bangladesh. The author is also thankful to the editors and anonymous reviewers for providing insightful suggestions and comments to improve the manuscript.

REFERENCES

Ferguson, C. R., & Kirkpatrick, A. T. (2001). *Internal Combustion Engines: Applied Thermosciences*. John Wiley & Sons.

Heywood, J. B. (1988). *Internal Combustion Engine Fundamentals*. McGraw-Hill.

Moran, M. J., & Shapiro, H. N. (2000). *Fundamentals of Engineering Thermodynamics*. John Wiley & Sons, New York.Bishop I. N. (1964). Effect of Design Variables on Friction and Economy. *Society of Automotive Engineering (SAE)*, 334-379.

Eduardo, A. M., & Fernando, A. (2017). Thermodynamic Properties of Propanol and Butanol as Oxygenate Additives to Biofuels. *InTech Journal*, 363-389.

Hakan, Ö., & Abdülvahap, Ç. (2018). Comparative exergy analysis of oxygenated fuel additives in a spark-ignition (SI) engine. *International Journal of Automotive Engineering and Technologies*, 7(3), 124-133.

Juan, E. T., José, I. H., Sebastián, O., Luis, F. Q., & José, E. N. (2018). The Effect of using Ethanol-Gasoline Blends on the Mechanical, Energy and Environmental Performance of In-Use Vehicles. *Energies*, 11, 1-17.

Kumar, D., Singh, A., & Sarma, A. K. (2015). Energy and Exergy Analysis of CI Engine for Karanja Biodiesel. *International Conference on Advances in Energy Research (ICAER)*.

Kuntesh, M., Ashish, J. M., & Dipak, G. (2017). Energy and Exergy Analysis on Si Engine by Blend of Ethanol with Petrol. *International Journal of Advanced Engineering Research and Science*, 4 (4), 49 - 61.

Mizanuzzaman, M. (2012). Effect of bore stroke ratios on overall friction model of SI engine. *MIST Journal of Science and Technology*, 1, 71-86.

Mizanuzzaman, M. (2013). Advantages of roller follower for different bore stroke ratios and effects on overall friction of SI engine. *MIST Journal of Science and Technology*, 2, 8-17.

Mizanuzzaman, M. (2017). Energy and Exergy Based Analysis of SI Engines Using Methane, Methanol and Octane. *MIST Journal of Science and Technology*, 5, 102-111.

Mizanuzzaman, M. (2018). Thermodynamic Analysis of Spark Ignition Engine Using Ethane, Ethanol and Octane. *BUP Journal*, 6, 99-111.

Rakopoulos, C. D. (1993). Evaluation of a spark ignition engine cycle using first and second law analysis techniques. *Energy Conversion and Management*, 34(12), 1299-1314.

Rakopoulos, C. D. & Giakoumis, E. G. (2006). Second law analyses applied to internal combustion engines operation. *Progress in Energy and Combustion science*, 32, 2-47.

Sezer, I., Altin, I., & Bilgin, A. (2009). Exergetic analysis of using oxygenated fuels in spark-ignition (SI) engines. *Energy & Fuels*, 23(4), 1801-1807.

Sezer, I., Altin, I., & Bilgin, A. (2008). Exergy analysis of SI engines. *International Journal of Exergy (IJEX)*, 5(2), 204-217.

Shirazi, S. A., Foust, T. D., & Reardon, K. F. (2020). Identification of Promising Alternative Mono-Alcohol Fuel Blend Components for Spark Ignition Engines. *Energies*,13, 1-16.

Simeon, I., & Kiril, H. (2012). Analysis of Engine Speed Effects on the Four Stroke GDI Engine Performance. *Proceeding in Manufacturing System*, 7(4), 229-234.

Haq, M. Z., & Morshed, A. (2013, July 29 - August 1). Energy and Exergy based analyses of a multy-fuelled SI engine. Proceedings of the ASME 2013 Power Conference, Boston, Massachusetts, USA. (Paper No. Power 2013-98279, ASME).

MIJST
MIST International Journal of Science and Technology

Assessment of Ecosystem Services and Disservices in Urban Environment Using Multispectral Image Analysis and Geospatial Mapping

Md. Nazmul Haque*[1], Irtija Alam[2], and Atif Aninda Rahman[3]

Department of Urban and Regional Planning, Khulna University of Engineering & Technology, Khulna-9203, Bangladesh

emails: *[1]nhaque13@urp.kuet.ac.bd; [2]alam1617012@stud.kuet.ac.bd; and [3]rahman1617020@stud.kuet.ac.bd*

ARTICLE INFO

Article History:

Received: 13th Decemberr 2020
Revised: 25th May 2021
Accepted: 29th May 2021
Published: 27th June 2021

Keywords:

Urban Environment
Ecosystem Services
Ecosystem Disservices
Image Analysis
ArcGIS

ABSTRACT

Ecosystem service and disservice components have a great impact on the environment as well as on urban life. The aim of the research is to assess the impact of ecosystem services and disservices by tracking the change over a span of 15 years (2005-2020) using satellite image analysis. It was conducted in wards 23 and 29 of Khulna City Corporation (KCC), an area adjacent to the river. The overall work breakdown has been rounded up in a methodological framework which cleaved into two parts focusing on ecosystem services, disservices and multispectral image analysis steps. Multispectral image analysis has been done using Normalized Difference Vegetation Index (NDVI) and Normalized Difference Build-up Index (NDBI). On the other hand, geospatial analysis has been done using Digital Elevation Model (DEM), Service Area Analysis (SAV) and other mapping tool including Geographic Information System (GIS) to show the changed impact of both ecosystem components. The study areas attain provisioning, habitat, cultural and regulatory service components and the disservice elements have been sorted out according to sources. Comparative study showed increase in the buildup area; vegetation coverage because of increasing vegetation, cultivation and gardening practices; good weather and water circulation condition and water body conservation which has significant positive impact on the area. The disservice component like poor drainage condition and solid waste management system and risky infrastructures have negative impact, need to address for the betterment of residence and environment.

1. INTRODUCTION

The trend of the fastest growing urbanization and internationalization creating a vast impact on the environment. Some of the impacts are increased population, developing industries with poor technologies, lack of proper provisioning and strong executing authority, unawareness is the reason for the environmental deterioration. This rapid urbanization has put compelling pressure on the urban ecosystem by biodiversity breakdown, habitat loss and environmental pollution (Tian *et al.*, 2020). Urban ecosystem glues a city and helps in building up a sound life with proper health, security and other core features of livelihood of the citizens (Bolund & Hunhammar, 1999; European Environment Agency, 2011; Odum, 1989; Tzoulas *et al.*, 2007). Also, it poses a negative effect on biodiversity and ecosystem and human well-being as well (Chabay, 2018). The urban ecosystem services usually refer to the opportunities provided by the urban ecosystem and its components (Andersson *et al.*, 2007; Gómez-Baggethun & Barton, 2013). Again ecosystem service is a heavy concept that presents the contribution of an ecosystem to human well-being (Isbell *et al.*, 2017). On the other hand ecosystem, disservice can be defined as feature, mechanism and properties of an environment which have created a perceived or actual detrimental effect on human well-being (Shackleton *et al.*, 2016).

Ecosystem-based researches are mainly focused on goods and services to identify the beneficial value to the ecosystem and humans as well (de Groot *et al.*, 2010). When the output of the ecosystem for humans and the environment are positive it is termed as "ecosystem

services" the component incorporates for service termed as "ecosystem service components". On the other hand, if the outputs are harmful the same ecosystem and incorporating components termed as "ecosystem disservice" and "Ecosystem disservice component" respectively (Rasmussen *et al*., 2017; Schaubroeck, 2017). The ecosystem and wellbeing are closely linked (Rasmussen *et al*., 2017). The Colombian Caribbean region is one of the most biodiverse regions in the world helping human well-being providing essential ecosystem services at the local, national and global levels (Aldana-Domínguez *et al.*, 2017; Le Saout *et al.*, 2013). Besides the study on ecosystem services, the study on ecosystem disservices is also very important to achieve sustainability and improvement of urban life in a systematic way. Identifying the relationship between and ecosystem services and disservices and addressing the root causes of disservices may enhance environmental management and ecological protection *(*Sun *et al.*, 2020). For economic disservice, a study had done in the marine ecosystem in the Polish Baltic sea defining disservices to be sea level rise, sea floods, erosion, toxic bloom, eutrophication, pollution etc. (Lyytimäki *et al.*, 2008). Another study has been done in northwest of Beijing to identify the environmental problems based on ecosystem disserve bundles for better environment management measures (Sun *et al.*, 2020).

There are many studies on ecosystem services all over the world. Hanna *et al.*, 2018 studied riverine ecosystem service to suggest effective measure to protect and manage the riverine ecosystem service bundles; Smart *et al.*, 2011 applied the ecosystem service concept to manage air quality in UK, Maskell *et al*., 2013 studied the ecosystem services in Great Britain to explore the ecosystem constaints to service delivery and biodiversity. According to (Rendón *et al.*, 2019) a linkage was buildup between the services and disservices of the existing area using a methodological framework. In Bangladesh, Islam *et al.*, studied to identify the natural and anthropogenic drivers of change that affect the ecosystem services of the Sundarbans Mangrove regions in Khulna, Satkhira and Bagerhat districts of Khulna Division based on secondary data and field interview (Islam *et al.*, 2018); Sarker *et al.* also studied on the ecosystem of Sundarbans to identify the variables which drive the mangrove biodiversity (Sarker *et al.*, 2019. Another study is done by Alam and Mohammad on applied ecosystem approach of regulation, monitoring, and management of Sundarbans as suitable means of conservation and sustainable development (Alam & Mohammad, 2018). In Khulna city-related studies regarding environmental profiling (Rabbi *et al.*, 2021) and environmental risk zone identification (Haque *et al.*, 2020) have been done. Works have been done on mapping out blue ecosystem services in the wards of Khulna city *(*Haque *et al.*, 2019) but further study on the disservices and services on land has not been yet done on Khulna city.

This research fills the gap in several ways. The spatiotemporal change from 2005 to 2020 based on ecosystem service and disservice components and its impacts on urban life are analyzed. Spatial analysis like DEM and two indices named NDVI and NDBI using multispectral image analysis for both service and disservice components are performed here. For disservice elements identification, location-based GIS mapping was done to sort out components like open dustbins, lack of tube wells, clogged or untreated drains, and risky buildings of the area. The study also relates the services and disservices of the area using proper reasoning of the framework. These changes and figures have helped to come to a conclusion about the service and disservice elements and assess them accordingly. But the study was not free from limitations. Due to a smaller study area and limited time period, the change was not that significant . Besides the quality analysis of waterbody, existing atmosphere analysis of dust particles was not possible due to limited time and the emergence of the COVID-19 outbreak.

The principal objective of the study was to make profile of ecosystem service and disservice components of the study area. Emphasis has been given on the comparison of vegetation, build environment coverage. It was done by the NDVI and NDBI respectively. A time extent from year 2005 to 2020 was taken for the study. Here environmental service indicators were taken as ecosystem service components. It was done to assess the environmental condition by justifying their role.

2. STUDY AREA

The selected study area is ward no. 23 and 29, the two adjacent areas of Khulna City Corporation. The area fall in the the ancient part of Khulna city near the Rupsha River. These two wards of the KCC have been explored based on secondary data, google earth and google map and found that they attained more ecosystem components than other wards in terms of: 1. Provisions like edible plants, water supply, fiber and fuel and raw material and ornament and medicine resources; 2. Regulating like air Quality, Climate condition, water regulation etc. 3. Habitat or Supporting like Nursery and 4. Cultural and Amenity like recreational activity, cultural heritage, spiritual and religious inspiration. A reconnaissance survey was conducted in the wards. It was found that those these wards attain a rich amount of ecosystem service and disservice components compared to other wards of the KCC boundary. Furthermore, this study has focused on the core unit (ward) of the urban area. There are some disservice components like poor drainage construction and sewerage system, no proper solid waste management system, degradation of blue ecosystem components like water body, lack of dustbin, and risky and old infrastructures. But authorities' concern is not sufficient to solve these problems. Finally, as the area consented to the study aim appropriately, it was selected as study area. The boundary road of the area is Khan-Jahan-Ali Road, South Central Road, Upper Jashore Road and Rupsha Stand Road. The total number of households of ward 23 is 3226 and total population is 13793. The total number of households of ward 29 is 4230 and total population is 17763. The population density of the total study area is 1030 sq. km under the Khulna Sadar Thana. Ward 29 is predominately a residential area but ward 23 is a commercial area. The road network and circulation, and adequacy of utility services condition are

comparatively good but the condition of the drainage and water service are not in good condition. In the candidate study area, the earliest settlements of the Khulna were developed and many buildings are having the sign of ancient heritage. There is a Missionary Community in the area and contributes to enriching the bio-diversity of the area by means of cultivation, gardening, conservation of water bodies and ornamentation.

3. RESEARCH METHODOLOGY

Figure 1 shows the location of ward 23 and 29 in KCC boundary.

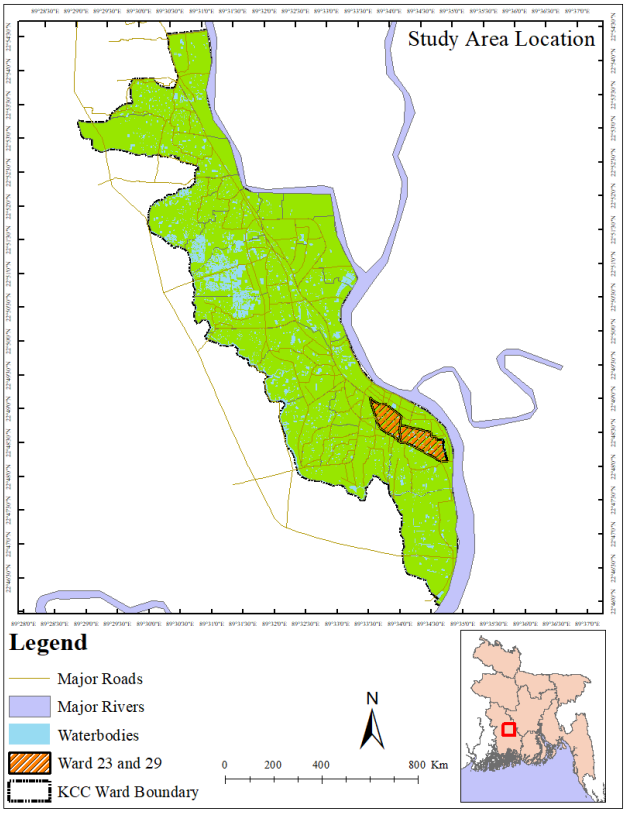

Figure 1: Location of ward 23 and 29 in KCC boundary

A . *Survey Design*

Firstly, a reconnaissance survey was conducted to know the overall environmental context and other features of the study area associated with ecosystem and environment. Data has been collected by questionnaire and checklist, prepared based on the available service and disservice components and the overall environmental condition of the study area from the observation of previous reconnaissance surveys. Among the bundle of service and disservice components, the accessible and available data were taken. The service components are water body, water supply point, agricultural land, greeneries, erosion protection, water regulation, cultural heritage and identity in the sense of place, design and belongings, spiritual and religious value, services comments, educational and scientific opportunities for formal and informal education and training (de Groot *et al.*, 2010) and the disservice components are waste dumping in the open places, risk of collapse and debris structures, sediment export on the water body (Sun *et al.*, 2020), poor drainage system, dust particles in the air. The survey based on the questionnaire was conducted in households and the checklist survey was conducted in both study areas and administration offices. Analysis was done based on the collected data. "Separation and Impact Analysis Methods" have been used where separation and discussion based on the impact of the elements were done. The desk analysis was based on a series of methods applied on the data retrieved from the field data collection. The obtained information was properly presented using mapping techniques in GIS. Further secondary data were collected from the USGS website for in-depth analysis of the study area for showing the temporal change.

B. *Technical Works for Presenting the Existing Scenario*

The service range of the dustbins which were only three in number was determined by creating a buffer of about 100m which was taken from the case study of Coimbatore India. The buffer tool of ArcGIS was used for this process. For determining the elevation of the areas, a tool known as the Training Center XML(TCX) converter was used and from google earth the latitude, longitude and altitude data were extracted and inserted in the TCX converter. Then processing the Inverse Distance Weighted (IDW), interpolation tool for Digital Elevation Model, in the ward boundary the elevation map of the area was determined. Waterbody depth data were collected in the field survey and Inverse Distance Weighted was also applied to determine the overall groundwater table in the area. Coordinates observed from field survey identified in google earth tool and converted the ".kml" file from there into shapefile points in GIS to locate open waste dumping point, tube well location, existing service facilities, deteriorated water bodies and risky infrastructures in the study area. Mainly these tools have helped to bring the study area in a precise and presentable manner.

C. *Methods Used in Spatiotemporal Indexing*

For a better understanding of the change in the study area environment temporal change was observed using satellite images extracted from the U.S. Geological Survey (USGS) website and the process followed is portrayed below:

i. *Data Collection and Preparation*

For image analysis LANDSAT images from 2005 and 2020 were taken from USGS (United State Geological Survey) website. The temporal gap was taken to observe the change in buildup area, vegetation and water bodies in the survey region. A primary survey was conducted to locate the places of prominent features of the area. The two LANDSAT images were Landsat 5 TM for 2005 and Landsat 8 OLI for 2020. The change of ecosystem components selected for the study and its impact are not evidencede in a short period. For this, an extent of 15 years time span has provided the research to explicate a significant change in ecosystem components and its impact on the area. The different electromagnetic radiations or the bands produced from these two satellites were used for determining processes such as Natural Difference Vegetative Index (NDVI), Natural Difference Water Index (NDWI) and Natural Difference Built-up Index (NDBI) defined in Table 1. The survey area a clear sky and free

from clouds during the early parts of month May during which the image from 2005 was taken and from the later parts of September from which the image from 2020 was taken. Both were free from cloud covers, then again while obtaining the data cloud covers have been taken to be less than 10% downloading from USGS. For both images, the path was 138 and the row was 44 with an image resolution of 30m.

Table 1
Showing the different band numbers and their attributes of the Landsat image indices

Indices	LANDSAT 8, OLI		LANDSAT 5, TM	
	Band number	Band attribute	Band number	Band attribute
NDVI	4 and 5	Visible red and NIR	3 and 4	Visible red and NIR
NDBI	5 and 6	NIR and SWIR	4 and 5	NIR and SWIR

ii. Multi-Spectral Image Dataset

The two sets of images taken here for modifications are from 2005 and 2020 which had the sensors TM (Thematic Mapper) and OLI (Operational Land Imager) respectively. The spectral resolution for both was 30m. To detect the change in vegetation and buildup area of the location, images from 13/04/2005 of LANDSAT 5 TM and 16/11/2020 of LANDSAT 8 OLI. Superior weather condition affects its transmission and scrambling (Sannier *et al.*, 2014). For this reason, data were taken from the weather condition which would give clear and accurate visuals and the least cloud cover. One of the affecting factors of sun azimuth and elevation are the differences that happen diurnally and seasonally (Singh, 1989). That is why which season to give the best results and the best time of the day was also taken into consideration. Table 2 presents the Multi-spectral image data description, of the two images used landsat-5 Thematic Mapper (TM) and landsat-8 Operation Land Imager (OLI).

Table 2
Multi-spectral image data description, of the two images used landsat-5 Thematic Mapper (TM) and landsat-8 Operation Land Imager (OLI)

Satellite	Sensor	Path/Row	DoY	Resolution (m)	Cloud cover (%)
Landsat-5 *(13 Apr. 2005)*	TM	138/44	120	30	10
Landsat-8 *(16 Nov. 2020)*	OLI	138/44	321	30	10

iii. Calculation of Normalized Difference Vegetation Index (NDVI)

NDVI shows the position of the good vegetation of the intended area. The darkest area is the greenest area and the brightest is the least green. For NDVI calculation two bands red and near-infrared radiation bands are used in the main equation. Here, the red band absorbs the most radiation and the near-infrared band radiates the most. The band no. 3 and 4 define red and near-infrared in Landsat-5 and for Landsat-8 it is band 4 and band 5.

$$NDVI = \frac{NIR - visible\ Red}{NIR + visible\ Red} \quad (1)$$

It varies from -1 to +1, -1 refers to the least number of vegetation and +1 the best vegetation present in the area.

iv. Calculation of Normalized Difference Build-Up Index (NDBI)

NDBI shows the condition of the buildup area of the region. The brightest area has least building conditions and the darkest area has dense buildings. For NDBI also two bands are used namely the short-wave infrared band and the near-infrared band. TheLandsat-5 calculation requires band 5 and 4 and for Landsat-8 it is band 6 and band 5.

$$NDBI = \frac{SWIR - NIR}{SWIR + NIR} \quad (2)$$

The value of NDBI also ranges from -1 to +1 where +1 refers to the dense buildup area and -1 refers to the least density of area having buildings.

The land use distribution for NDVI from lowest to highest was a buildup area, paved road, grassland, shrubs and dense vegetation. And that for NDBI from lowest to highest is good vegetation, shrubs, bare land, metaled surface and buildup area. The lower limit and the higher limit of the NDVI and NDBI value were not the same but it needs to be normalized the value for corresponding category selection. For this, the value of the lower limit and the higher was calculated by averaging the all-lower limits and the higher limit respectively. Table 3 presents the Land use distribution, value range and category for NDVI and NDBI indices

Table 3
Land use distribution, value range and category for NDVI and NDBI indices (Haque et al., 2020)

NDVI Value Range	Category	Land Use	NDBI Value Range	Category	Land Use
0.004 – 0.072	Very Low	Build up Area	-0.183 – -0.067	Very Low	Good vegetation
0.072 – 0.118	Low	Paved Road	-0.067 – -0.001	Low	Shrubs
0.118 – 0.167	Moderate	Grass Land	-0.001 – 0.047	Moderate	Bare Land
0.167 – 0.227	Medium	Shrubs	0.047 – 0.088	Medium	Metaled Surface
0.227 – 0.360	High	Dense Vegetation	0.088 – 0.268	High	Build up Area

Here, the change in value has been categorized from very low to high, where the lowest value defines the lowest amount of the calculated index and the highest value defines the highest amount of that calculated index. For vegetation, it showed 0.227 – 0.36 which was categorized as high. The same went for NDBI where the highest and dense buildup area had the highest range of NDBI value. Here it was 0.088–0.268, for the dense buildup area the value range was -0.183 – -0.067. The land use was from good vegetation. The overall research was mainly divided into two parts, fieldwork and desk work. Fieldwork comprised the findings of the region profile and desk work was built around imagery analysis and presenting them using mapping techniques of ArcGIS.

Methodological framework of the overall research is presented in Fig. 2. NDVI it showed -0.004 – 0.072 for the metaled road so it was categorized as very low vegetation there.

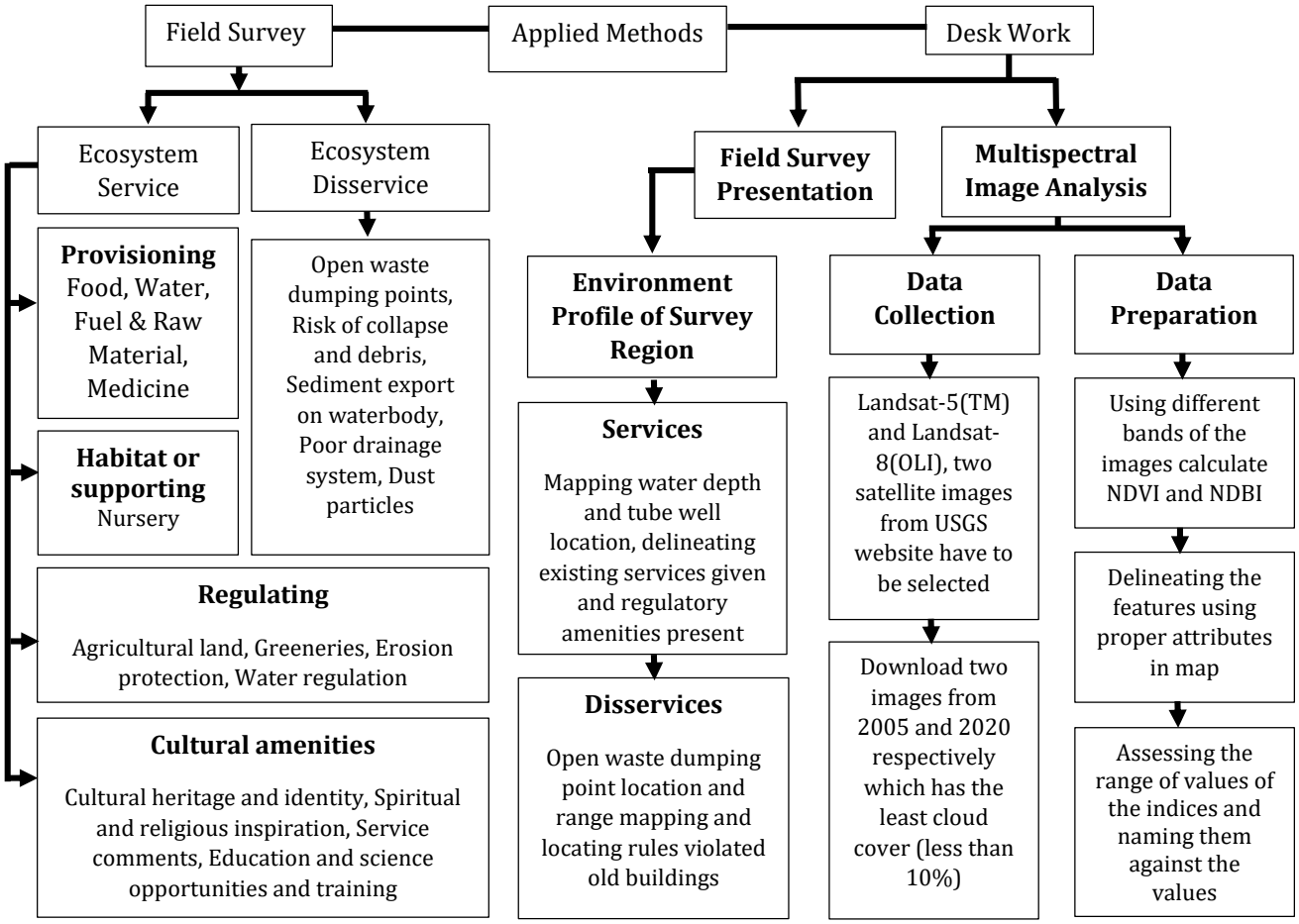

Figure 2: Methodological framework of the overall research

4. RESULT AND DISCUSSION

A. Temporal Change in Climatic Elements

The cloud coverage is positively correlated with humidity, rainfall determined by Random Effect Model (Rokonuzzaman & Rahman, 2017) but in the study area there is a negative impact on humidity as well as sunshine, and temperature is quite uncertain. Data of 2009 were taken because no compact data of 2005 was available for Khulna city. The data was collected from secondary source where meteorological data of every month from 2009 to 2020 are recorded. For ease of presentation and analysis it the twelve months have been categorized into major 4 seasons summer, monsoon, autumn and winter, and explained the findings as well. In 2020, the average precipitations between April to June and July to September are 226 mm and 589 mm, respectively which is recorded highest amount of rainfall since 2009 though there was no significant difference between the rainy day showed in Table 4. This record amount of rainfall and high visibility range for the year 2020 is correlated with cloud coverage, evaporation and declination of various kinds of pollutants for closing the industries all over the world in this pandemic situation for COVID-19. Table 4 also shows the humidity, sunny hour and sunny days which has a negative correlation with clouds coverage, precipitation, visibility range and wind speed in the year 2020 compared to 2009. Maximum and average wind speed shows a parallel relation but the trend breaks in 2019 and continued to 2020 for cyclone Foni (2019), super cyclone Amphan (2020), a heavy thunderstorm occurred in both years.

Table 4
Yearly change in the meteorological attributes

Components	Jan-Mar		Apr-Jun		Jul- Sept		Oct-Dec	
Year	09	20	09	20	09	20	09	20
Max. Avg. Temp (°c)	32	31	36	36	31	32	28	30
Min. Avg. Temp (°c)	18	19	27	26	26	27	19	21
Avg. Precipitation (mm)	3	27	70	226	200	589	40	322
Rain Days (No.)	6	17	50	69	91	91	20	30
Avg. Wind Speed (km/hr.)	8.3	8.6	11.5	14.87	9.4	14.7	7.1	8.3
Max. Wind Speed (km/hr.)	8.3	14.2	11.5	22.4	9.4	20.7	7.1	12.4
Visibility (km)	9.8	9.8	9.6	9.3	7	8.7	9.2	9.6
Cloud (%)	6	15	23	46	55	67	14	32
Humidity (%)	145	148	206	202	271	236	222	146
Sunny Days (No.)	81	74	30	22	1	1	69	31
Sunny Hr. (hr.)	258	282	352	206	214	143	226	191

B. Ecosystem Service Components

The more diversity in vegetation indicates the more enriched ecosystem and this rich ecosystem serves us a healthier environment in urban areas where life is stagnant in between the buildup areas, pollutions and so on. The NDVI and NDBI analysis represent a comparison from the year 2005 to 2020, it evident that the vegetation and building area playing an important role as ecosystem service components which is further described by image analysis in the next subsection.

i. Temporal Change in Vegetation Coverage

The comparative changes in vegetation type from the year 2005 to 2020 of KCC wards 23 and 29 are shown in Figure 3. From Table 5 ward 23 shrubs type vegetation increases by 225 km^2 and others decreased for predominately rooftop gardening and ground gardening. Table 5 also shows grass and dense vegetation land transformed into the buildings (mainly residential area) and the roof of the maximum buildings are adorned with different shrub type vegetation (filed observation). Inward 29 grassland, shrubs and dense vegetation increased by 1260, 1728 and 819 km^2 respectively from the year 2005 to 2020. This increased amount of vegetation indicates the area holding a rich ecosystem developed over time and that is resulted for mainly 3 reasons observed in filed survey, 1) The people of the Christian Missionary planting more shrubs, grass, dense vegetation like mango tree garden for beautification, eating, medicine, shade and other service purposes; 2) vegetation (grass, shrub and dense vegetation) growing on the surface of water body and edges more than before; 3) Rooftop gardening and road side plantation. As the band uses to develop NDVI mainly used for identification of vegetation, for rooftop gardening, road side planation and plants on the edge and surface of water body all seems as vegetation land rather than water body or build or paved area and for this the result from Table 6 shows significant amount of decrease in build area but the scenario is not real for both wards.

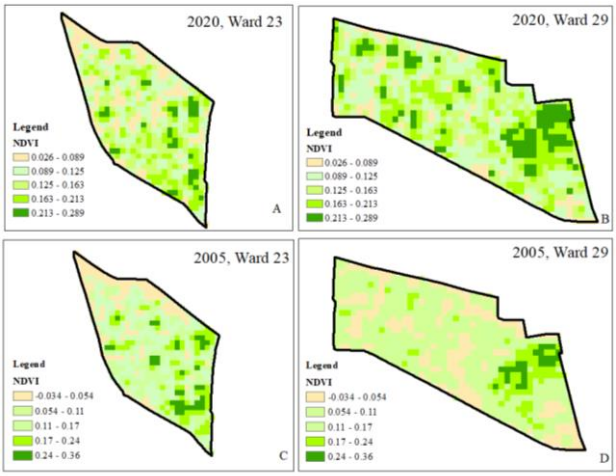

Figure 3: Normalized Difference Vegetation Index, (A) 2020, ward 23; (B) 2020, ward 29; (C) 2005, ward 23; and (D) 2005, ward 29

Table 5
Change in Vegetation Coverage from the Year 2005 to 2020

NDVI Value Range	Land Use	Area (km^2) Ward 23		Area (km^2) Ward 29	
		2005	2020	2005	2020
-0.04 – 0.09	Build-up Area	1044	1152	1764	180
0.09 – 0.13	Paver Road	1602	1512	2952	729
0.13 – 0.17	Grass Land	1494	1269	1197	2457
0.17 – 0.24	Shrubs	684	909	648	2376
0.24 – 0.36	Dense Veg.	324	306	243	1062

Table 6
Change in Build-up Area from the Year 2005 to 2020

NDBI Value Range	Land use	Area (km^2) Ward 23		Area (km^2) Ward 29	
		2005	2020	2005	2020
-0.293 – -0.098	Good veg.	306	297	324	315
-0.098 – -0.047	Shrubs	657	1008	873	738
-0.047 – -0.012	Bare Land	1494	1647	1755	1368
-0.012 – 0.19	Paved Surface	1647	1431	2205	2448
0.19 – 0.268	Buildup Area	1116	837	1647	1935

ii. Temporal Change in Building Areas

Changes in buildup areas represented in Figure 4 from the year 2005 to 2020 of KCC ward 23 and 29 indirectly

playing a role as an ecosystem service component. In ward 29, the paved surface and build-up areas have been increased by transforming the vegetation land and bare land but most of the buildings are modern residential buildings with rooftop gardening. The study area symbolizes the ancient settlement in the whole Khulna region near the river bank and most of the buildings are old-fashioned, reused for other purposes like schools, madrasas are often covered or beautified with vegetation and the new buildings are densely adorned with vegetation (Field observation). For this reason, the result of ward 23 was somehow distorted and it is false fully showing the increased amount of Bare Land and Shrubs and decrease amount of Metaled Land and Buildup Area whereas ward 29 and ward 23 are one of the most prominent developing commercial areas of Khulna city. So, the increased amount of build areas with vegetation are playing the role of a great ecosystem service component as a whole.

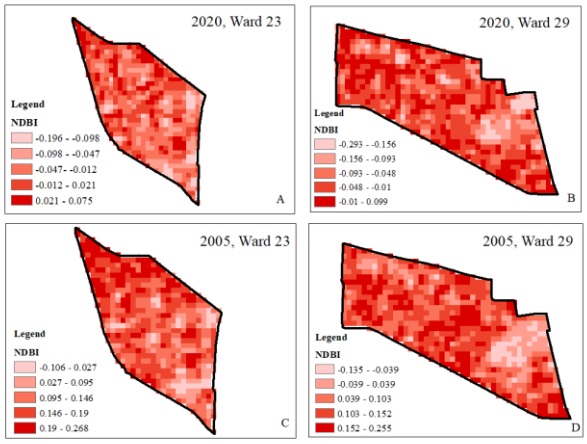

Figure 4: Normalized Difference Build-up Index, (A) 2020, ward 23; (B) 2020, ward 29; (C) 2005, ward 23; and (D) 2005, ward 29

Assessment of the component of four category indicators present in our study area and their importance discussed in the following points:

iii. Provisioning Service Indicators

Food, water body and water supply point and ornament species, these three are present in our area of the six indicators. Edible plants in both rooftop gardens and ground gardens, and animals from 2 poultry farms, fish storage farms serve food. The 50 water bodies in the area with an average depth of 7-8 ft. Minimum 4-5 ft. is enough for healthy aquaculture (Staff, 2018). These water bodies holding a rich aquaculture of them maximums are leased and private-owned, both of which are used for fisheries purpose. Ground water through road side community tube well and private electric motor means of water supply. Ornament species often use for beautification of every residences and institutions is like a characteristic of the area.

iv. Habitat or Supporting Indicators

Nursery is the only supporting service component present in the area. There are two big nurseries that cultivate and conserves different local species of flower, fruit and other

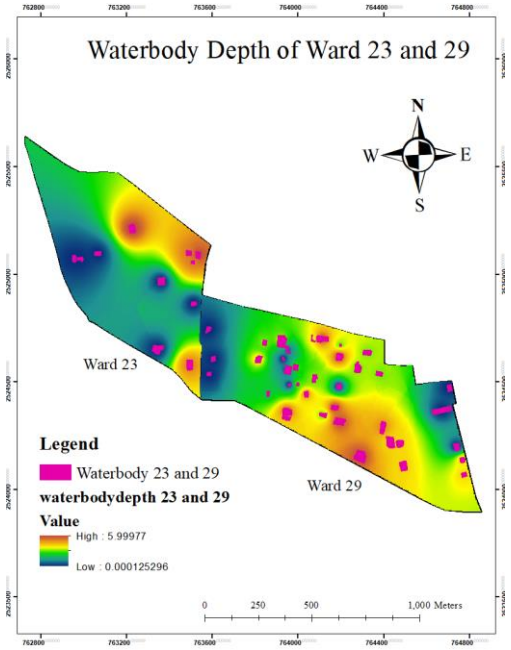

Figure 5: Waterbody depth

ornament species for commercial purpose or for scientific experiment for production of the healthy and superior plant, preservation of rare species and conserve the bio-diversity (Field observation) which enriching the ecosystem of the area.

iv. Regulating Service Indicators

Agricultural land, greeneries, erosion protection of the water bodies and water regulation are present as regulating service indicator. Under the ownership of the Christian missionary, most of the agricultural and vacant land

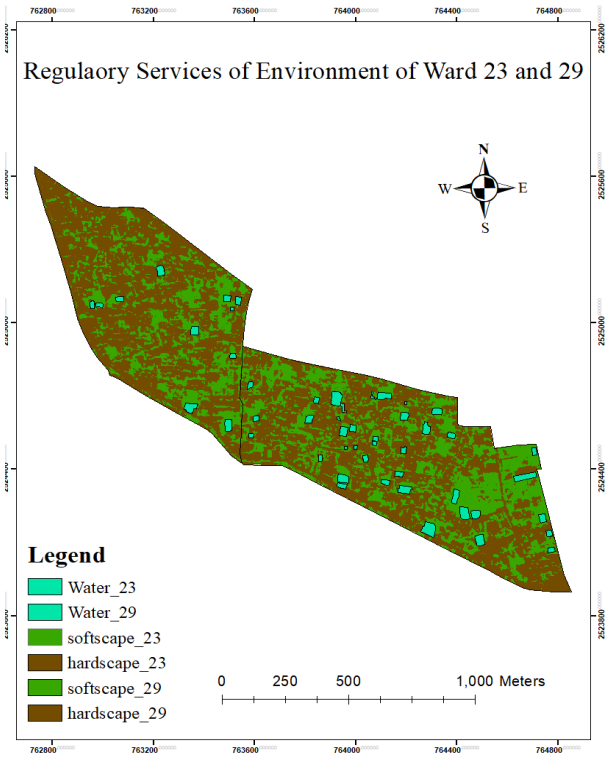

Figure 6: Regulatory services: Land use

cultivates vegetables, fruits, ornament species, herbal species and trees produce wood in both wards serving the people in many ways and holding a rich biodiversity culture trend. Other private vacant land in front of residential building and agricultural land use for gardening and cultivate vegetable or native fruits, shrubs and ornament species. There are four categories of greeneries based on height in our area such as 1. Big trees like mango, coconut, palm and herbal trees; 2. Medium height trees of fruits and flowers 3. Shrubs like flowers, ornament and darnel species. Except 3 water body 47 are embanked by soil and others are embanked by concrete. The soil type of the area is fine graded that tend to erode. Naturally developed grass and different big and medium height trees planted to prevent erosion of the earthen embankment. These water body are playing a vital role of regulating the water circulation and draining the storm water in the area. The old developed drainage condition of the area is very miserable. Blocked and broken drains are all full of waste and water cannot be drained out effectively through drains and resulted quick water logging and pollution. The amount of annual precipitation is 1736mm which is quite high but for the water bodies in the area water logging do stay more than one day even if in heavy rainfall condition. Regulating indicator presented in the study area serving a good environment effectively.

v. Cultural & Amenities Service Indicators

Cultural and amenities indicators of the area are 1. Cultural heritage and identity in the sense of place and belongings, 2. Spiritual and religious inspiration, 3. Education and science opportunities and training, 4. Dustbins 5. Amenities. Study area have the ancient settlement near the Rupsha river symbolizing the traditional Bengali architecture on building patterns and designs of old residential and religious buildings, educational and administrative institutions and restaurants are now playing the role as a sense of heritage and identity for the present generation. Presently the buildings have no warrior or public building are converted the use such as the old office of the General Deputy Postmaster of Khulna division converting to the museum, some residence like "White House" in ward 23 converted to a restaurant. Many mosques, two Hindu temples and one Church and graveyard of Christian serve as the religious and spiritual inspiration to the people of the study area. There are many schools, two colleges and one orphanage as an educational center in the area. Local Government Engineering Department is an experiment center that experiments with construction materials, road circulation and handles local level physical development. "Karitash" operated by Christian Missionaries and "BRAC" these two NGOs provide technical and skill development training and "AVA Center" serves as the training center of the people of the area. The area has all necessary urban amenities and utilities and dustbins for collection.

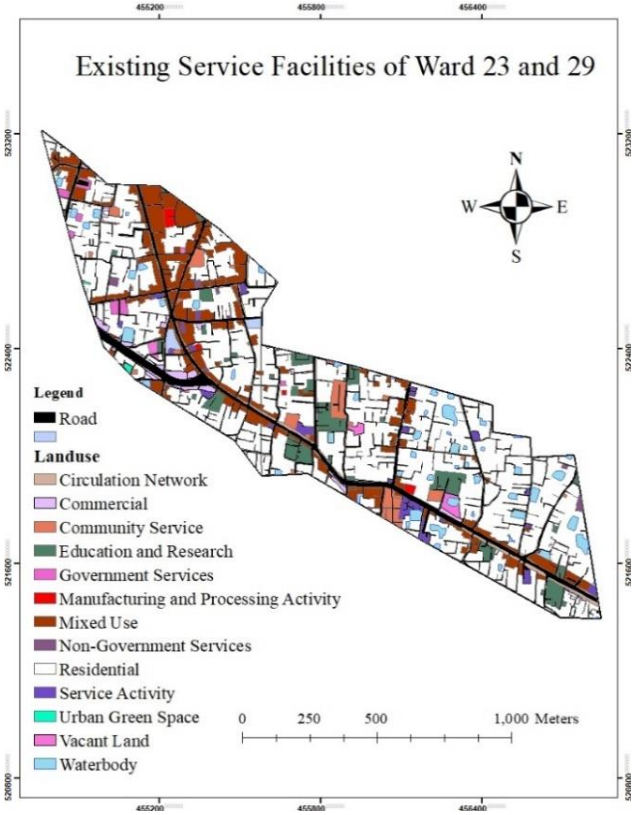

Figure 7: Service facility distribution

C. Ecosystem Dis-service Components

The study area has different disservice component that is not convenient, risky and hazardous in some cases. The following disservices are present in our study area:

i. Open Waste Dumping Points

There are only three waste dumping points in which a few amounts of people, are insufficient for gathering the waste generated by the people of the area. Moreover, the dustbins are open, Privatization of waste management systems,

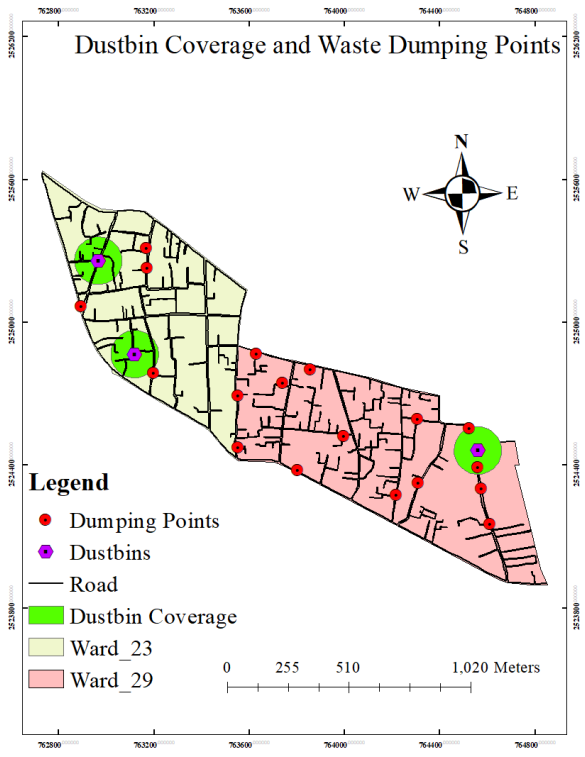

Figure 8: Maps showing waste dumping points and their range with pictures of those areas

irregularity of waste collection, just one-time waste collection per day and insufficiency of dustbins people throw waste in road sides, drains, water bodies and open spaces that so much unhealthy and in case of unmanaged clinical waste it is hazardous for the people of the area. Identification of the location of all the open waste dumping points have been done and 4 of them are beside the hospital and the clinical waste was kept open and scattered. In this pandemic situation this can cause severe health hazard for the people.

ii. Sediment Export on Water Body and Water Quality Degradation

Sediment export on some water bodies resulted from land filling, silt comes from water runoff and nearby contractions reduce the depth of the water body, toxic chemical contamination and degrades the water quality which is unhealthy for the aquaculture in some cases and posed threat to the ecosystem in the water body. Different types of water hyacinths, darnel species and waste in the surface of the water body (Location: 763928.16mE, 2524686.99 mN Figure 9(A) and 764065.21mE, 2524692.17 mN Figure 9(B) also degrades the water quality which can destroy the function of the water body and the ecosystem in it.

Figure 9: Water quality degradation on two areas A and B of the existing area

iii. Poor Drainage System

Open, blocked with a waste, broken slab of close drain resulted from poor construction method, damage of construction material for ending of the lifecycle of the construction material, poor maintenance, poor service capacity and abuse of the drains. The impact of the poor drainage system is waterlogging, insects bore for blockage, insect-borne diseases in the summer and winter (No water runoff happen then) season can cause a health hazard and mainly the drains are not functioning well. The area being low lying also posed negative effects.

iv. Violation of Rule and Risk of Collapse and Debris

Under the "Bangladesh Water Act 2013" Article S20 and S21states that structure is not allowed to be constructed above or in the embankment of the water body which would changes the water flow and deteriorated the water quality. But the office of the ward 29 is situated above a water body and a mosque is constructed close to embankment. Waste generated from the office and adjacent mosque continuously deteriorating the water quality. The slab of the drain which is mainly used for footpath are often broken. Old damaged residential building are still used by people which is very risky, can cause severe accident like death due to the collapse of the structures. The map in Figure 11 shows the risky old building which is still used for different purposes which were about four in number. The area being an old area the presence of old buildings was a unique characteristic of the region and the Figure 10 (a, b, c) shows some pictures of the risky buildings and structures on the survey region.

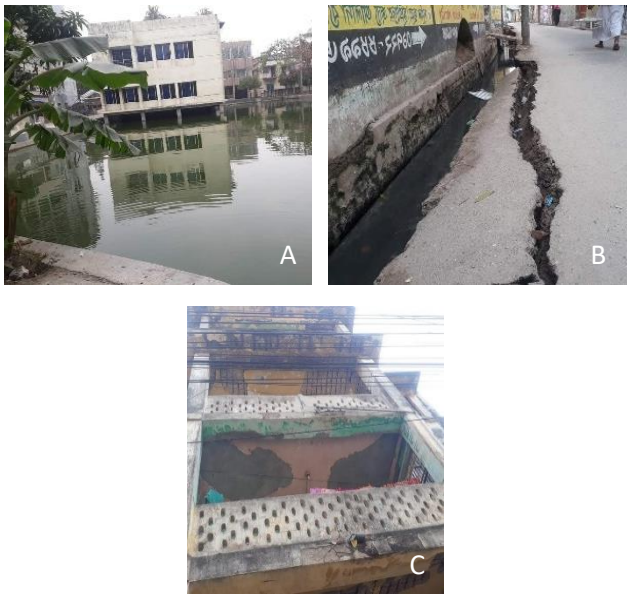

Figure 10: Violation of Rule and Risk of Collapse and Debris

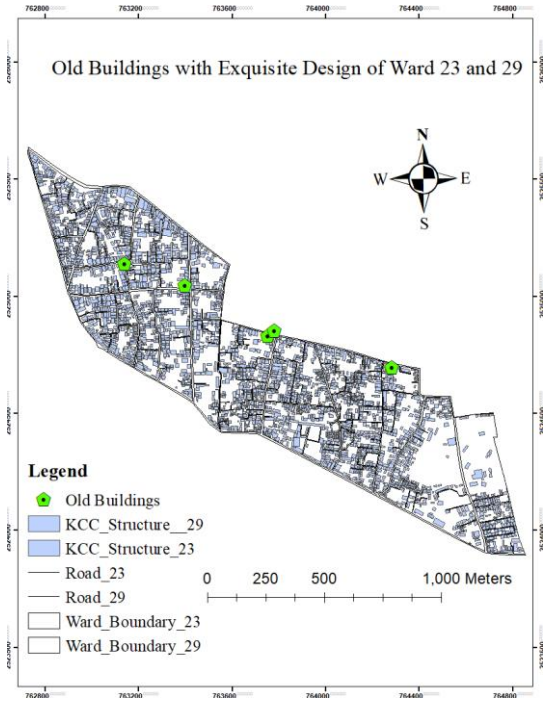

Figure 11: Risk prone old building location

5. CONCLUSIONS

The vegetation coverage of the area has shown satisfactory result over the year and indicates that improvement of a diverse and enriched ecosystem through increased vegetation, cultivation and gardening practices. With increase of buildup area, the rooftop gardening practice also indirectly balancing the impact of reduction of the

vegetation land in the ecosystem. The environmental service components have positioned the environment of the study area at a satisfactory level which ultimately is a positive sign for the urban environment and also balance the ecosystem as well. But the disservice element of the study area like open waste dumping points and drains, risk of collapsed and debris, sedimentation and water quality degradation, violation of rule are very inconvenient for people, environment and ecosystem of the study area. In some cases, it might pose a threat to people and street animals as well. The study addressed the change in environmental condition of the area over the years through imagery analysis but certain scopes were yet to be touched where blue ecosystem condition could have been analyzed. Also, in depth field data were not been able to be collected due to COVID-19 pandemic. So, the research is open for further investigation and analysis of both land and water ecosystem services sorting out the disservices and finding solutions for better overall environment condition.

ACKNOWLEDGEMENTS

Authors would like to express their gratitude to the Department of Urban and Regional Planning, Khulna University of Engineering & Technology, Khulna-9203, Bangladesh. The authors also would like to thank the Editors and anonymous reviewers of the the MIJST for their insightful comments to improve the contents of the article.

REFERENCES

Alam, S., & Mohammad, S. N. (2018). Applying the ecosystem approach to the Sundarbans of Bangladesh: Possibilities and challenges. *Review of European, Comparative and International Environmental Law*, *27*(2), 115–129. https://doi.org/10.1111/reel.12230

Aldana-Domínguez, J., Montes, C., Martínez, M., Medina, N., Hahn, J., & Duque, M. (2017). Biodiversity and Ecosystem Services Knowledge in the Colombian Caribbean: Progress and Challenges. *Tropical Conservation Science*, *10*, 1–41. https://doi.org/10.1177/1940082917714229

Andersson, E., Barthel, S., & Ahrné, K. (2007). Measuring social-ecological dynamics behind the generation of ecosystem services. *Ecological Applications*, *17*(5), 1267–1278. https://doi.org/10.1890/06-1116.1

Bolund, P., & Hunhammar, S. (1999). Ecosystem services in urban area. *Ecological Economics*, *29*(2), 293–301. https://doi.org/10.1017/S174217051300046X

Chabay, I. (2018). Land degradation and restoration. In *Companion to Environmental Studies*. https://doi.org/10.4324/9781315640051-105

de Groot, R. S., Alkemade, R., Braat, L., Hein, L., & Willemen, L. (2010). Challenges in integrating the concept of ecosystem services and values in landscape planning, management and decision making. *Ecological Complexity*, *7*(3), 260–272. https://doi.org/10.1016/j.ecocom.2009.10.006

European Environment Agency. (2011). Green infrastructure and territorial cohesion. In *Tecnical Report (Number 18)* (Issue 18).

Gómez-Baggethun, E., & Barton, D. N. (2013). Classifying and valuing ecosystem services for urban planning. *Ecological Economics*, *86*(February), 235–245. https://doi.org/10.1016/j.ecolecon.2012.08.019

Hanna, D. E. L., Tomscha, S. A., Ouellet Dallaire, C., & Bennett, E. M. (2018). A review of riverine ecosystem service quantification: Research gaps and recommendations. *Journal of Applied Ecology*, *55*(3), 1299–1311. https://doi.org/10.1111/1365-2664.13045

Haque, M. N., Morshed, S. R., Fattah, M. A., Ishra, A. K., & Saroar, M. (2020). Environmental Risk Zone Identification of an Urban Unit Using GIS and Remote Sensing. *BAUET JOURNAL*, *2*(2), 25–39.

Isbell, F., Gonzalez, A., Loreau, M., Cowles, J., Díaz, S., Hector, A., MacE, G. M., Wardle, D. A., O'Connor, M. I., Duffy, J. E., Turnbull, L. A., Thompson, P. L., & Larigauderie, A. (2017). Linking the influence and dependence of people on biodiversity across scales. *Nature*, *546*(June), 65–72. https://doi.org/10.1038/nature22899

Islam, M. M., Sunny, A. R., Hossain, M. M., & Friess, D. A. (2018). Drivers of mangrove ecosystem service change in the Sundarbans of Bangladesh. *Singapore Journal of Tropical Geography*, *39*(2), 244–265. https://doi.org/10.1111/sjtg.12241

Le Saout, S., Hoffmann, M., Shi, Y., Hughes, A., Bernard, C., Brooks, T. M., Bertzky, B., Butchart, S. H. M., Stuart, S. N., Badman, T., & Rodrigues, A. S. L. (2013). Protected areas and effective biodiversity conservation. *Science*, *342*(6160), 803–805. https://doi.org/10.1126/science.1239268

Lyytimäki, J., Petersen, L. K., Normander, B., & Bezák, P. (2008). Nature as a nuisance? Ecosystem services and disservices to urban lifestyle. *Environmental Sciences*, *5*(3), 161–172. https://doi.org/10.1080/15693430802055524

Maskell, L. C., Crowe, A., Dunbar, M. J., Emmett, B., Henrys, P., Keith, A. M., Norton, L. R., Scholefield, P., Clark, D. B., Simpson, I. C., & Smart, S. M. (2013). Exploring the ecological constraints to multiple ecosystem service delivery and biodiversity. *Journal of Applied Ecology*, *50*(3), 561–571. https://doi.org/10.1111/1365-2664.12085

Odum, E. P. (1989). Ecology and our endangered life-support systems. *Environmental Entomology*, *20*(1), 283. https://doi.org/10.2307/1352581

Rabbi, M. F., Sami, F. Y., Rimi, A. A., & Haque, M. N. (2021). Environmental profiling of an urban unit. In Imam, Rahman, & Pal (Eds.), *Proceedings of the 5th International Conference on Advances in Civil Engineering (ICACE 2020)* (Issue May, pp. 65–72).

Rasmussen, L. V., Christensen, A. E., Danielsen, F., Dawson, N., Martin, A., Mertz, O., Sikor, T., Thongmanivong, S., & Xaydongvanh, P. (2017). From food to pest: Conversion factors determine switches between ecosystem services and disservices. *Ambio*, *46*(2), 173–183. https://doi.org/10.1007/s13280-016-0813-6

Rendón, O. R., Garbutt, A., Skov, M., Möller, I., Alexander, M., Ballinger, R., Wyles, K., Smith, G., McKinley, E., Griffin, J., Thomas, M., Davidson, K., Pagès, J. F., Read, S., & Beaumont, N. (2019). A framework linking ecosystem services and human well-being: Saltmarsh as a case study. *People and Nature*, *1*(4), 486–496. https://doi.org/10.1002/pan3.10050

Rokonuzzaman, M., & Rahman, M. M. (2017). Effect of Cloud Coverage on Sunshine, Humidity, Rainfall and Temperature for Different Weather Stations in Bangladesh: A PanelAnalysis. *IOSR Journal of Environmental Science, Toxicology and Food Technology*, *11*(03), 01–06. https://doi.org/10.9790/2402-1103010106

Sannier, C., McRoberts, R. E., Fichet, L. V., & Makaga, E. M. K. (2014). Using the regression estimator with landsat data to estimate proportion forest cover and net proportion deforestation in gabon. *Remote Sensing of Environment*,

151(August), 138–148. https://doi.org/10.1016/j.rse.2013.09.015

Sarker, S. K., Reeve, R., Paul, N. K., & Matthiopoulos, J. (2019). Modelling spatial biodiversity in the world's largest mangrove ecosystem—The Bangladesh Sundarbans: A baseline for conservation. *Diversity and Distributions*, *25*(5), 729–742. https://doi.org/10.1111/ddi.12887

Schaubroeck, T. (2017). A need for equal consideration of ecosystem disservices and services when valuing nature; countering arguments against disservices. *Ecosystem Services*, *26*(August), 95–97. https://doi.org/10.1016/j.ecoser.2017.06.009

Shackleton, C. M., Ruwanza, S., Sinasson Sanni, G. K., Bennett, S., De Lacy, P., Modipa, R., Mtati, N., Sachikonye, M., & Thondhlana, G. (2016). Unpacking Pandora's Box: Understanding and Categorising Ecosystem Disservices for Environmental Management and Human Wellbeing. *Ecosystems*, *19*(4), 587–600. https://doi.org/10.1007/s10021-015-9952-z

Singh, A. (1989). Review Articlel: Digital change detection techniques using remotely-sensed data. *International Journal of Remote Sensing*, *10*(6), 989–1003. https://doi.org/10.1080/01431168908903939

Smart, J. C. R., Hicks, K., Morrissey, T., Heinemeyer, A., Sutton, M. A., & Ashmore, M. (2011). Applying the ecosystem service concept to air quality management in the UK: A case study for ammonia. *Environmetrics*, *22*(5), 649–661. https://doi.org/10.1002/env.1094

Staff, K. (2018). *Dimensions : Dig DIFFERENT Sized Fish Ponds*. https://krishijagran.com/news/dimensions-dig-different-sized-fish-ponds

Sun, Y., Hao, R., Qiao, J., & Xue, H. (2020). Function zoning and spatial management of small watersheds based on ecosystem disservice bundles. *Journal of Cleaner Production*, *255*(May), 1–10. https://doi.org/10.1016/j.jclepro.2020.120285

Tian, Y., Wu, H., Zhang, G., Wang, L., Zheng, D., & Li, S. (2020). Perceptions of ecosystem services, disservices and willingness-to-pay for urban green space conservation. *Journal of Environmental Management*, *260*(110140), 1–12. https://doi.org/10.1016/j.jenvman.2020.110140

Tzoulas, K., Korpela, K., Venn, S., Yli-Pelkonen, V., Kaźmierczak, A., Niemela, J., & James, P. (2007). Promoting ecosystem and human health in urban areas using Green Infrastructure: A literature review. *Landscape and Urban Planning*, *81*(3), 167–178. https://doi.org/10.1016/j.landurbplan.2007.02.001

CALL FOR PAPERS

MIJST invites to submit Unpublished, Original, and Innovative research works from any branch of Engineering, applied sciences, and related areas.

Submitted manuscripts will undergo a double-blind peer-review process. For submission of Manuscript template and authors' instructions, please visit journal website at: ***https://mijst.mist.ac.bd/mijst/index.php/mijst/***

MIJST offers a faster peer-review process. There will be no charges for Registration, Online submission, Publication of manuscripts, and access to the published articles. Best selected papers will also be awarded by MIJST.

ABOUT MIJST

MIST International Journal of Science and Technology (MIJST), published biannually (June and December), is a peer-reviewed open-access journal of the Military Institute of Science and Technology (MIST). This journal is a continuation of the 'MIST Journal of Science and Technology', published by MIST, under ISSN 1999-2009 from 2009 to 2011, ISSN 2224-2007 from 2012 to 2019, & E-ISSN 2707-7365 since 2020.

MIJST publishes original research findings as regular papers, review papers (by invitation). The Journal provides a platform for Engineers, Researchers, Academicians, and Practitioners who are highly motivated in contributing to the Engineering, Science, and Technology and Applied Sciences disciplines. MIJST welcomes contributions that address solutions to the specific challenges of the developing world.

The Journal is now indexed in the "DOI Crossref", "BaglaJOL", "Creative Common", "Microsoft Academic Search", "Publons", "Semantic Scholar" and "Open Journal System" databases and is accessible through the Google Scholar. The journal is also planned to be registered under the Asian Citation Indexing, Directory of Open Access Journals (DOAJ), SCOPUS, and Emerging Source Citation Indexing (ESCI) in course of time. The Journal aims to be one of the leading journals of the Country and the Region for its contributions in the advancement of Science and Technology. Unpublished innovative world-class research papers under the following subject areas are invited. Contributions from other areas of Engineering and Applied Sciences are also welcome.

SUBJECT AREAS:

- **AEROSPACE AND AVIONICS ENGINEERING**
- **APPLIED PHYSICS & SCIENCE**
- **ARCHITECTURE**
- **BIOMEDICAL ENGINEERING**
- **CHEMISTRY**
- **CIVIL ENGINEERING**
- **COMPUTER SCIENCE AND ENGINEERING**
- **ELECTRICAL, ELECTRONIC AND COMMUNICATION ENGINEERING**
- **ENVIRONMENTAL, WATER RESOURCES, AND COASTAL ENGINEERING**
- **INDUSTRIAL AND PRODUCTION ENGINEERING**
- **MATERIALS SCIENCE & ENGINEERING**
- **MECHANICAL ENGINEERING**
- **NAVAL ARCHITECTURE AND MARINE ENGINEERING**
- **NUCLEAR SCIENCE & ENGINEERING**
- **PETROLEUM AND MINING ENGINEERING**

E-ISSN: 2707-7365

Journal URL